

NASA TECHNICAL NOTE



NASA TN D-5102

2.1

NASA TN D-5102



LOAN COPY: RETURN TO
AFWL (WLIL-2)
KIRTLAND AFB, N MEX

**LARGE-SCALE TESTS OF AN AIRPLANE
MODEL WITH A DOUBLE-DELTA WING,
INCLUDING LONGITUDINAL AND LATERAL
CHARACTERISTICS AND GROUND EFFECTS**

*by Victor R. Corsiglia, David G. Koenig,
and Joseph P. Morelli*

*Ames Research Center
Moffett Field, Calif.*



LARGE-SCALE TESTS OF AN AIRPLANE MODEL WITH A DOUBLE-DELTA
WING, INCLUDING LONGITUDINAL AND LATERAL
CHARACTERISTICS AND GROUND EFFECTS

By Victor R. Corsiglia, David G. Koenig, and Joseph P. Morelli

Ames Research Center
Moffett Field, Calif.

NATIONAL AERONAUTICS AND SPACE ADMINISTRATION

For sale by the Clearinghouse for Federal Scientific and Technical Information
Springfield, Virginia 22151 - CFSTI price \$3.00

LARGE-SCALE TESTS OF AN AIRPLANE MODEL WITH A DOUBLE-DELTA
WING, INCLUDING LONGITUDINAL AND LATERAL
CHARACTERISTICS AND GROUND EFFECTS

By Victor R. Corsiglia, David G. Koenig, and Joseph P. Morelli

Ames Research Center

SUMMARY

A wind-tunnel investigation has been undertaken to determine the lateral directional, and longitudinal aerodynamic characteristics of a supersonic transport configuration with a double-delta wing of aspect ratio 1.66. Ground effects were also investigated.

There was no large reduction in static longitudinal stability at high angles of attack. The trimmed lift coefficient in ground effect, at gear height, was 1.25 times that out of ground effect at the angle of attack for takeoff or landing. Calculations of takeoff performance showed that the takeoff distance can be reduced by increasing the speed beyond that corresponding to the ground limit value of angle of attack. To improve the lift-drag ratio in the takeoff climb, it is desirable to accelerate after lift-off, because the speed for maximum L/D is about 250 knots relative to a takeoff speed of about 190 knots. The improved L/D results in reduced noise at distances greater than 3 miles from brake release and results in more efficient flight.

INTRODUCTION

One aircraft configuration that has been considered in recent supersonic transport design studies has a fixed double-delta wing and no horizontal tail or canard. Elevons are used for longitudinal and lateral control. The double-delta wing has a sharp leading edge that produces flow separation at angles of attack which would be used for landing and takeoff. This separated flow forms two vortex cores that extend above the wing. These vortex cores affect the aerodynamic forces and moments by interacting with the wing and vertical tail. In reference 1, it is pointed out that the use of strakes on a delta wing to form a double-delta wing increases the lift at a given angle of attack but reduces longitudinal stability. The double-delta wing, then, must be designed to obtain adequate lift at a given angle of attack and to avoid excessive reductions in stability with increasing angle of attack.

A large-scale wind-tunnel investigation has been undertaken to determine the lateral, directional, and longitudinal aerodynamic characteristics of a supersonic transport configuration with a double-delta wing of aspect ratio 1.66. Longitudinal aerodynamic characteristics in the proximity of the ground

were also obtained. The model was equipped with leading-edge flaps, a rudder, and elevons. The effects of Krueger flap and of increasing fuselage length were also investigated.

NOTATION

| | |
|------------|--|
| b | wing span, 29.0 ft |
| c | wing local chord, in. |
| \bar{c} | reference chord, $2/S \int_0^{b/2} c^2 dy$, strakes off, 21.68 ft |
| C_D | drag coefficient, drag/qS |
| C_L | lift coefficient, lift/qS |
| C_m | pitching-moment coefficient, pitching moment/qS \bar{c} , positive nose up |
| C_n | yawing-moment coefficient, yawing moment/qSb, positive nose right |
| C_y | side-force coefficient, side force/qS, positive right |
| C_l | rolling-moment coefficient, rolling moment/qSb, positive right wing down |
| F_1, F_2 | fuselage configuration, see figure 2(a) |
| h | height of moment center above ground plane or above the runway, ft |
| L/D | lift-drag ratio |
| N | engine nacelles (no engines) |
| n | load factor |
| q | free-stream dynamic pressure, lb/ft ² |
| S | reference area, strake off, 505.9 ft ² |
| T/W | thrust-weight ratio |
| t | wing-section thickness |
| V | vertical tail or speed |
| W | wing including strake or gross weight |
| Z | ordinate of wing section mean line measured from wing reference line |

| | |
|------------|--|
| z_u, z_L | upper and lower surface ordinates of wing section measured from wing reference line, in. |
| α | angle of attack of wing reference line, positive leading edge up, deg |
| α_0 | twist, angle between wing section chord and wing reference line, positive leading edge up, deg |
| β | angle of yaw, positive nose left, deg |
| δ_a | aileron deflection, (left side/right side), $\delta_e(\text{left}) - \delta_e(\text{right})$, deg |
| δ_e | elevon deflection, positive trailing edge down, deg |
| δ_K | Krueger flap deflection, positive leading edge down, deg |
| δ_n | leading-edge flap deflection, positive leading edge down, deg |
| δ_r | rudder deflection, positive trailing edge left, deg |
| γ | flight-path angle, deg |
| η | span location, fraction of semispan |

Subscripts

| | |
|------------|---------------------------------------|
| FS | fuselage station |
| u | uncorrected |
| α | wind-stream angularity |
| β | derivative with respect to β |
| δ_a | derivative with respect to δ_a |

MODEL AND APPARATUS

When data out of ground proximity were desired, the model was mounted on the conventional support system shown in figure 1(a). For the portion of the tests when ground effects were measured, the model was mounted on the ground plane support system (fig. 1(b)). When ground effects were measured, a different set of struts was used for each ground height.

The model consisted of the wing, fuselage, vertical tail, and nacelle combination shown in figure 2(a). It was equipped with leading-edge flaps, a rudder, and elevons along the wing trailing edge. The leading edge of the basic wing and strake was sharp. Details of the Krueger flap are also shown in figure 2(a). This flap was removed when not used. The elevons consisted of three trailing-edge flaps on each wing. Aileron control was obtained by deflecting the outboard two elevons on each wing.

Fuselage contours are shown in figure 2(b). To obtain the extended fuselage configuration, F_2 , a constant area extension was inserted in the center portion of the fuselage.

Details of the wing sections are shown in figure 2(c). The four control sections for the wing are shown on this figure. The wing surface between the control sections was defined by straight-line elements at constant percent chord. The spanwise variation of twist and maximum thickness are shown in the table of figure 2(c). The mean lines of the control sections are also plotted on this figure. The wing surface ordinates in table I are measured down from the wing reference plane.

For the three outboard wing control sections, the wing thickness is a parabolic distribution with the maximum thickness at 55-percent chord. The root control section ($\eta = 0.0833$) has a somewhat different thickness distribution. As indicated on figure 3(a), the thickness of the strake is formed by straight-line elements at constant percent of the exposed span of the strake between fuselage stations 105.5 and 264.4. From the 55-percent chord of the root control section to the point on the root control section which is an extension of the 55-percent chord line of the basic wing (see fig. 2(c)), the thickness is constant. The remainder of the section is a parabolic thickness distribution with the maximum thickness at the constant thickness portion of the section.

Details of the strake and the nacelles are shown in figures 3(a) and 3(b), respectively.

TEST PROCEDURE AND CONDITIONS

Force and moment data were obtained for angles of attack from -2° to $+32^\circ$ at angles of yaw from -12° to $+12^\circ$. Ground height ranged from out of ground effect to a height of $h/\bar{c} = 0.19$ (a typical value corresponding to lift-off and touchdown). Table II is an index of the configurations tested.

The free-stream dynamic pressure was 35 lb/ft^2 for most of the tests, which corresponds to a Reynolds number (based on \bar{c}) of 23.8×10^6 and a Mach number of 0.15.

DATA REDUCTION AND CORRECTIONS

Forces and moments for the model were measured with the wind-tunnel balance system with the moment data referred to $0.25\bar{c}$. The position of this moment center is shown in figure 2(a). The reference area and lengths were $S = 505.9 \text{ ft}^2$, $\bar{c} = 21.68 \text{ ft}$, and $b = 29.00 \text{ ft}$. Force data are referred to wind axis, and moment data to stability axis.

The data obtained with the model mounted on the conventional support system (i.e., the data representative of the characteristics out of ground proximity) were corrected for wind-tunnel wall effects and strut tare as follows:

$$\alpha = \alpha_u + 1.46 C_L$$
$$C_D = C_{D_u} + 0.02 C_L^2 - (\Delta C_D)_{\text{tare}}$$

The strut tare corresponded to the force and moment measured for the struts alone with the model removed from the wind tunnel. This tare was negligible for lift and moment coefficient and was 0.0027 for drag coefficient.

For data taken to determine ground effects, no wind-tunnel wall corrections were applied since they are negligible. However, the following strut tare and wind-stream angularity corrections were included:

$$C_L = C_{L_u} - C_{D_u} \sin \alpha_\alpha$$

$$C_D = C_{D_u} - (\Delta C_D)_{\text{tare}} + C_{L_u} \sin \alpha_\alpha$$

$$C_M = C_{M_u} - (\Delta C_M)_{\text{tare}}$$

$$\alpha = \alpha_u + \alpha_\alpha$$

The magnitude of the tare (which varied with ground height) was negligible for lift coefficient and less than 0.012 and 0.008 for drag and moment coefficients, respectively.

RESULTS AND DISCUSSION

Longitudinal Characteristics

As shown in figure 4, the variation of pitching-moment coefficient with lift coefficient was nearly linear, with no serious abrupt changes in pitching moment in the range of C_L used for landing and takeoff ($C_L = 0.5$ to 0.6). There is slight gradual reduction in longitudinal stability as lift

increases. This curvature in the pitching-moment curve is associated with the presence of the leading-edge vortex flow field above the wing (ref. 1). The magnitude of this curvature is such that the aerodynamic center shifted forward about 4 to 8 percent of \bar{c} (depending on the elevon deflection) as C_L was increased from 0 to 1.0.

The longitudinal control effectiveness remained essentially unchanged for the range of deflections tested for lift coefficients up to 1.0.

Effects of leading-edge flaps.- The effects of deflecting the leading-edge flaps on the lift, drag, and pitching-moment characteristics of the model are shown in figures 4(b), (c), (d), and (e). These results are summarized in terms of L/D and angle of attack in figure 5. As shown, the L/D improvement at $C_L = 0.5$ is about 0.3; however, at climbout values of C_L (0.3 to 0.4) the L/D improvement increases to about 1.0. The angle-of-attack penalty due to deflection of the leading-edge flaps is about 1.0° .

As an alternative to using leading-edge flaps, the use of Krueger flaps to improve L/D at high lift coefficients was considered. A sketch of these flaps is seen in figure 2(a). The data with the Krueger flaps installed are presented in figure 6. A summary showing the L/D and angle-of-attack variation with Krueger flap deflection appears in figure 7. At $C_L = 0.5$ the maximum L/D increase is about the same as obtained with the use of leading-edge flaps; at lower C_L (0.3), however, the L/D increase is less. The angle-of-attack penalty remained about the same as for leading-edge flaps at all C_L .

As shown in figure 2(a), the leading-edge flaps had three panels on each side, each with approximately the same spanwise extent. Data with leading-edge flap deflection varying spanwise are presented in figure 8. The spanwise variation of leading-edge flap deflection produced modest effects on pitching-moment characteristics, and only minor effects on lift and drag characteristics. These results suggest that moderate improvements in stability can be achieved by spanwise variation of leading-edge flap deflection.

In the data shown above, the leading-edge flaps were deflected down to increase L/D at a given C_L . However, this was accompanied by an increase in angle of attack required for a given C_L . Therefore, the use of upward deflection of the leading-edge flaps to reduce the angle of attack required for a given C_L was considered. The results of this investigation are presented in figure 9. It is shown that an upward 20° deflection of the leading-edge flaps reduced the angle of attack by only 0.3° at $C_L = 0.5$, compared to the configuration with 0° flap deflection. In addition, there was an increase in C_D for a given C_L .

Effects of ground proximity.- The characteristics of the model in the presence of the ground are presented in figures 10 through 12. Figure 13 is a summary of the ground effects. The effect on elevon effectiveness was slight. Lift-curve slope and static margin changed 0.030 and 0.08, respectively, for a change in ground height from out of ground effect to $h/c = 0.19$. This corresponds to about a 50-percent increase in lift-curve slope. In the same range of ground height, the drag was reduced 20 percent

of the out of ground effect value. With the elevons fixed ($\delta_e = -5^\circ$), the lift coefficient in ground effect was about 1.6 times the value out of ground effect. However, with the pitching moment trimmed by use of the elevons, this multiple was reduced to 1.25.

Lateral-Directional Characteristics

Figure 14 presents data with various angles of sideslip for the short fuselage configuration. Data with the vertical fin and the nacelles removed are presented in figures 15 and 16, respectively.

Lateral stability.- A summary of the data showing the variation of C_{l_β} with sideslip and lift coefficient is presented in figure 17. The value of C_{l_β} varies between -0.0018 and -0.0030 for C_L from 0.4 to 1.0. C_{l_β} was obtained by crossplotting C_l versus β and then measuring the slope.

Directional stability.- The data for the configuration with the extended fuselage are presented in figure 18. Figure 19 is a summary of the yawing moment due to sideslip characteristics of the model as shown in figures 14(b) and 18(b). The variation of yawing moment with angle of sideslip is stable at lift coefficients up to 0.8, but the level of stability is reduced considerably at a lift coefficient of 1.0. This is due to the effect of the interaction of the windward wing leading-edge vortex and the forebody vortices with the vertical tail. The only significant effect of extending the fuselage was to reduce C_{n_β} for low values of sideslip and to cause the destabilizing tendency at high lift to become more severe. The value of C_{n_β} measured at low values of lift coefficient and sideslip is 0.0020 for the extended fuselage configuration.

Lateral control.- Data with various aileron deflections at zero elevon are presented in figure 20. The ailerons are seen to be effective for values of C_L from 0 to 1.0. The value of $C_{l_{\delta_a}}$ was 0.00088 at zero lift. The yawing-moment coefficient due to aileron deflection is adverse at high lift coefficients but not at low lift coefficients (C_L below 0.23). The values of $C_{n_{\delta_a}}$ are -0.0001 and -0.0002 for $C_L = 0.4$ and 0.8, respectively.

Figure 21 presents data for various angles of sideslip with the ailerons deflected. An aileron deflection of $\delta_a = 40^\circ$ was adequate to trim up to 12° of sideslip at $C_L = 0.8$.

Directional control.- Data with various rudder deflections are presented in figure 22. The rudder effectiveness is linear and can be seen to be independent of C_L for values of C_L from 0 to 1.0. The value of $C_{n_{\delta_r}}$ was measured to be -0.0014. Figure 23 presents data for various angles of sideslip with the rudder deflected. The maximum rudder deflection tested ($\delta_r = +27^\circ$) was not adequate to trim 12° of sideslip ($\beta = 12^\circ$) for C_L from 0.2 to 0.8. At $C_L = 0.6$ this rudder deflection would trim about 10° of sideslip.

COMPARISON WITH THEORY

Out of Ground Effect

A theoretical method to predict the normal forces and pitching moments on low-aspect-ratio wings with leading-edge vortex flow is presented in reference 2. This method has been applied to the wing fuselage configuration used in the present investigation, and the results are shown in figure 24. As shown, the lift curve is slightly under that predicted with a maximum error in C_L of 0.07. The aerodynamic center location at low lift is predicted well. However, the theory predicted an increase in longitudinal stability with increasing C_L instead of the slight reduction in stability obtained experimentally. At $C_L = 0.5$, the error in longitudinal stability is 6-percent \bar{c} .

In Ground Effect

For the prediction of ground effect, the theory of Gersten (refs. 3 and 4) was used. A summary of the ground effect on lift results, as measured in the present investigation, is compared with Gersten's theory in figure 25. It is seen that for the range of ground heights tested the agreement between theory and experiment is good.

TAKEOFF PERFORMANCE

A double-delta wing transport has aerodynamic characteristics considerably different from those of conventional subsonic jet transports. Three characteristics are especially noteworthy. First, the lift coefficient available for takeoff and landing is limited by the low lift-curve slope and the ground clearance limit on angle of attack (about $\alpha = 12^\circ$). Second, the lift-drag ratio is low (about 5) at values of lift coefficient used for take-off and landing. Finally, the thrust-weight ratio is quite high (about 0.38).

Figure 26 presents trimmed values of C_L as a function of L/D , and α for this double-delta configuration both in and out of ground effect. A representative value of angle of attack for lift-off is about $\alpha = 12^\circ$, so that the maximum available lift coefficient for lift-off with leading-edge flaps deflected 30° is $C_L = 0.64$. The value of L/D out of ground effect at this lift coefficient is approximately half the maximum value.

Takeoff Velocity and Distance

The takeoff characteristics have been predicted for an airplane having the aerodynamic characteristics presented here and the thrust and weight characteristics representative of a supersonic transport airplane. Some of

the parameters used in this computation are listed in table III, and a brief description of the computational technique is given in appendix A. Figure 27 presents the takeoff distances to flight speeds corresponding to lift-off and 50-foot altitude for various values of gross weight. For comparison, the flight-test results of a KC-135A jet tanker are also presented (ref. 5). Pertinent parameters of the KC-135A are also listed in table III. Lift-off velocities are about 20 knots higher for the SST (due to the low value of C_L available). However, because of its superior acceleration ability (due to the higher thrust-weight ratio), the takeoff distance to an altitude of 50 feet for the SST (for $W = 590,000$ lb) is about 1500 feet less than that of the KC-135A (for $W = 240,000$ lb).

Optimum Lift-Off Speed

Minimum lift-off speed is not the speed for optimum takeoff for this aircraft. For the takeoff computation shown in the previous figure, lift-off occurred near the limit value of angle of attack. This was done to limit the speed at lift-off to a near minimum value. An improved L/D at takeoff can be achieved by increasing the lift-off speed. Increased lift-off speed will reduce the C_L below that available at $\alpha = 12^\circ$ and thereby increase the L/D (see fig. 26(b)). As shown in figure 28, increasing the lift-off speed from 170 to 189 knots improved the second segment rate of climb by 9 percent without increasing the distance required to attain an altitude of 35 feet.

Takeoff Climb Profile

To operate at an improved L/D after lift-off, it is necessary to accelerate to higher speed (i.e., lower C_L) rather than to climb at the maximum angle available at takeoff speed. This will result in reduced airplane altitude in the vicinity of the airport. However, to reduce the noise heard on the ground, it is desirable to attain high altitude and high L/D (low thrust). These climb technique considerations are shown in figure 29, where two climb profiles are presented. One represents a high climb gradient technique, the other an acceleration type. For the high climb gradient takeoff (i.e., aircraft A, fig. 29), the angle of attack was increased from 12° at lift-off to 14° , resulting in a load factor of 1.2 (standard day). This load factor was maintained until a climb speed of 196 knots was reached, then the load factor was reduced to 1.0 while constant speed was maintained, so that a constant climb gradient was achieved. The initial acceleration type of takeoff was performed by maintaining a much smaller constant load factor throughout the entire climb ($n = 1.05$ standard day).

At a point 3 miles from brake release, the higher climb gradient aircraft was 700 feet higher; however, the speed was 55 knots lower than that of the reduced climb gradient aircraft. The thrust-to-weight ratio (corresponding to 500 fpm rate of climb and constant speed) of the higher aircraft was about 27 percent greater than that of the lower aircraft because of the lower L/D corresponding to the lower speed. Noise of the two aircraft at the 3-mile

point was calculated using the method described in reference 6. The noise heard on the ground at the 3-mile point is essentially the same for the two takeoff techniques; that is, the increase in noise due to the increased thrust of the higher aircraft is compensated for by the attenuation in noise due to the increased altitude. However, at distances from brake release greater than 3 miles, the altitudes of the two aircraft will approach one another, and therefore the higher speed aircraft will produce less noise on the ground.

Also shown in figure 29(a) is a small portion of the climb profile of the KC-135A jet tanker. For this aircraft, the speed for maximum L/D in the takeoff configuration corresponds to about lift-off speed, hence an initial acceleration would not improve climb performance.

CONCLUDING REMARKS

The following conclusions were obtained from the results of a large-scale wind-tunnel investigation to determine the aerodynamic characteristics of a double-delta supersonic transport configuration:

1. No large reduction in static longitudinal stability in the normal operating range of angle of attack was found.
2. The trimmed lift coefficient in ground effect, at gear height, was 1.25 times that out of ground effect at the same angle of attack.
3. The lift coefficient, both in and out of ground effect, was predicted within about 10 percent.
4. The aerodynamic center was predicted satisfactorily out of ground effect. However, the theory predicted a slight increase in longitudinal stability with angle of attack rather than the slight reduction in stability found experimentally.
5. Takeoff performance can be improved by increasing lift-off speed beyond that corresponding to the limit value of angle of attack.
6. Noise heard on the ground can be reduced at distances from brake release greater than about 3 miles by accelerating after lift-off. The reduced noise results from the improved L/D available at higher speed (i.e., at lower C_L).

Ames Research Center
National Aeronautics and Space Administration
Moffett Field, Calif. 94035, Nov. 8, 1968
720-01-00-01-00-21

APPENDIX A

DESCRIPTION OF THE COMPUTATIONAL TECHNIQUE FOR ESTIMATING TAKEOFF PERFORMANCE

The computation is performed on a digital computer on which the longitudinal equations of motion are integrated in a step-by-step fashion with time. At each point in time, the forces and moments on the aircraft are obtained from the aerodynamic data, the engine data, and the weight force.

The takeoff maneuver is considered in three phases: ground roll, transition, and climb-out. Ground roll consists of an initial acceleration during which thrust, C_L , and C_D are assigned through input. At the time a prescribed rotation velocity is reached, the elevons are deflected, and the resulting angle of attack is computed. The transition phase begins right after lift-off when the target value of angle of attack has been reached. During this phase thrust, C_L , C_D , and α are assigned consistent with the appropriate ground height. This phase continues until the aircraft is out of ground effect. For the climb-out phase, the load factor is assigned and C_L is computed to yield the assigned load factor. The angle of attack and the drag coefficient are then obtained from the aerodynamic data. One trial computation is generally required so that the load factor at the end of the transition matches the assigned value for climb-out.

REFERENCES

1. Kelly, Mark W.; Corsiglia, Victor R.; and Koenig, David G.: Experimental and Theoretical Studies of Wing-Leading-Edge Vortex Flow. NASA SP-124, 1966, pp. 297-311.
2. Sacks, A. H.; Lundberg, R. E.; and Hanson, C. W.: A Theoretical Investigation of the Aerodynamics of Slender Wing-Body Combinations Exhibiting Leading-edge Separation. NASA CR-719, 1967.
3. Gersten, Klaus: Über Die Berechnung des Induzierten Geschwindigkeitsfeldes Von Tragflügeln. Jahrbuch 1957 der WGL, pp. 172-190, Braunschweig, 1958.
4. Gersten, Klaus: Calculation of the Aerodynamic Characteristics of Wings of Finite Span Near the Ground. Library Translation No. 1054, Royal Aircraft Establishment, December 1963.
5. Yancey, M. H.; and Gandy, C. L.: KC-135A Performance Test With Leading-Edge Flaps. AFFTC-TR-58-26, October 1959.
6. Anon.: Jet Noise Prediction. Society of Automotive Engineers AIR 876, July 10, 1965.

TABLE I. - WING SURFACE ORDINATES

[Measured down from wing reference plane]

| x/c | $\eta = 0.0833$ | | x/c | $\eta = 0.0833$ | |
|-------|-----------------|------------------|--------|-----------------|----------------|
| | Z _U | Z _L | | Z _U | Z _L |
| 0 | 0 | 0 | 0.55 | 0 | 13.065 |
| .0638 | | 0 | .68 | | 13.065 |
| .10 | | STRAKE ↑ ↓ | .715 | | 12.756 |
| .15 | | | .75 | | 12.070 |
| .20 | | | .786 | | 11.050 |
| .25 | | | .822 | | 9.744 |
| .30 | | | .86 | | 8.350 |
| .35 | | | 12.060 | .89 | 6.696 |
| .40 | | | 12.160 | .93 | 4.625 |
| .45 | | | 12.620 | .964 | 2.276 |
| .50 | | | 12.940 | 1.00 | 0.0 |

| x/c | $\eta = 0.2155$ | | $\eta = 0.3879$ | | $\eta = 1.00$ | |
|------|-----------------|----------------|-----------------|----------------|----------------|----------------|
| | Z _U | Z _L | Z _U | Z _L | Z _U | Z _L |
| 0 | 6.493 | 6.493 | 4.515 | 4.515 | 0.795 | 0.795 |
| .05 | 5.203 | 6.500 | 3.919 | 4.723 | .823 | .676 |
| .10 | 4.164 | 6.691 | 3.364 | 4.931 | .851 | .565 |
| .15 | 3.320 | 7.025 | 2.850 | 5.139 | .879 | .461 |
| .20 | 2.627 | 7.441 | 2.377 | 5.347 | .908 | .364 |
| .25 | 2.035 | 7.717 | 1.946 | 5.452 | .917 | .276 |
| .30 | 1.509 | 7.927 | 1.556 | 5.515 | .918 | .194 |
| .35 | 1.049 | 8.069 | 1.207 | 5.537 | .913 | .121 |
| .40 | .657 | 8.145 | .900 | 5.518 | .899 | .055 |
| .45 | .331 | 8.153 | .633 | 5.459 | .878 | -.004 |
| .50 | .072 | 8.096 | .408 | 5.357 | .850 | -.055 |
| .55 | -.119 | 7.971 | .224 | 5.214 | .814 | -.098 |
| .60 | -.228 | 7.762 | .092 | 5.020 | .769 | -.133 |
| .65 | -.236 | 7.454 | .021 | 4.764 | .712 | -.155 |
| .70 | -.145 | 7.045 | .012 | 4.447 | .644 | -.167 |
| .75 | -.218 | 6.402 | -.040 | 4.044 | .572 | -.175 |
| .80 | -.162 | 5.430 | -.022 | 3.428 | .474 | -.156 |
| .85 | -.122 | 4.372 | .024 | 2.796 | .372 | -.134 |
| .90 | -.131 | 3.065 | -.009 | 1.962 | .260 | -.101 |
| .95 | -.140 | 1.557 | .010 | 1.057 | .135 | -.056 |
| 1.00 | 0 | 0 | 0 | 0 | 0 | 0 |

TABLE II.- INDEX TO CONFIGURATIONS

| Figure | Configuration | δ_e | δ_n | δ_k | δ_a | δ_r | β | h/\bar{c} | q |
|--------|---------------------------------------|------------|------------|------------|------------|------------|---------|-------------|----|
| 4(a) | W+F ₁ +V+N | Vary | 0 | Off | 0 | 0 | 0 | 0 | 35 |
| 4(b) | | | 10 | | | | | | |
| 4(c) | | | 20 | | | | | | |
| 4(d) | | | 30 | | | | | | |
| 4(e) | | | 40 | | | | | | |
| 5 | W+F ₁ +V+N | 0 | Vary | | | 0 | 0 | | |
| 6 | W+F ₂ +V+N | 0 | 0 | Vary | | | | | 25 |
| 7 | | | | | | | | | |
| 8 | W+F ₁ +V+N | | Vary | Off | | | | | 35 |
| 9 | W+F ₂ +V+N | | | | | | | | 25 |
| 10(a) | W+F ₂ +V | Vary | 0 | | | | | .19 | |
| 10(b) | | | | | | | | .31 | |
| 10(c) | | | | | | | | .42 | |
| 11 | | -5 | Vary | | | | | .19 | |
| 12 | | Vary | 30 | | | | | | |
| 13 | | -5° | 0 | | | | | Vary | |
| 14(a) | W-F ₁ +V+N | 0 | 0 | | | | Vary | ∞ | 35 |
| 14(c) | | | 30 | | | | | | |
| 14(e) | | -10 | 0 | | | | | | |
| 15(a) | W+F ₁ +N | 0 | | | | | | | |
| 15(c) | | | 30 | | | | | | |
| 16 | W+F ₁ | | 0 | | | | | | |
| 17 | W+F ₁ +V+N | | | | | | | | |
| 18 | W+F ₂ +V+N | | | | | | | | |
| 19 | W+F ₁ +V+N, F ₂ | | | | | | | | |
| 20(a) | W+F ₁ +V+N | | | | Vary | | 0 | | |
| 20(c) | | -5 | | | | | | | |
| 21 | | 0 | | | +40 | | Vary | | |
| 22 | | | | | 0 | Vary | 0 | | |
| 23 | | | | | | +27 | Vary | | |

TABLE III.- AIRCRAFT PARAMETERS USED FOR THE TAKEOFF COMPUTATION

SST

$$W = 590,000 \text{ lb}$$

$$W/S = 70 \text{ lb/ft}^2$$

$$\delta_n = 30^\circ$$

Maximum angle of attack at lift-off, $\alpha = 12^\circ$

$$\text{Gear height } h/\bar{c} = 0.19$$

$$T/W = 0.39, \text{ sea-level static thrust}$$

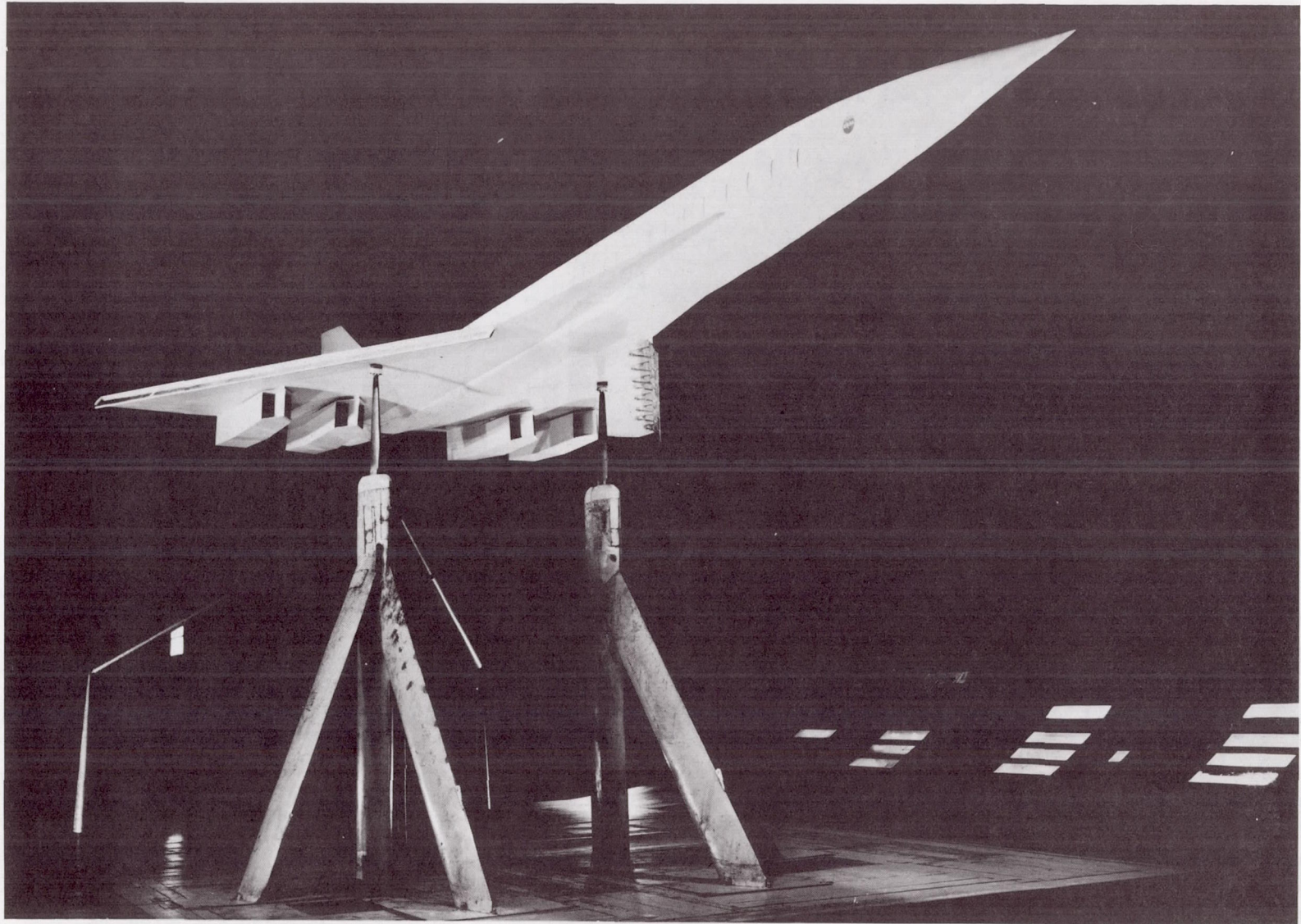
KC-135A

$$W = 240,000 \text{ lb}$$

$$W/S = 98.5 \text{ lb/ft}^2$$

Trailing-edge flaps = 20°

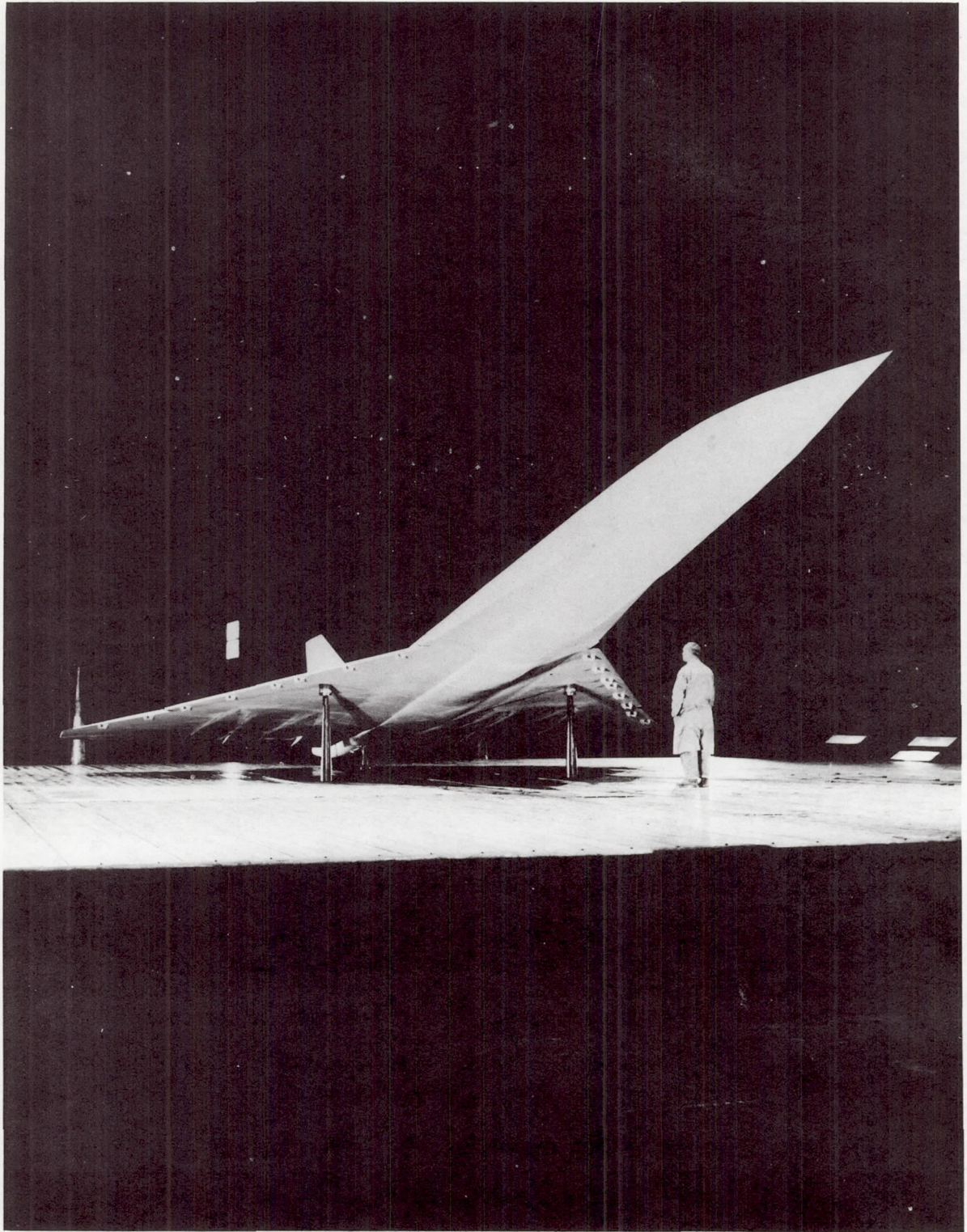
$$T/W = 0.216, \text{ sea-level static thrust}$$



(a) Conventional support system.

A-35307

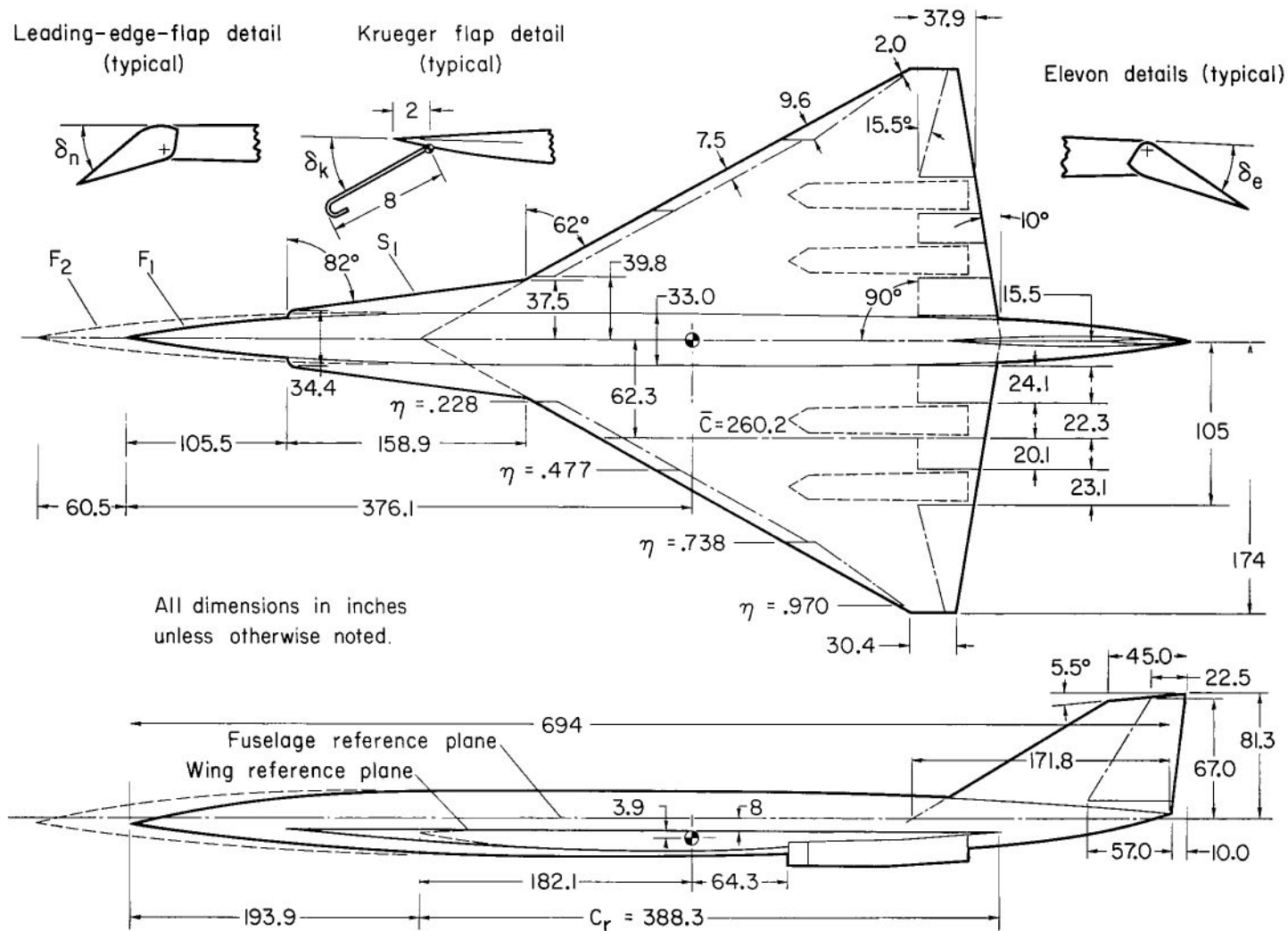
Figure 1.- The model mounted in the Ames 40- by 80-Foot Wind Tunnel.



(b) Ground plane support system.

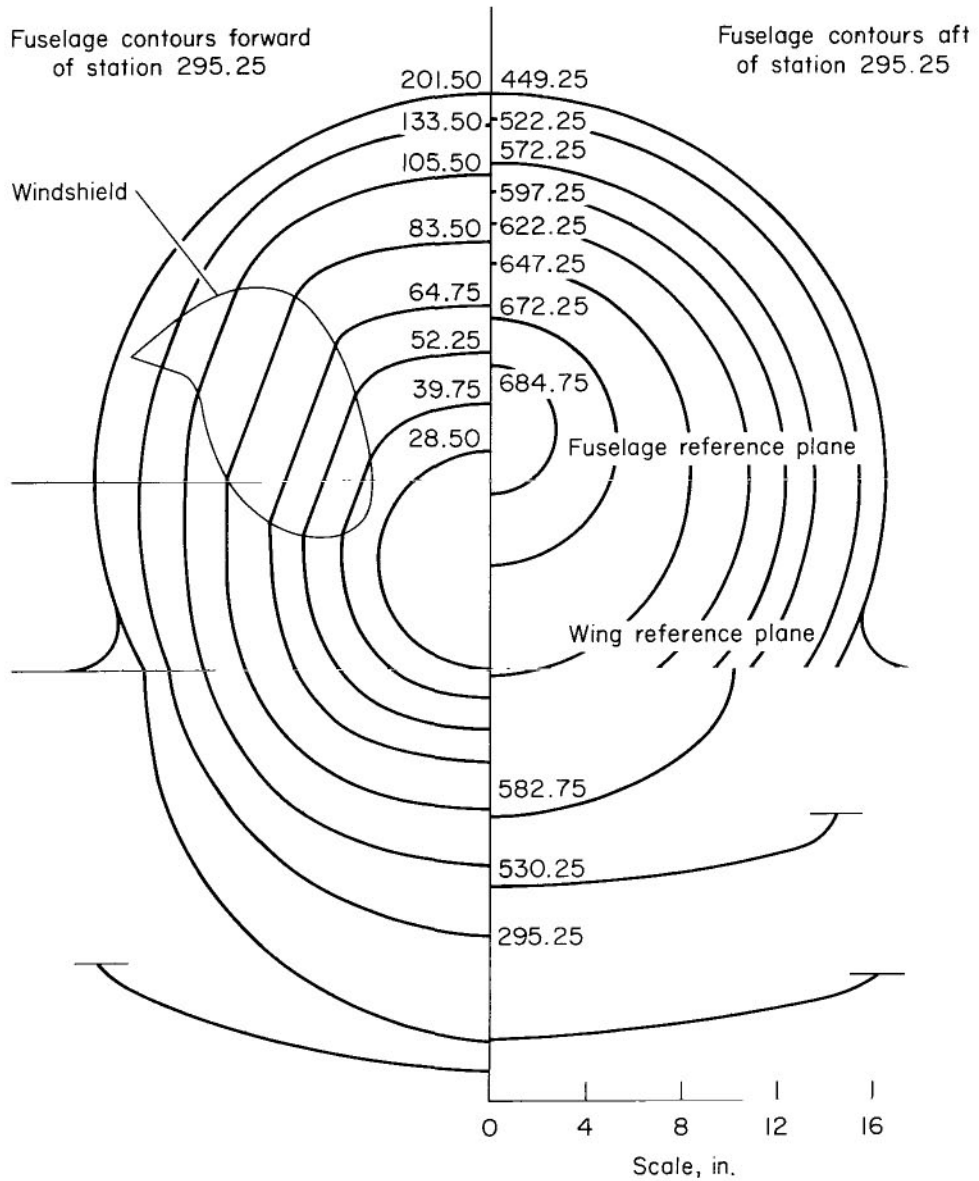
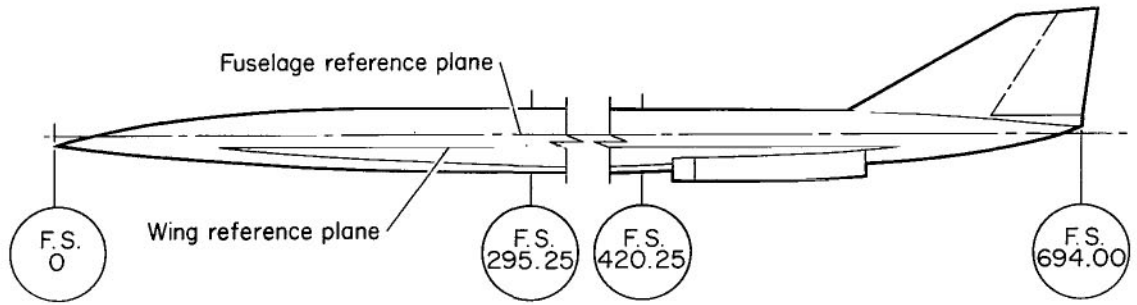
A-36360

Figure 1.- Concluded.



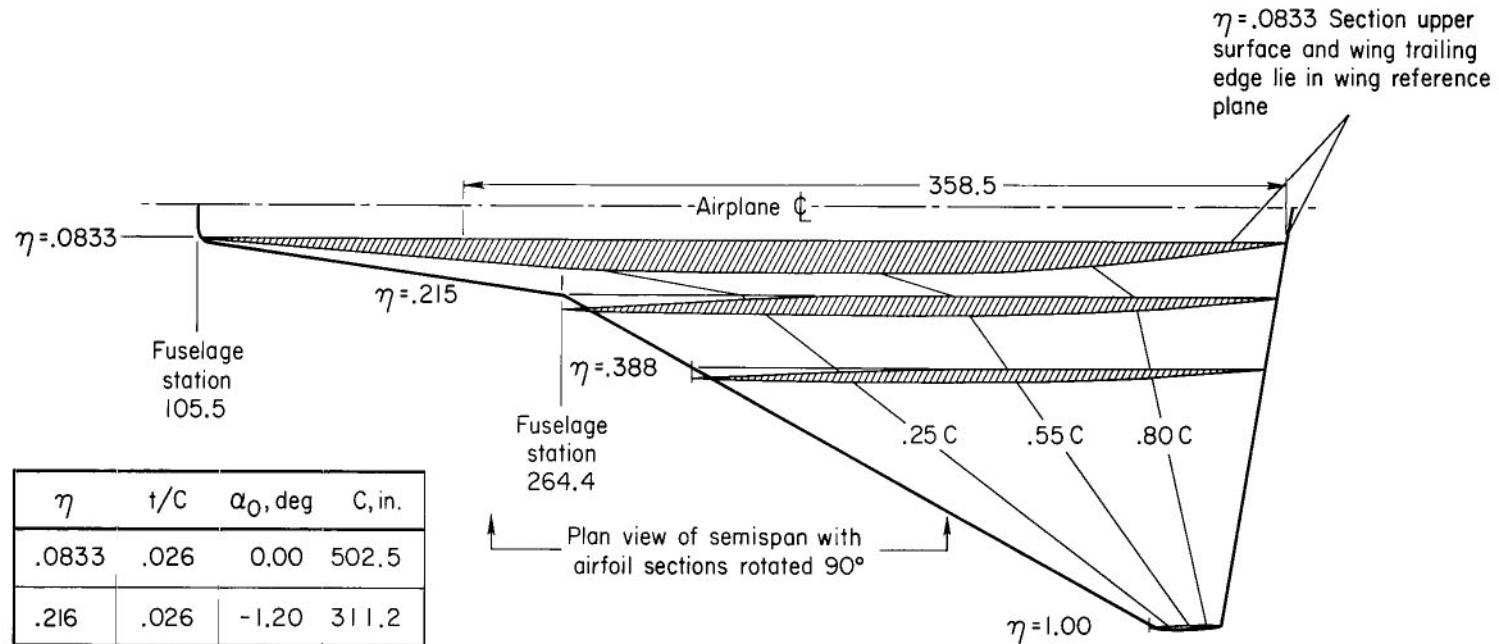
(a) Two views of the model.

Figure 2.- Geometric details of the wing and fuselage.

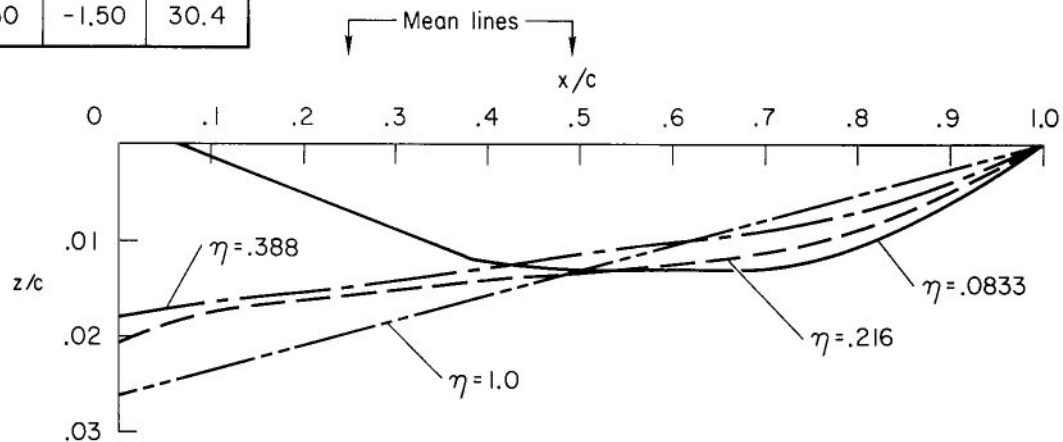


(b) Fuselage contours.

Figure 2.- Continued.

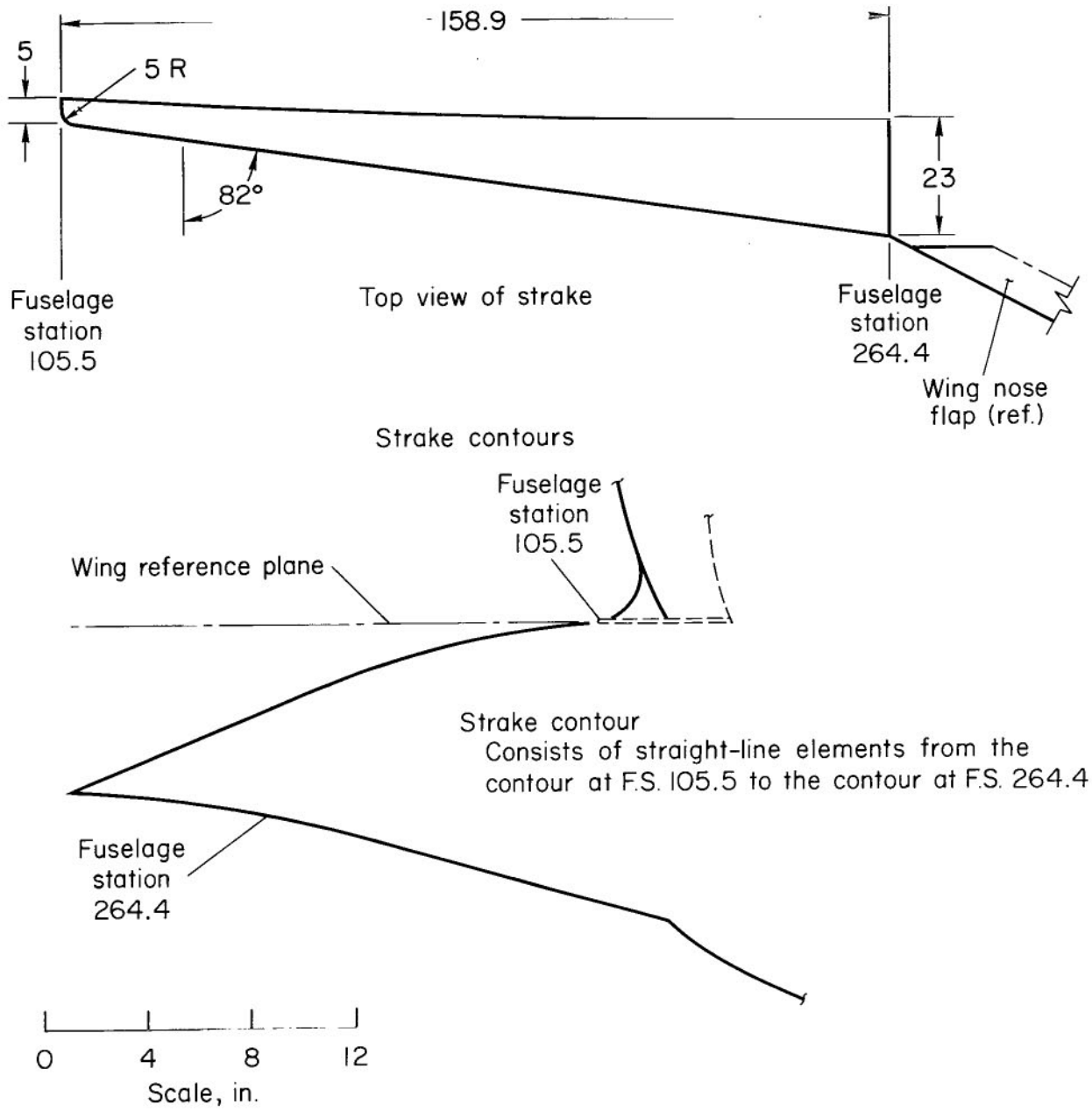


| η | t/c | α_0 , deg | C, in. |
|--------|------|------------------|--------|
| .0833 | .026 | 0.00 | 502.5 |
| .216 | .026 | -1.20 | 311.2 |
| .388 | .020 | -1.00 | 249.5 |
| 1.00 | .030 | -1.50 | 30.4 |



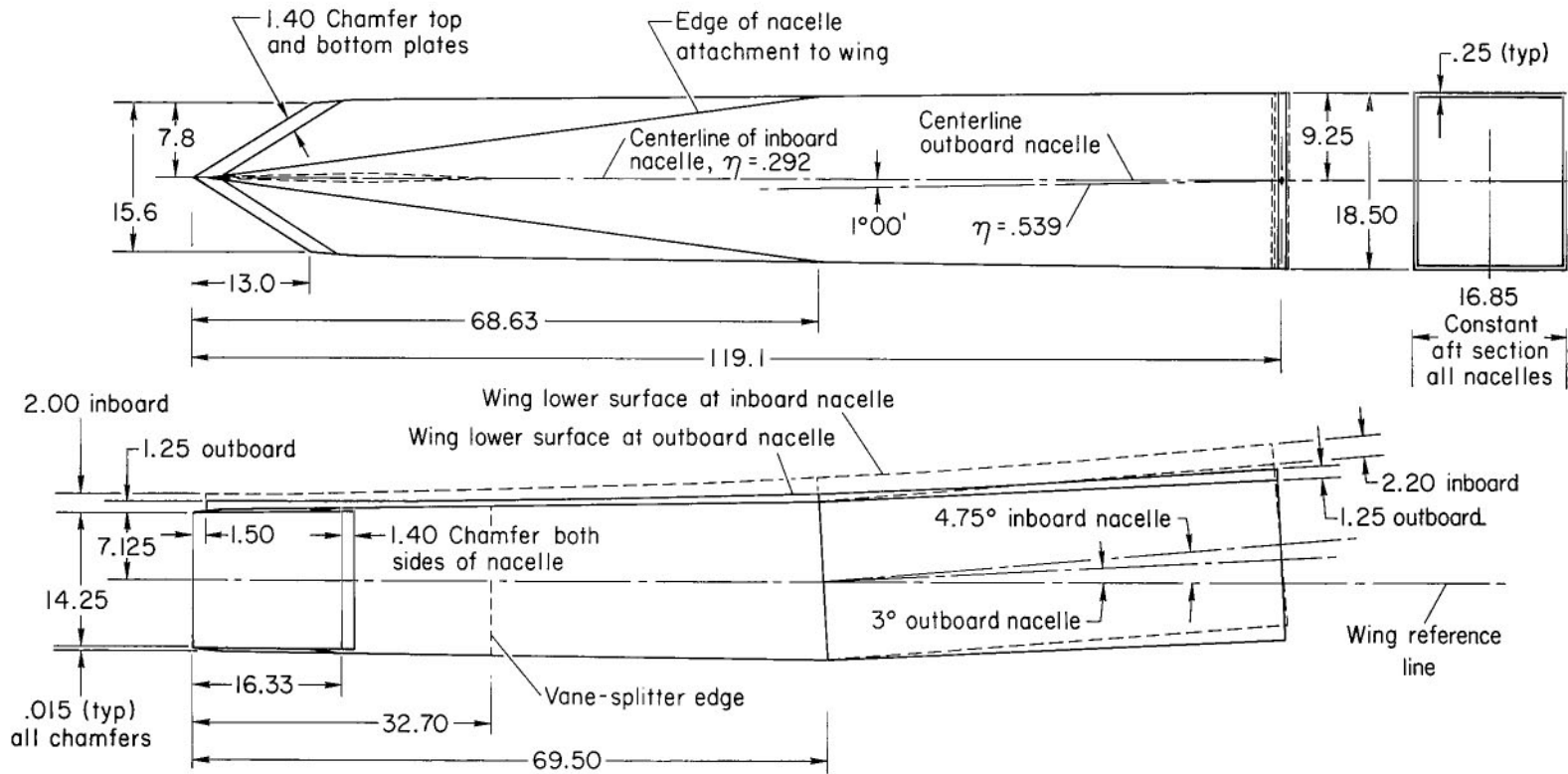
(c) Wing section details.

Figure 2.- Concluded.



(a) Strake details.

Figure 3.- Strake and engine nacelle details.



(b) Engine nacelle details.

Figure 3.- Concluded.

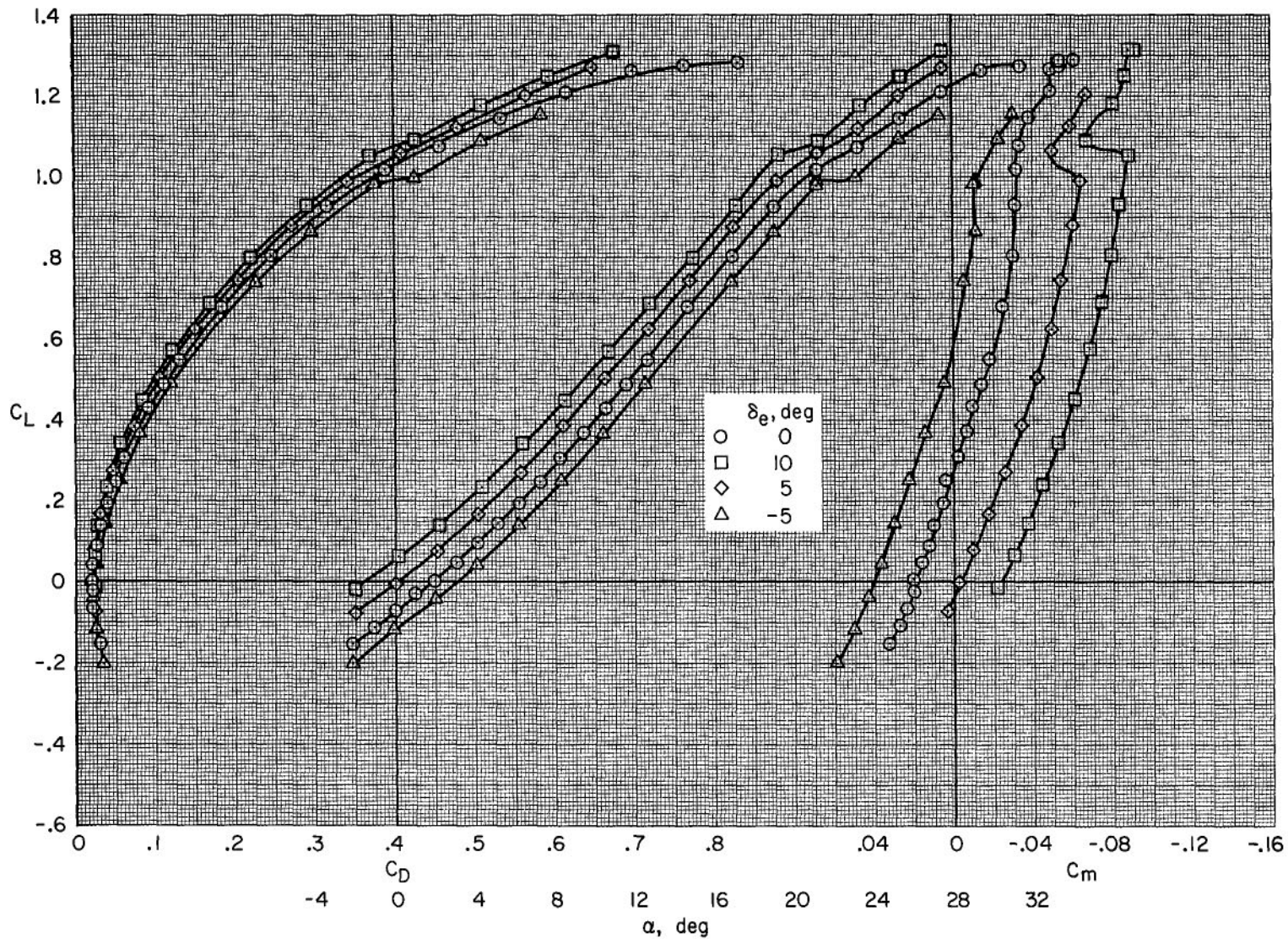
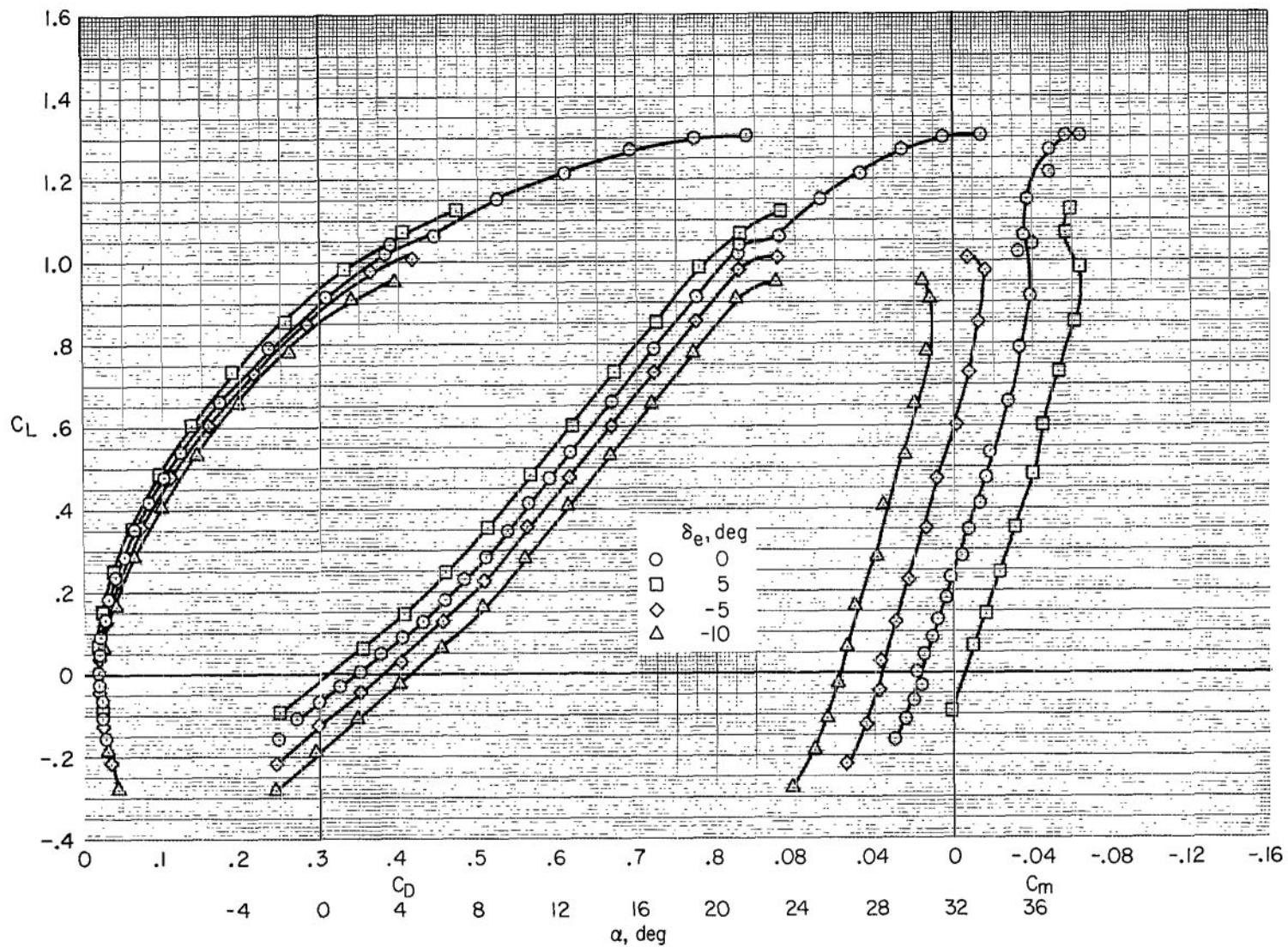
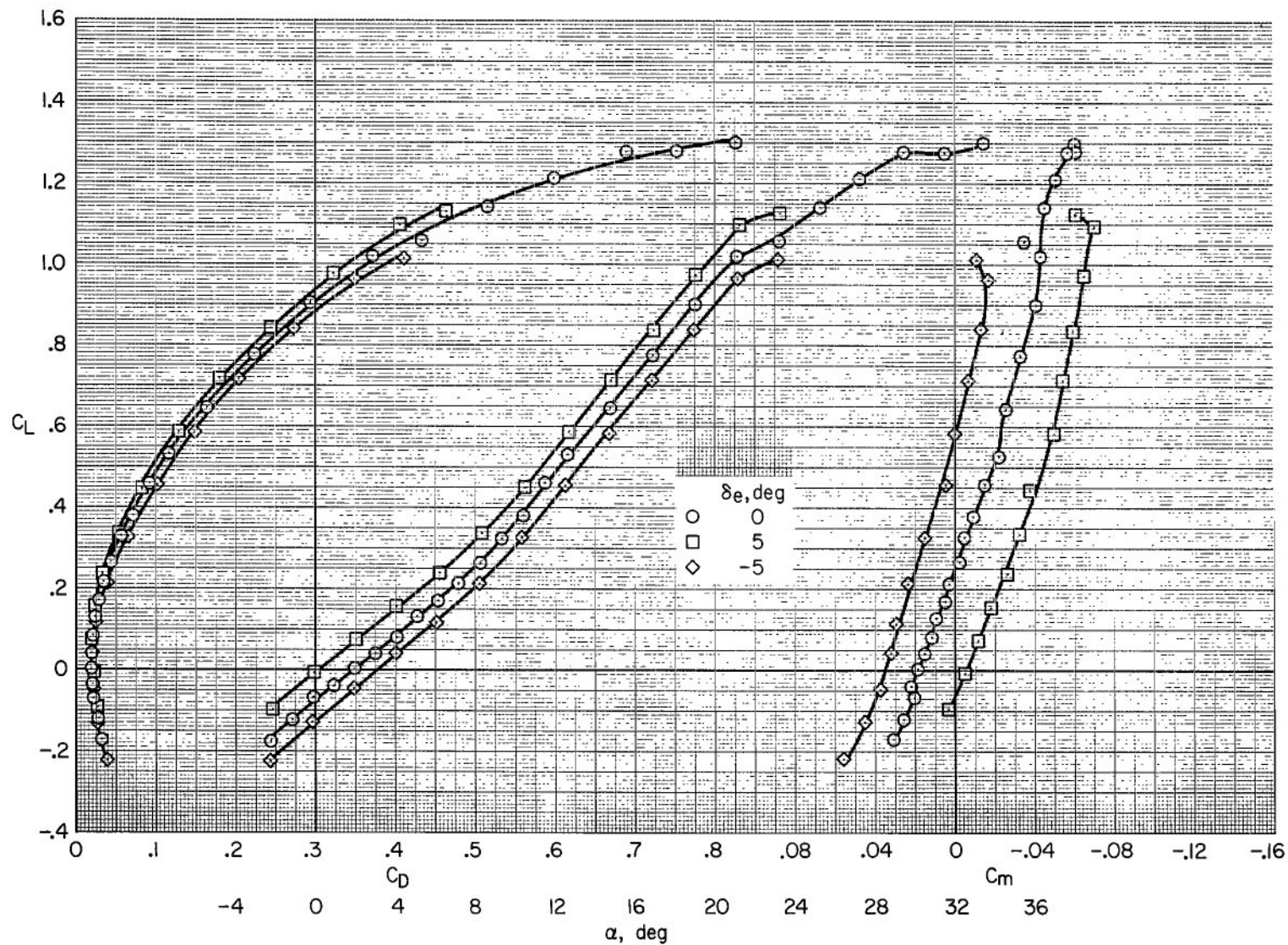
(a) $\delta_n = 0^\circ$

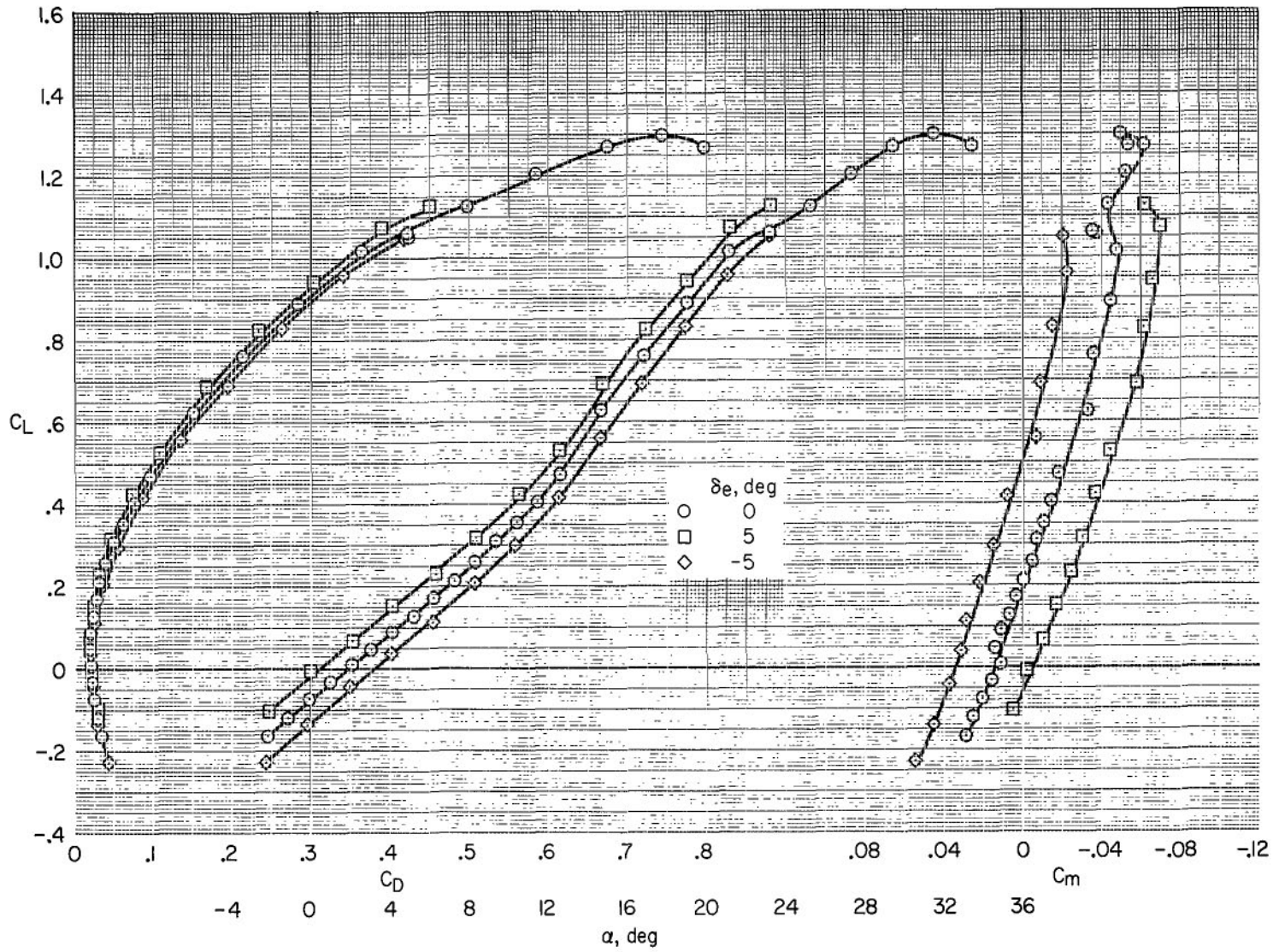
Figure 4.- The effect of variation of elevon deflection on the characteristics of the model with the short fuselage; $h/\bar{c} = \infty$.



(b) $\delta_n = 10^\circ$

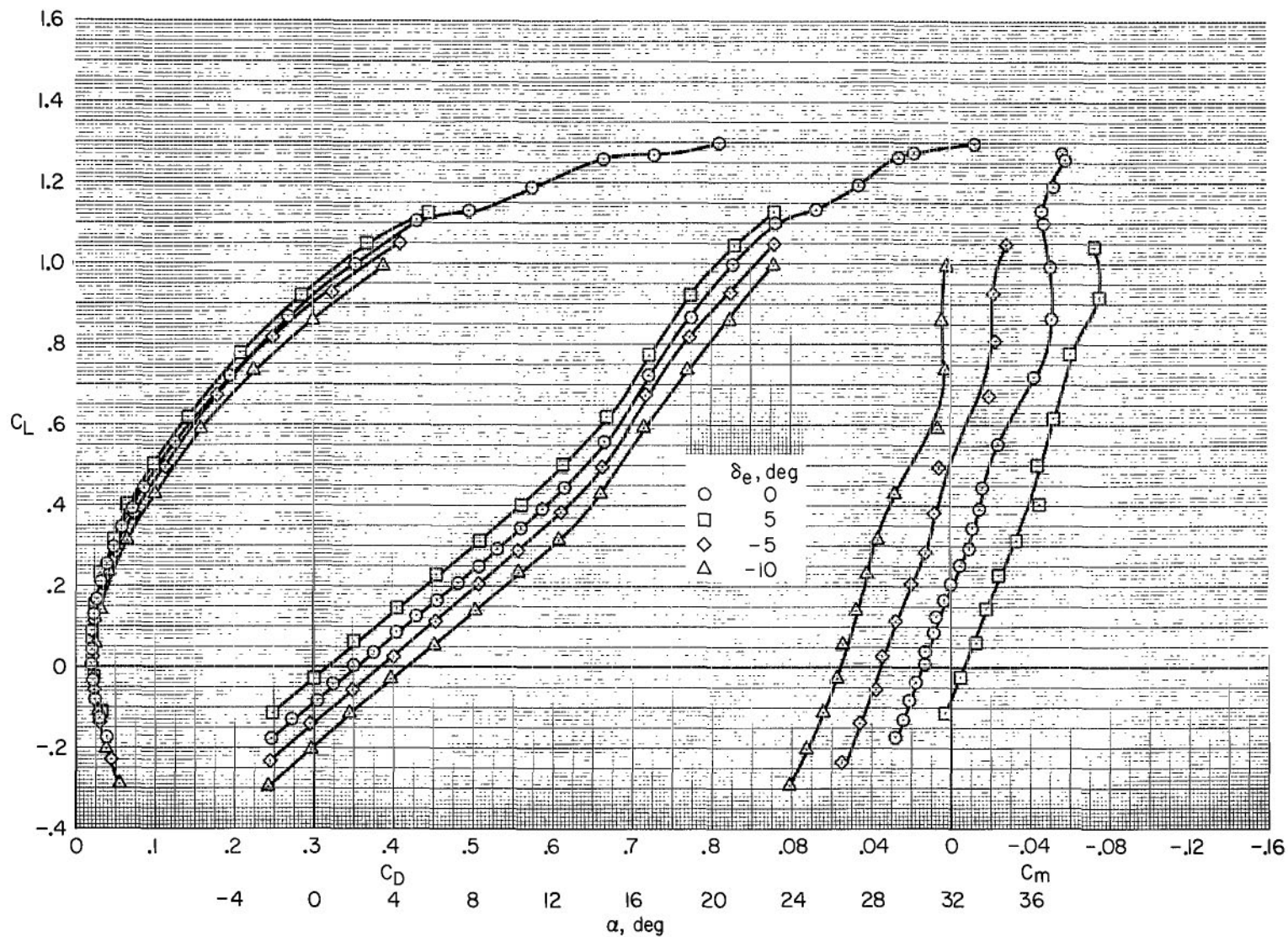
Figure 4.- Continued.

(c) $\delta_n = 20^\circ$



(d) $\delta_n = 30^\circ$

Figure 4.- Continued.



(e) $\delta_n = 40^\circ$

Figure 4.- Concluded.

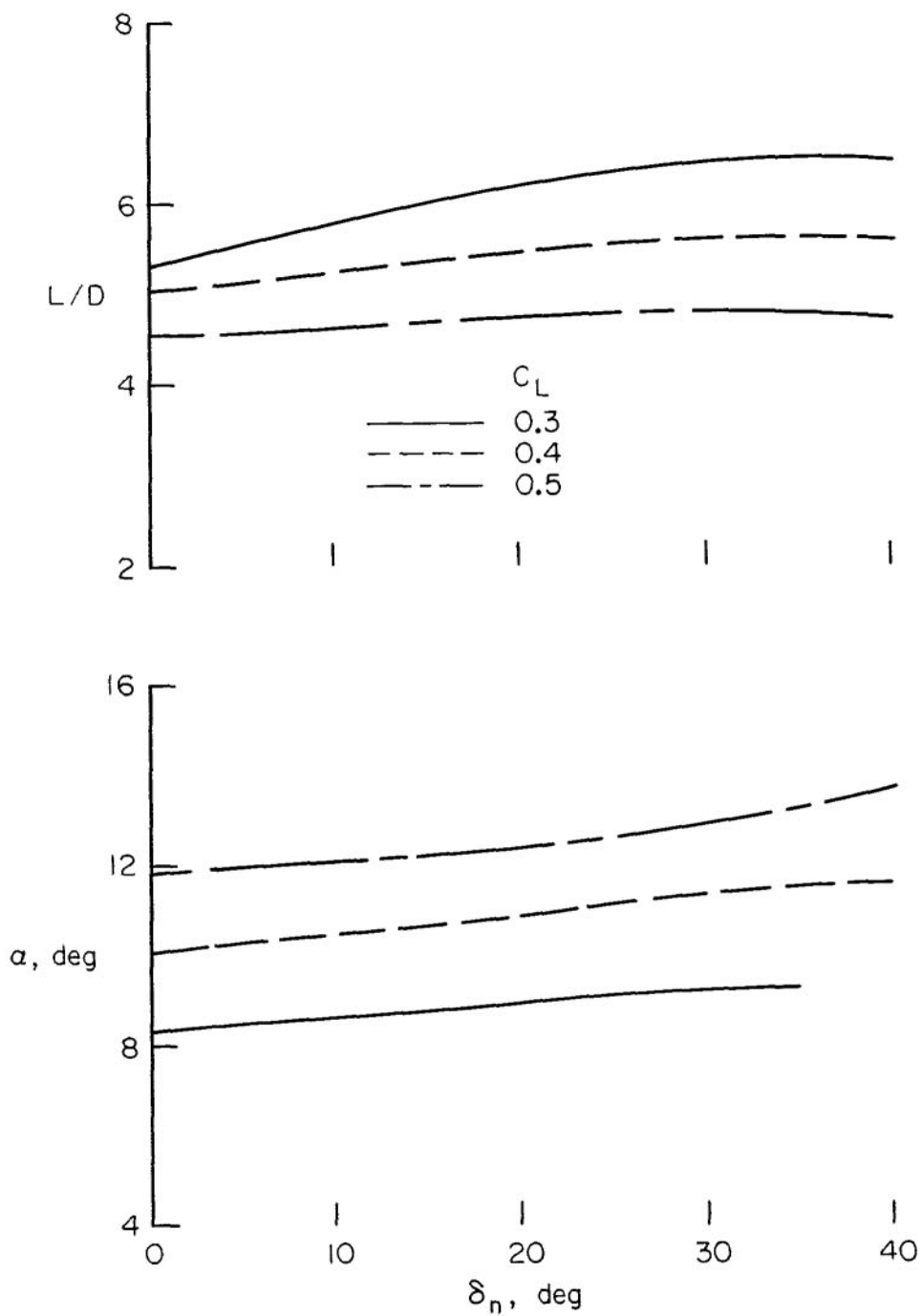


Figure 5.- The effectiveness of the nose flaps on the model with the short fuselage; $\delta_e = 0^\circ$, $h/\bar{c} = \infty$.

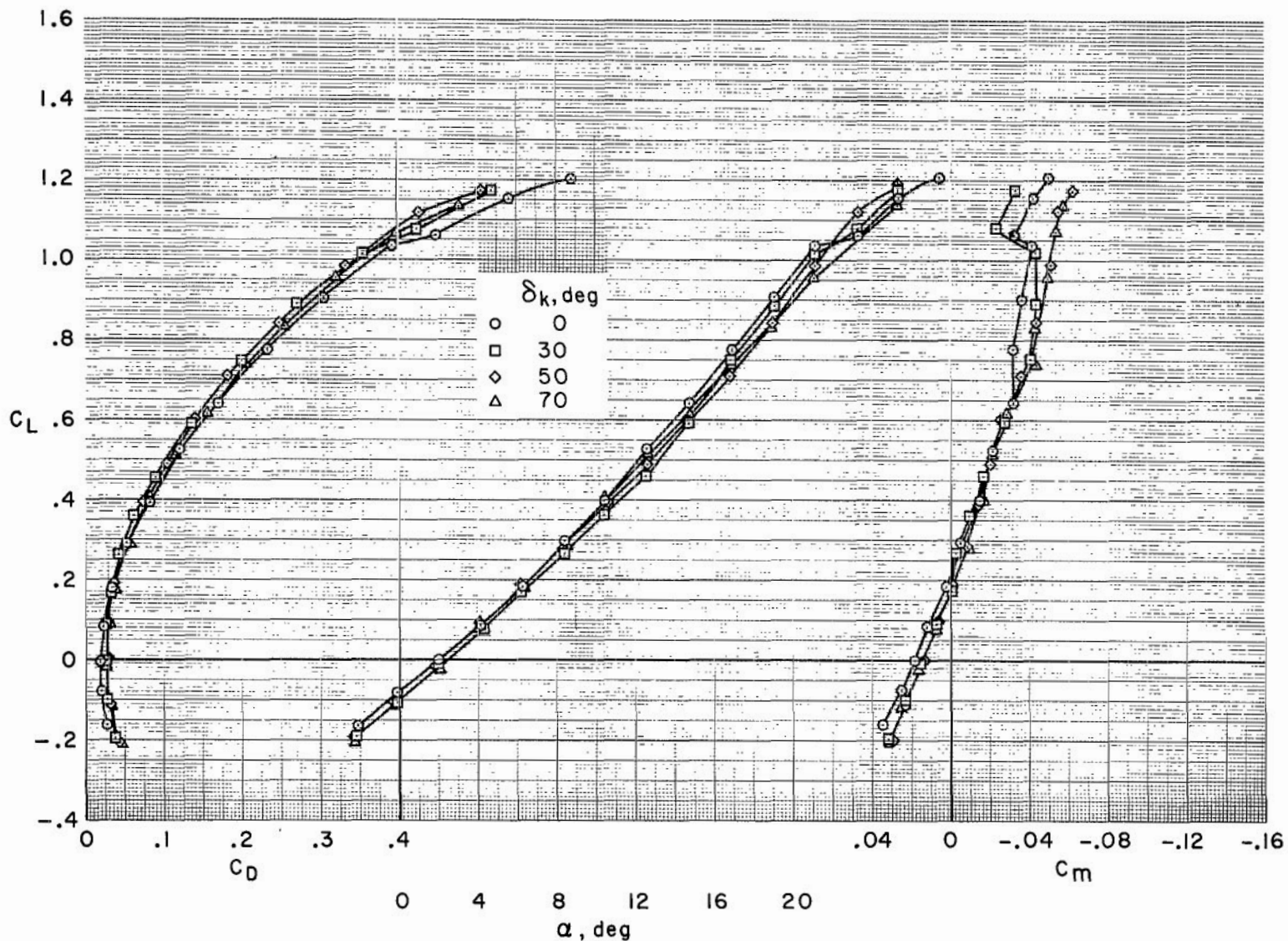


Figure 6.- The effect of variation of Krueger flap deflection on the configuration with the extended fuselage; $\delta_n = 0^\circ$, $\delta_e = 0^\circ$, $h/\bar{c} = \infty$.

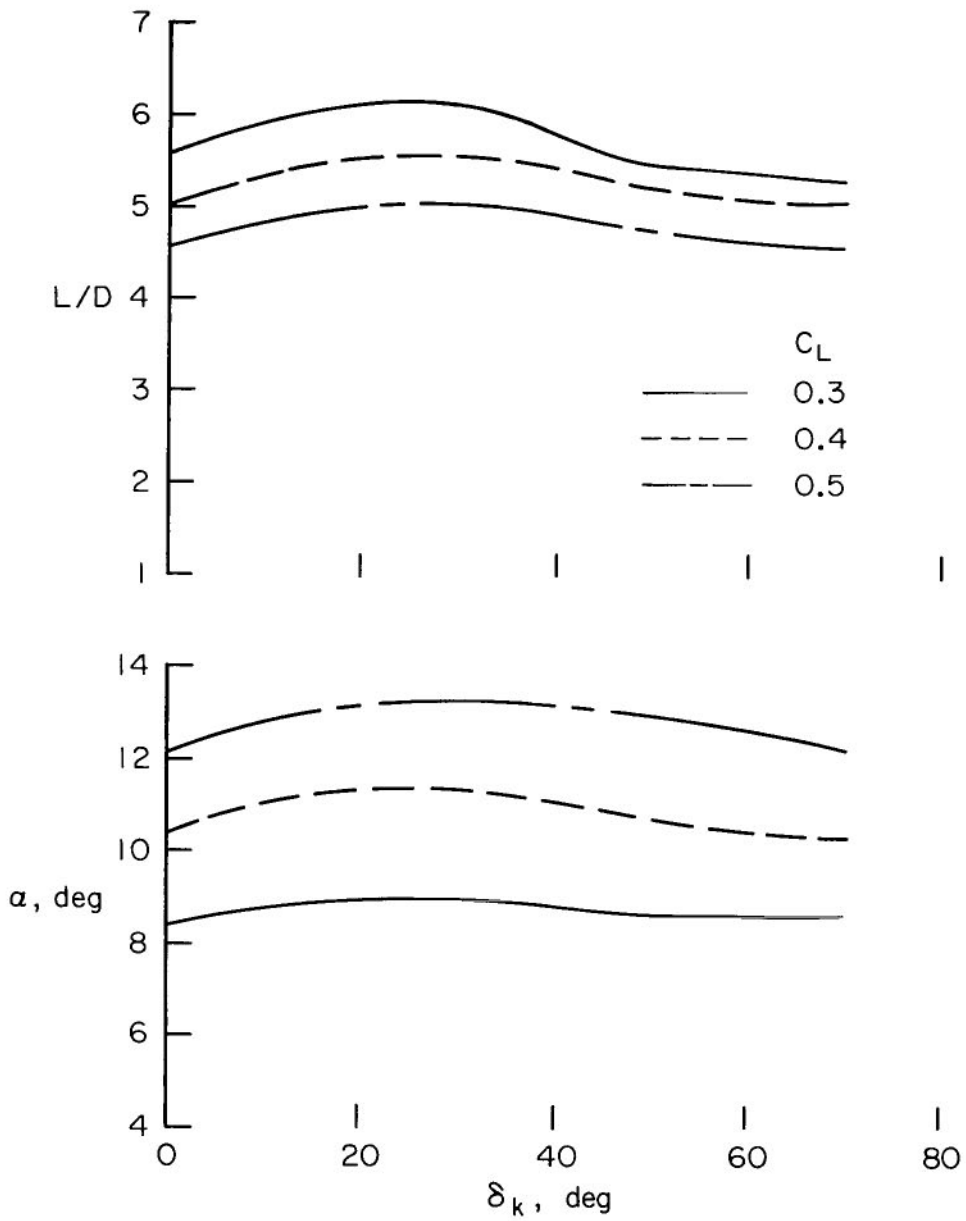
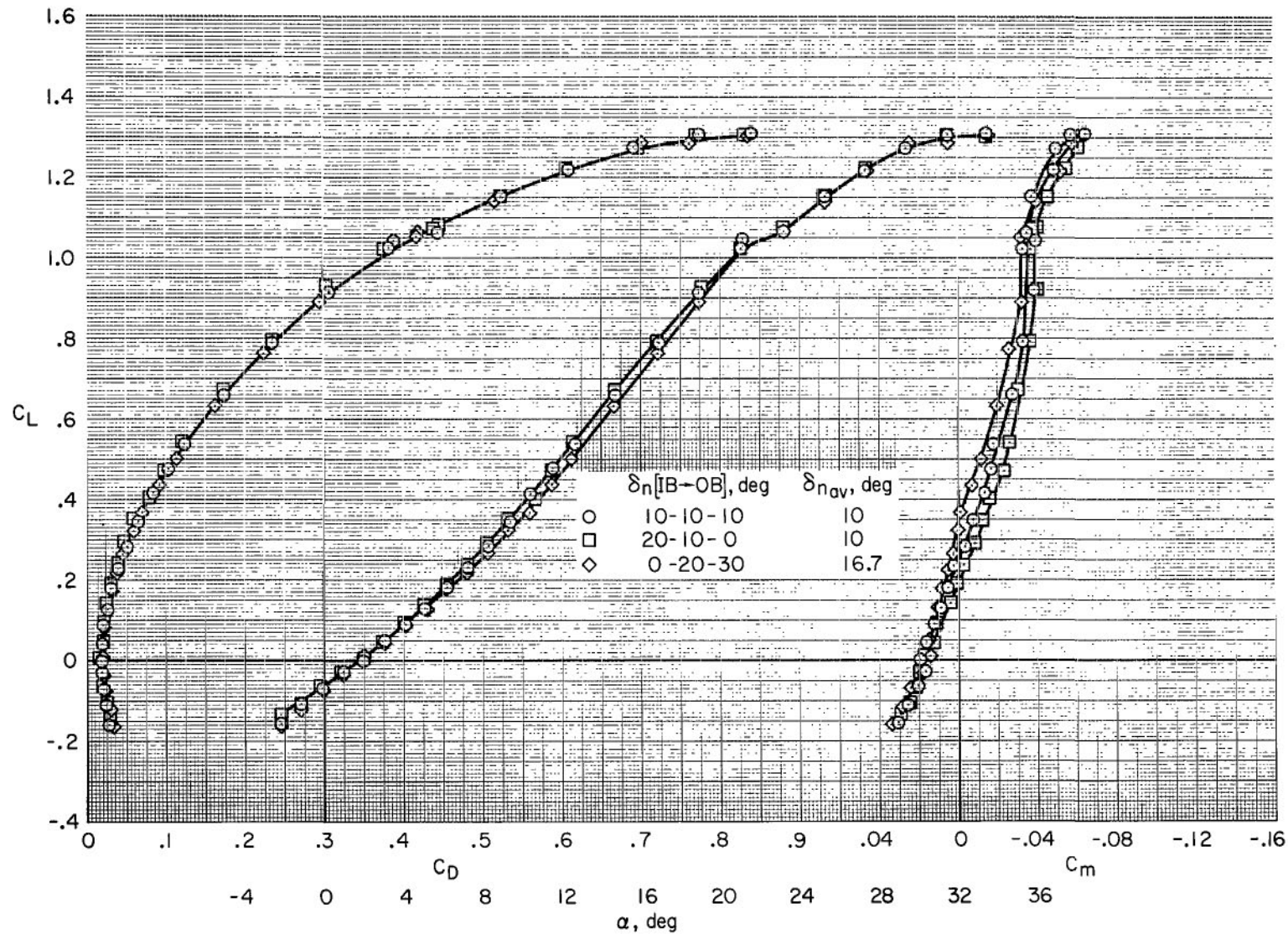
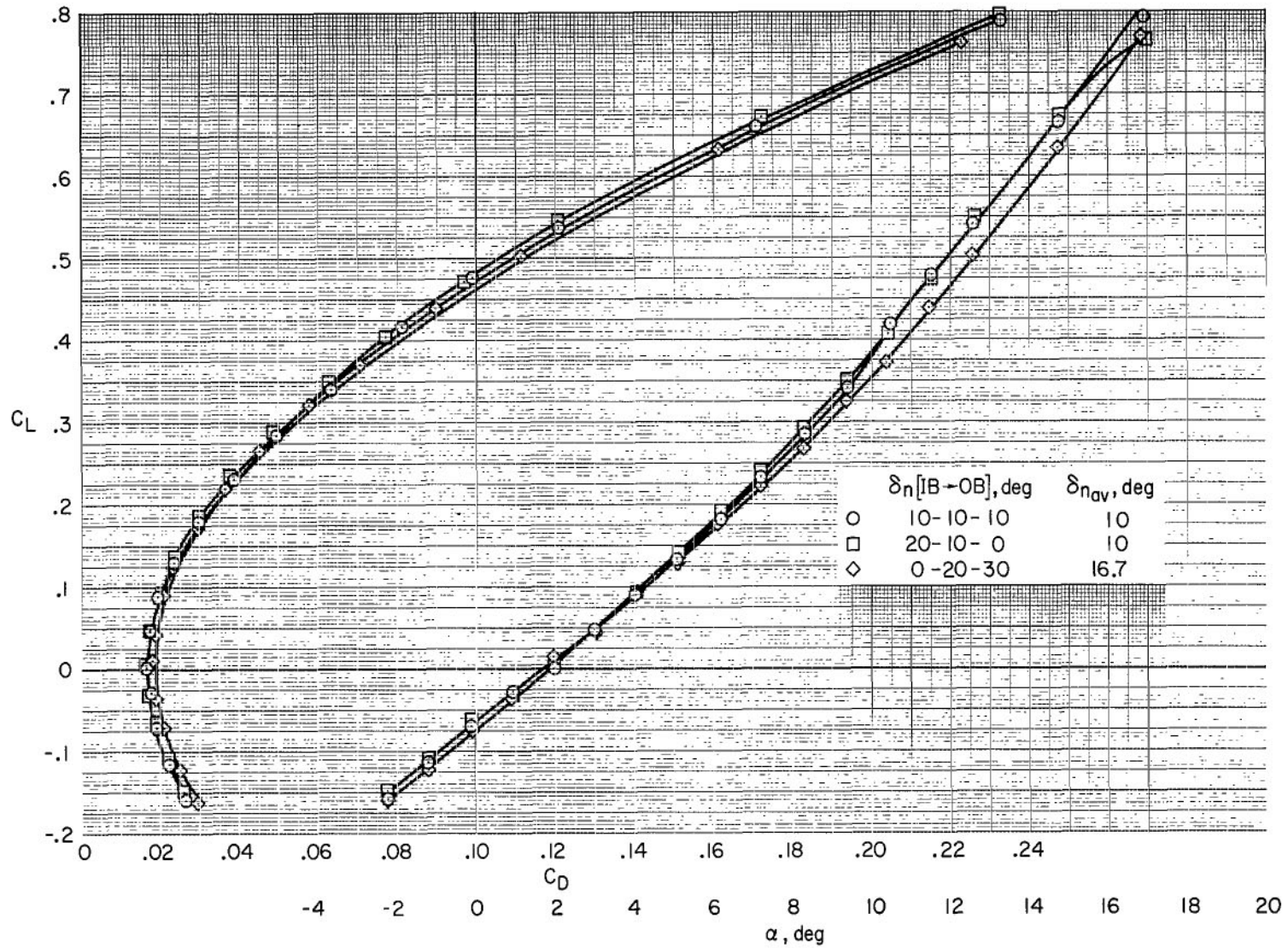


Figure 7.- The effectiveness of the Krueger flaps on the model with the extended fuselage; $\delta_e = 0^\circ$, $\delta_n = 0^\circ$, $h/\bar{c} = \infty$.



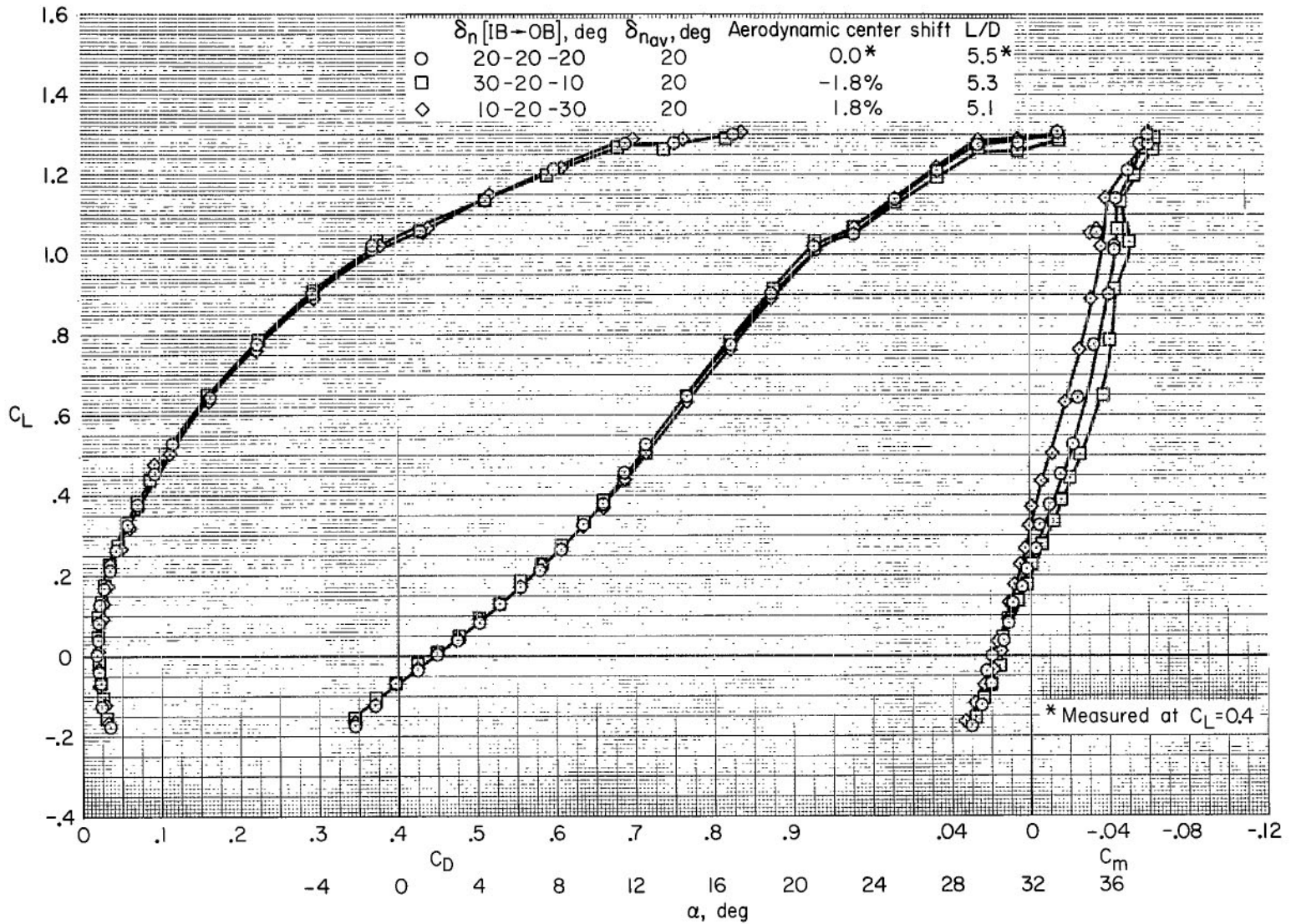
(a) $\delta_{n_{av}} = 10^\circ, 16.7^\circ$; C_L vs. C_D , α , C_m .

Figure 8.- The effect of spanwise variation of nose flap deflection on the characteristics of the model with the short fuselage; $\delta_e = 0$, $h/\bar{c} = \infty$.



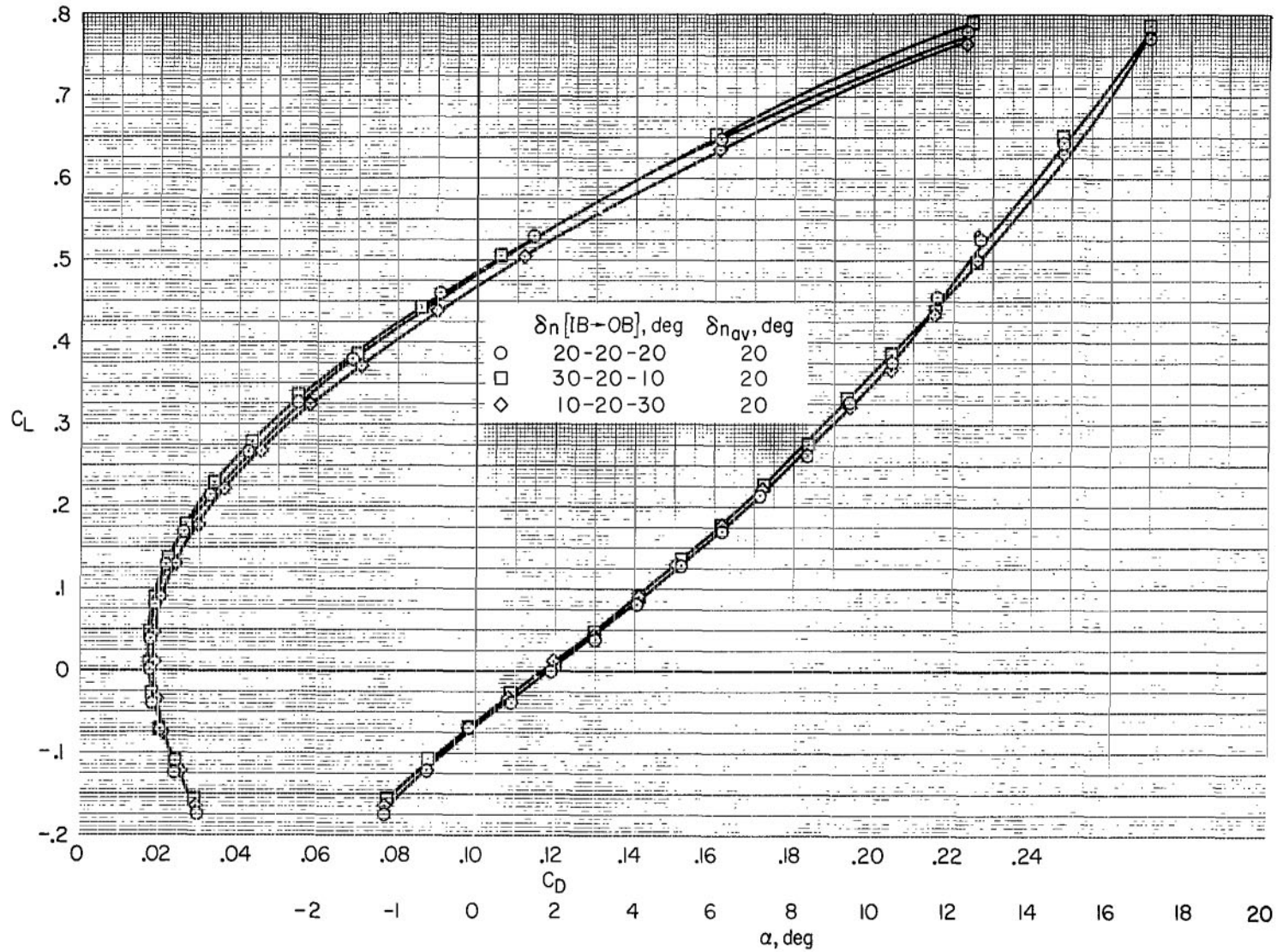
(b) $\delta_{n_{av}} = 10^\circ, 16.7^\circ$; large scale, C_L vs. C_D , α

Figure 8.- Continued.



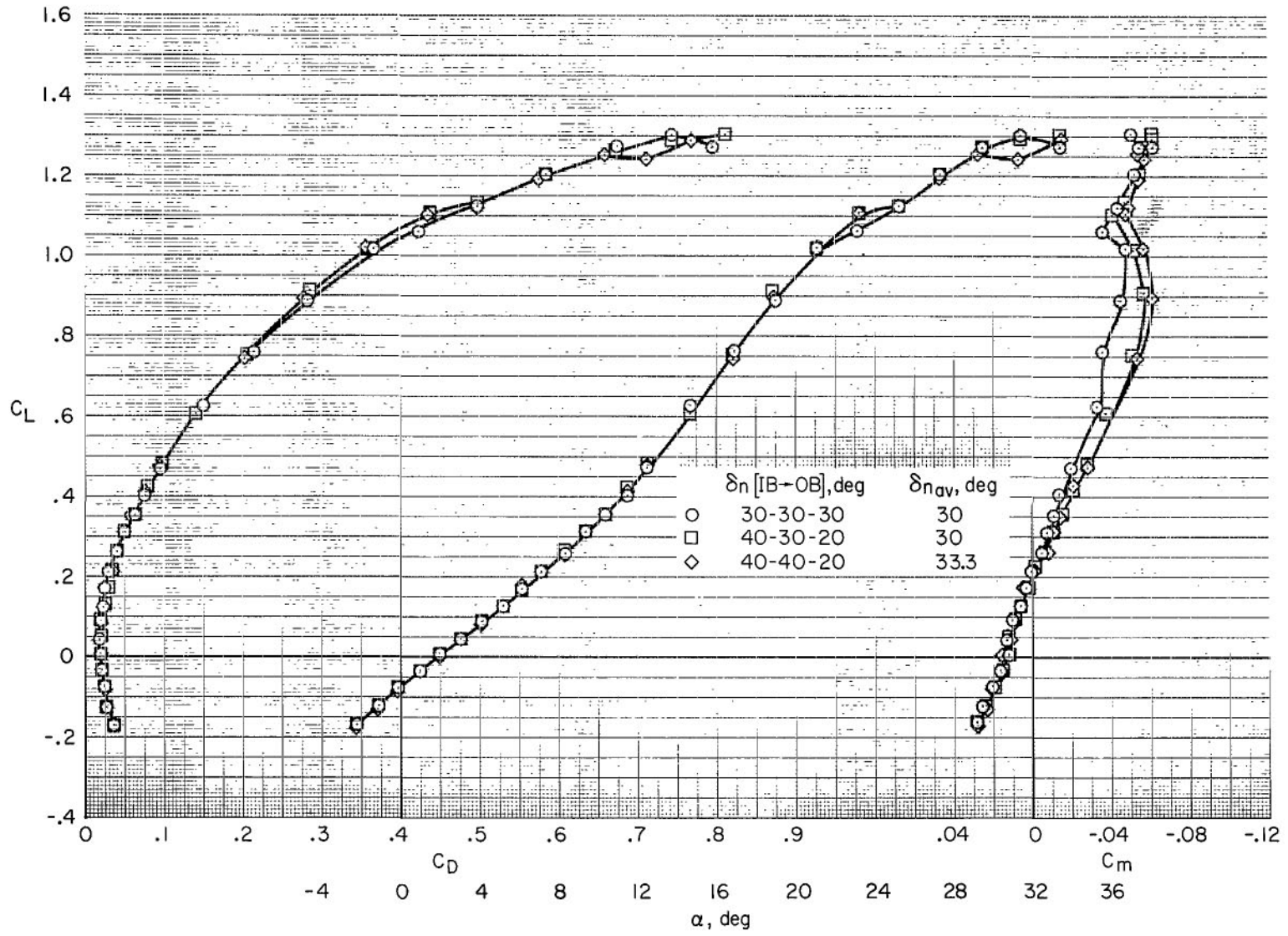
(c) $\delta_{n_{av}} = 20^\circ$; C_L vs. C_D , α , C_m

Figure 8.- Continued.



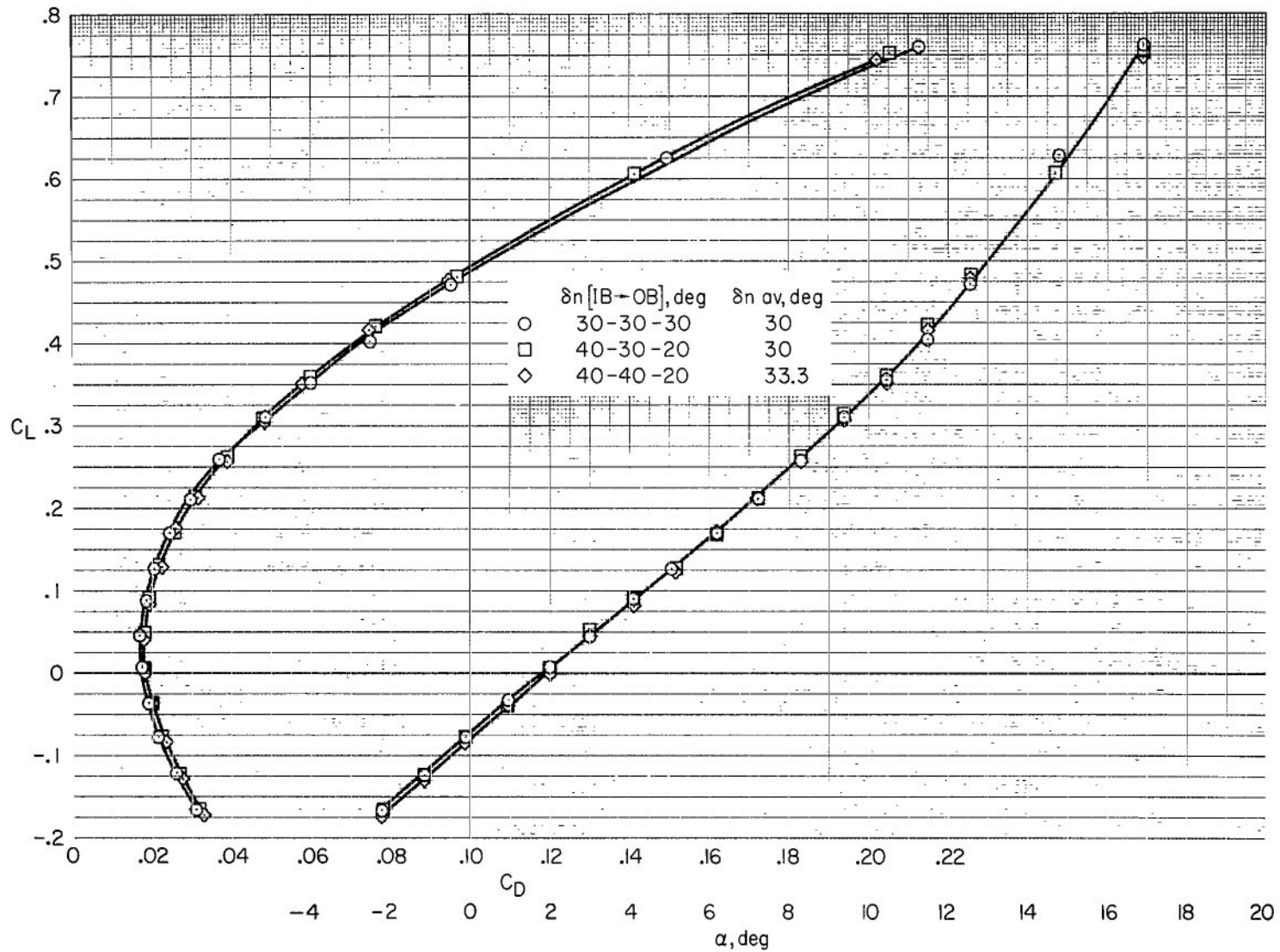
(d) $\delta_{n_{av}} = 20^\circ$; large-scale, C_L vs. C_D , α

Figure 8.- Continued.



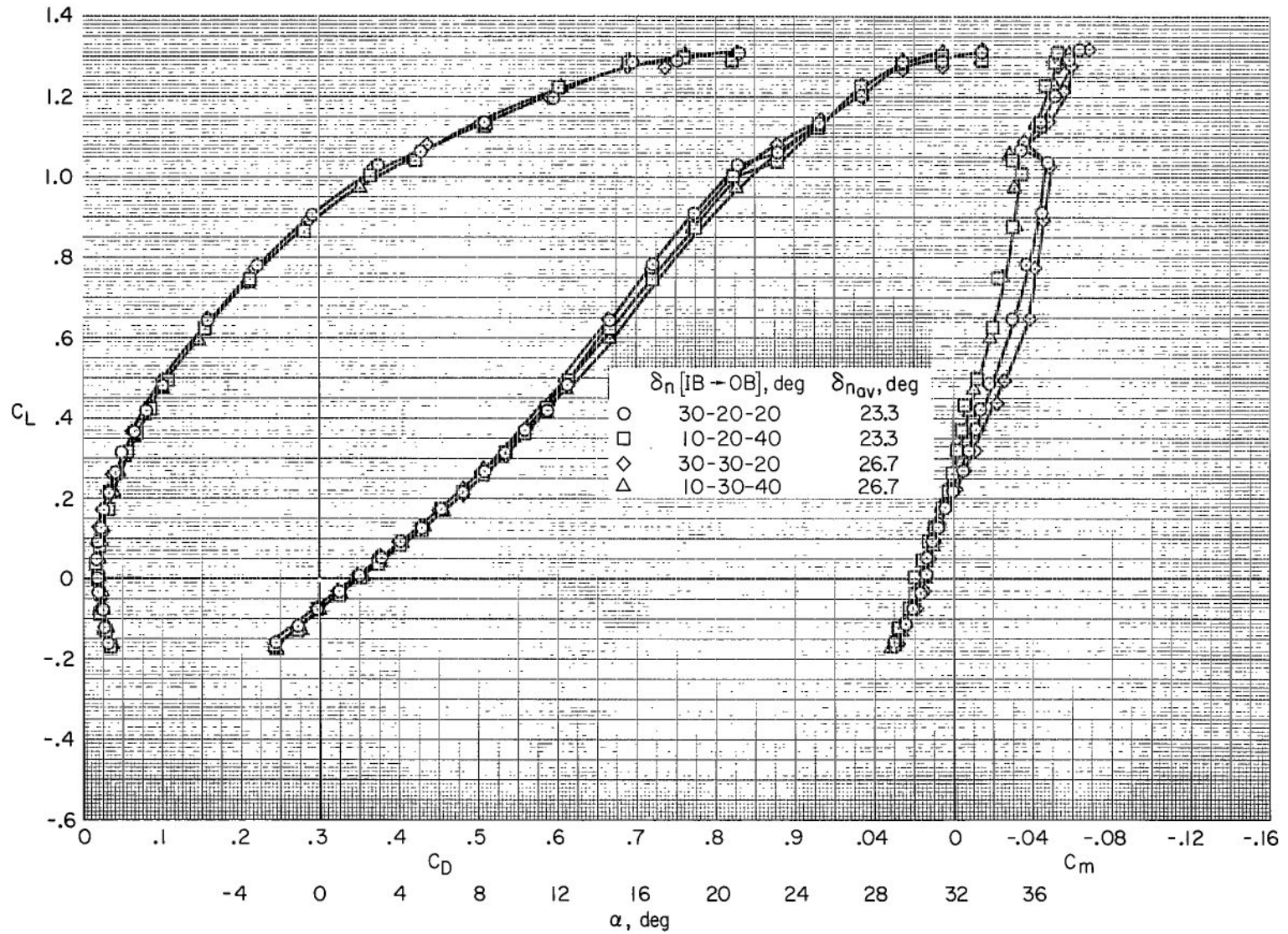
(e) $\delta_{n_{av}} = 30^\circ, 33.3^\circ$; C_L vs. C_D , α , C_m

Figure 8.- Continued.



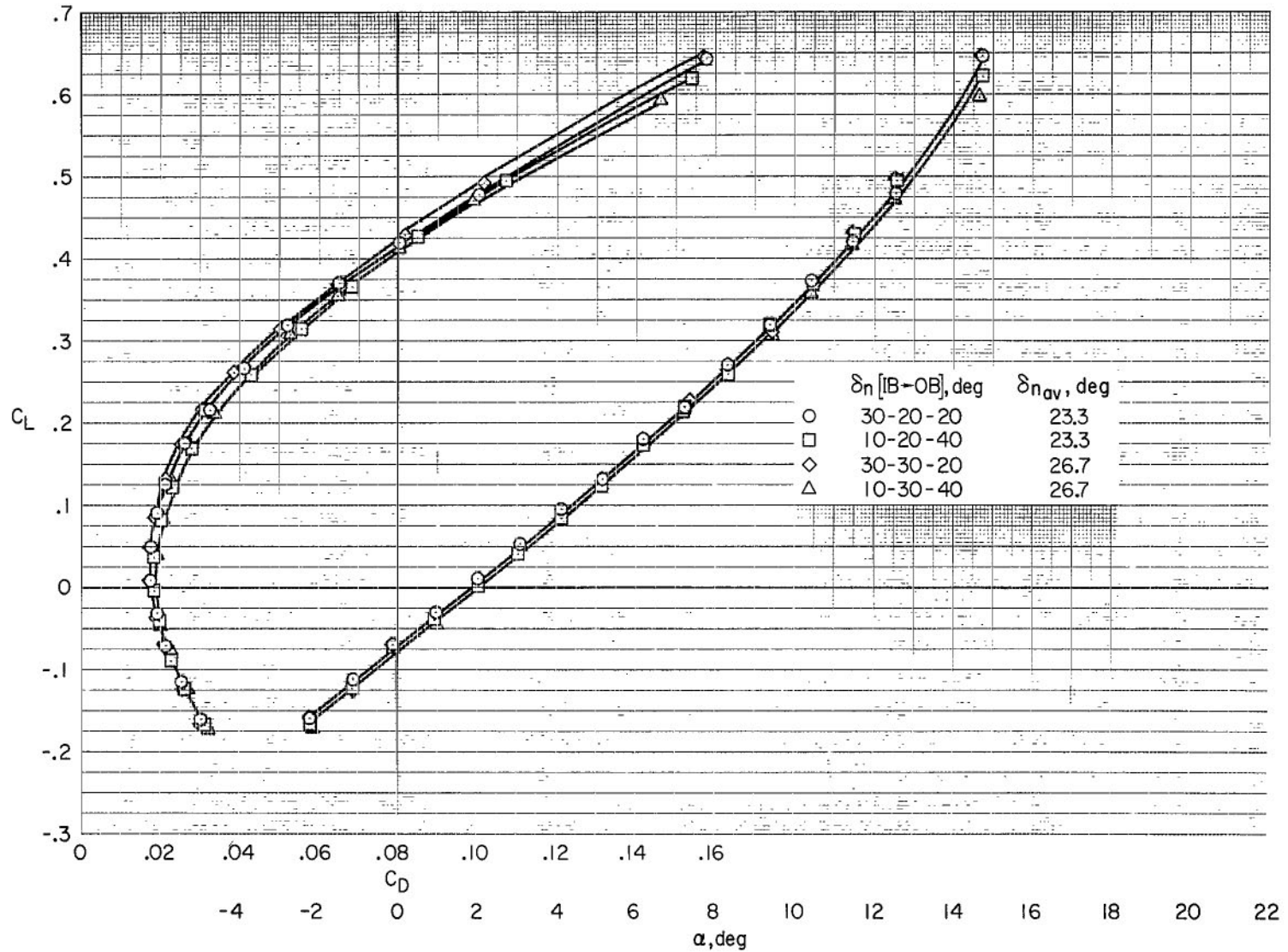
(f) $\delta n_{av} = 30^\circ, 33.3^\circ$; large-scale, C_L vs. C_D, α

Figure 8.- Continued.



(g) $\delta_{n_{av}} = 23.3^\circ, 26.7^\circ$; C_L vs. C_D , α , C_m

Figure 8.- Continued.



(h) $\delta_{n_{av}} = 23.3^\circ, 26.7^\circ$; large-scale, C_L vs. C_D, α

Figure 8.- Concluded.

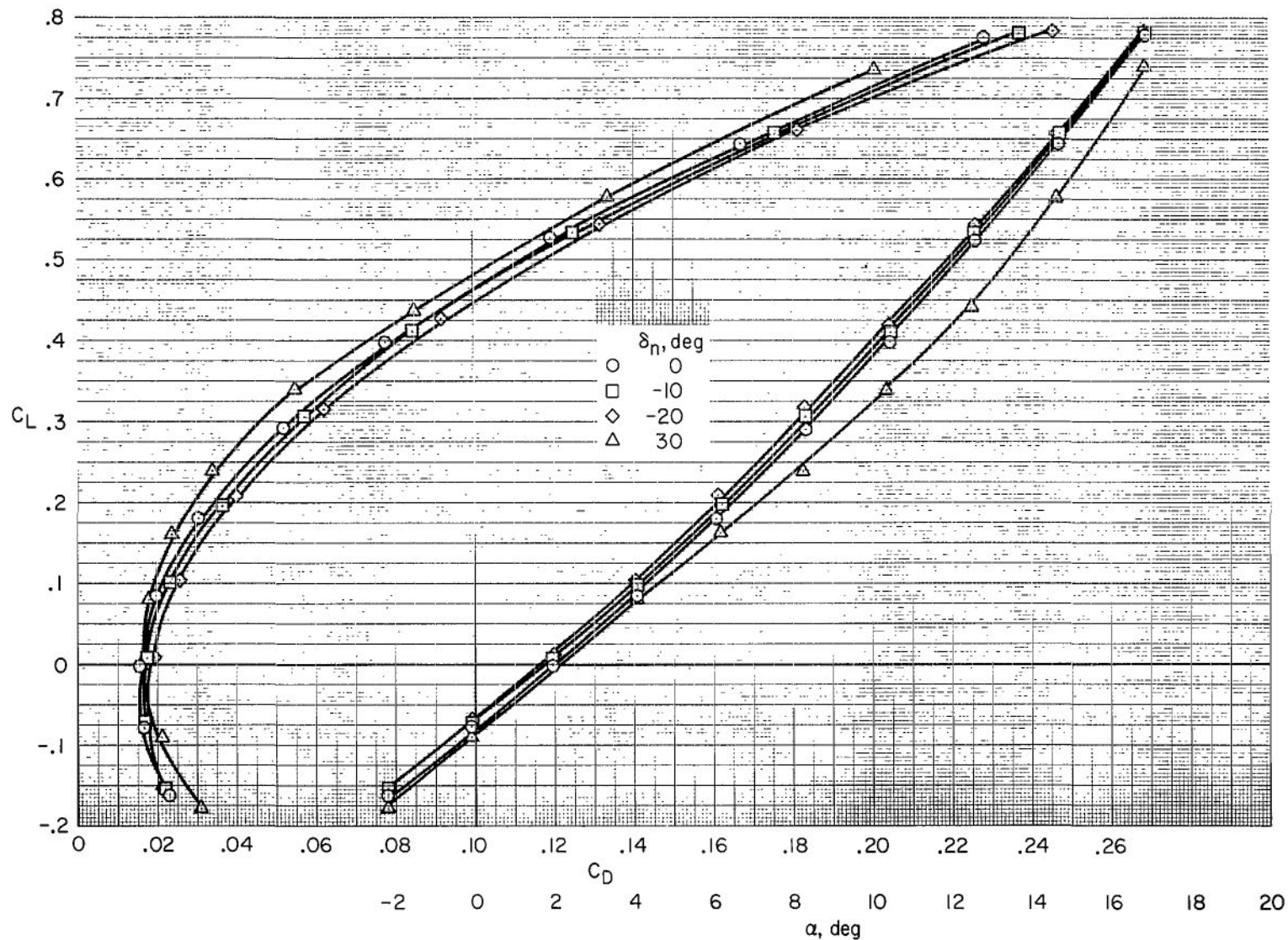
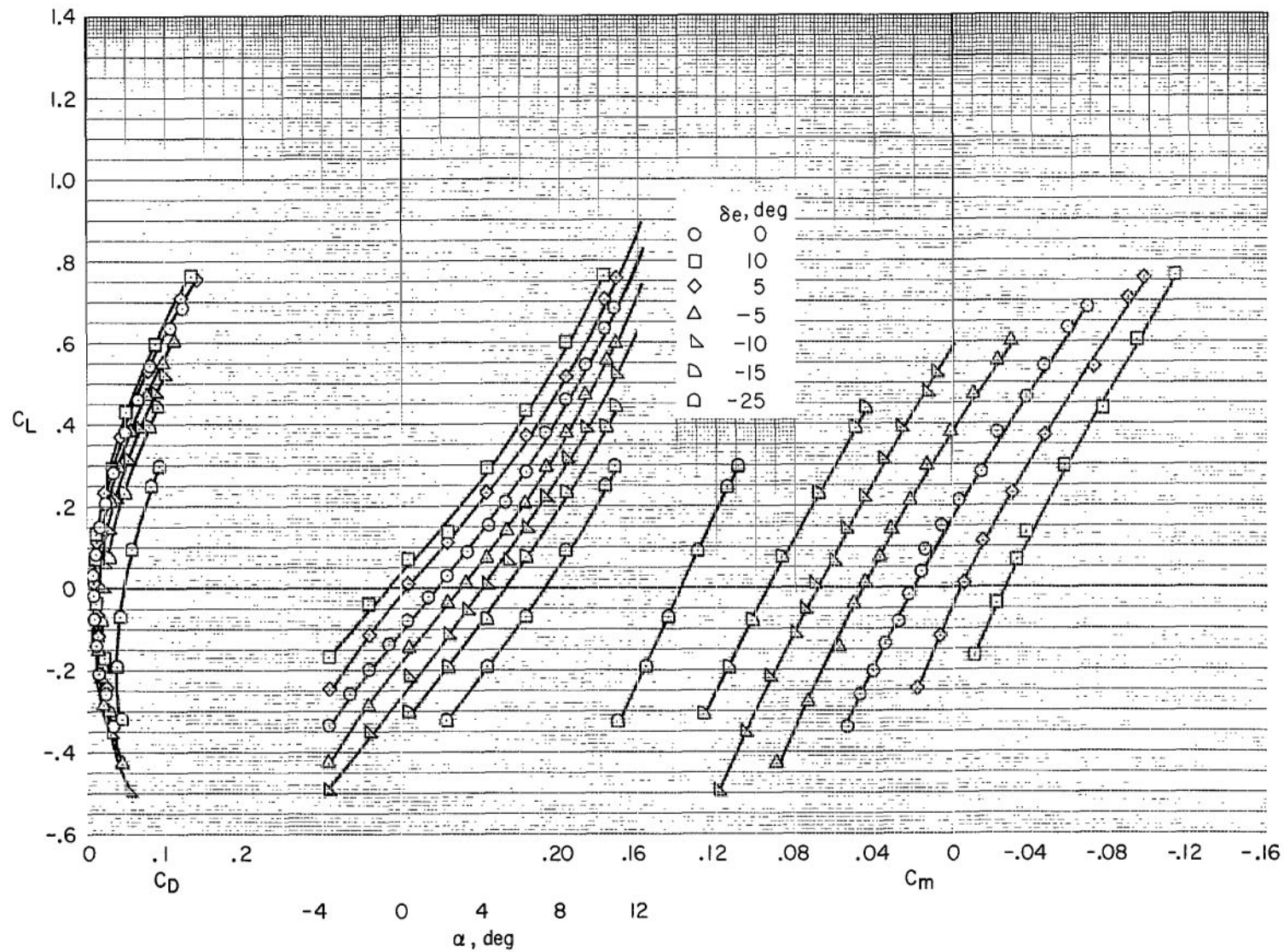


Figure 9.- The effect of deflecting the nose flaps to negative deflection on the characteristics of the model with the extended fuselage; $\delta_e = 0^\circ$, $h/\bar{c} = \infty$.



(a) $h/\bar{c} = 0.19$

Figure 10.- The effect of elevon deflection on the characteristics of the model with the extended fuselage and the nacelles removed in the presence of the ground; $\delta_n = 0$.

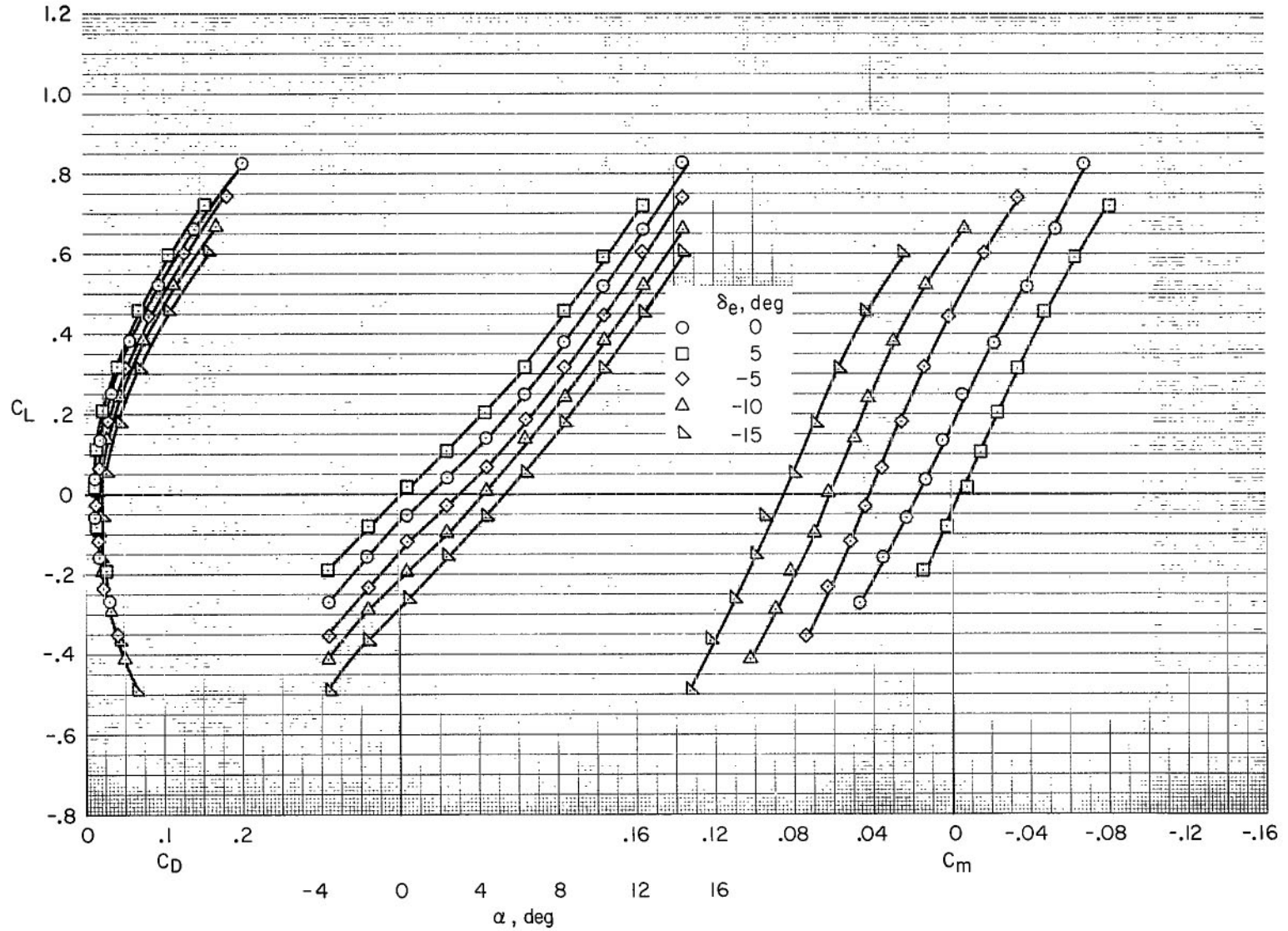
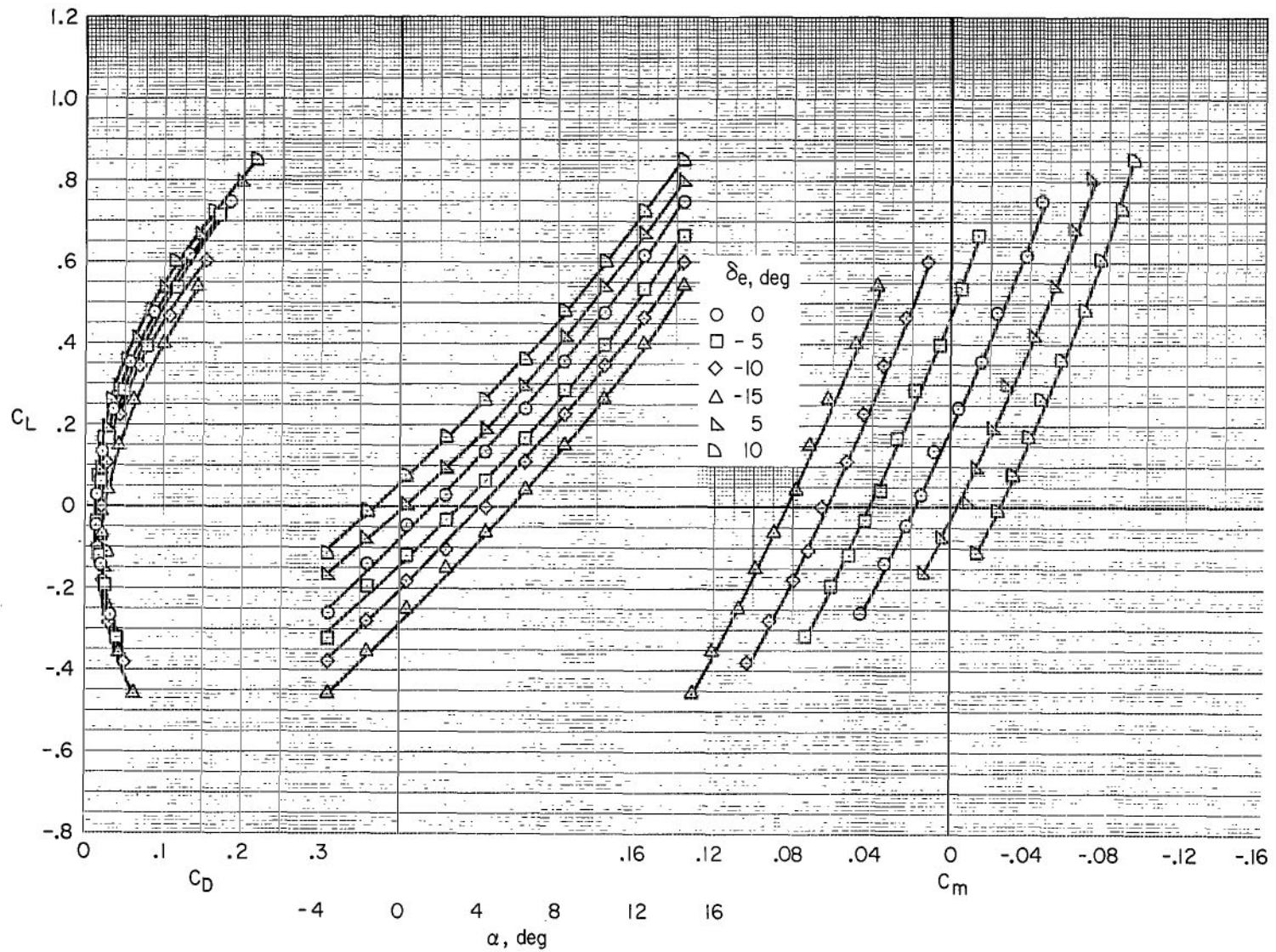
(b) $h/\bar{c} = 0.31$

Figure 10.- Continued.



(c) $h/\bar{c} = 0.42$

Figure 10.- Concluded.

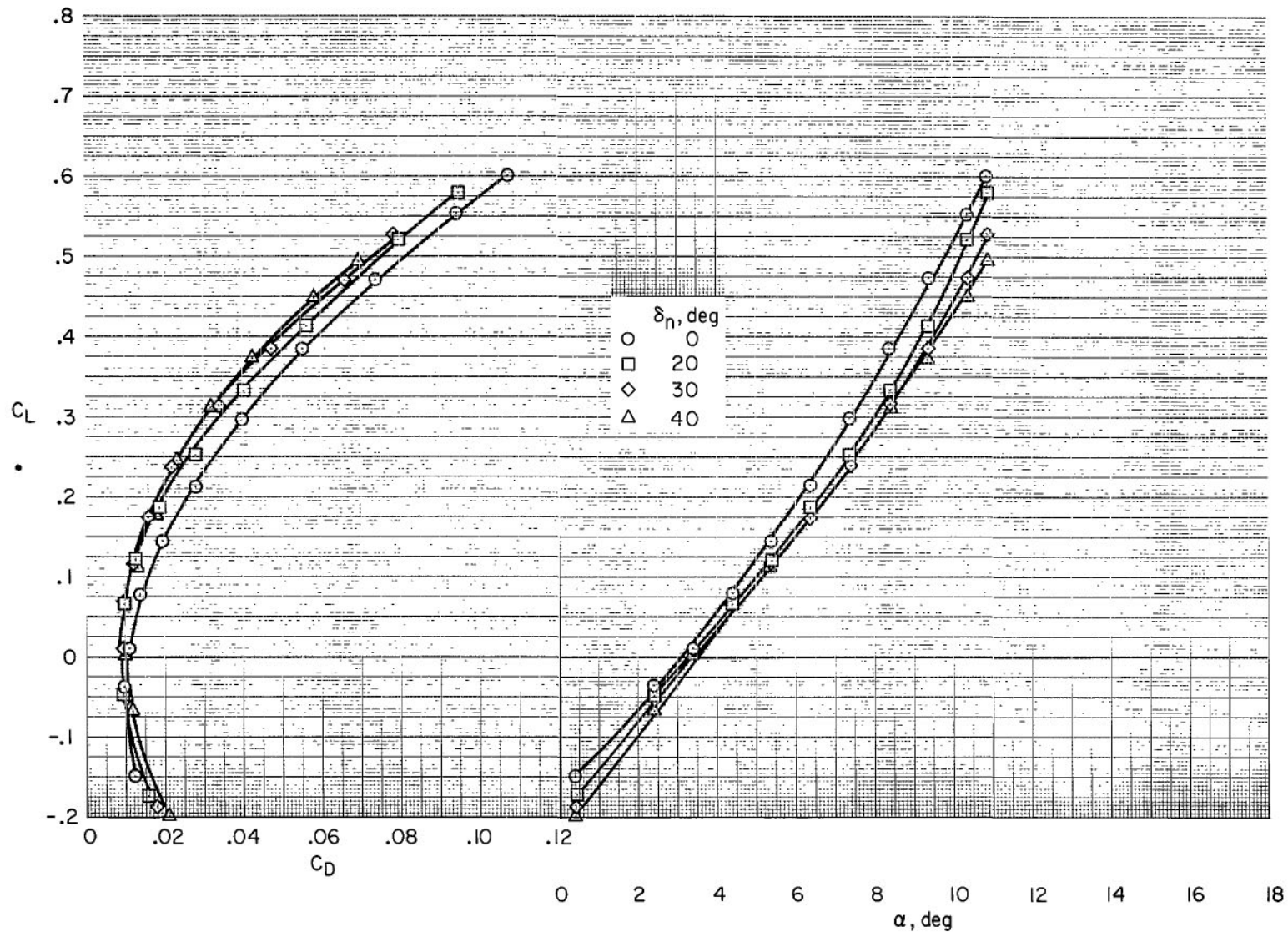


Figure 11.- The effect of nose flap deflection on the characteristics of the model in the presence of the ground; $h/\bar{c} = 0.19$, $\delta_e = -5$, extended fuselage, nacelles removed.

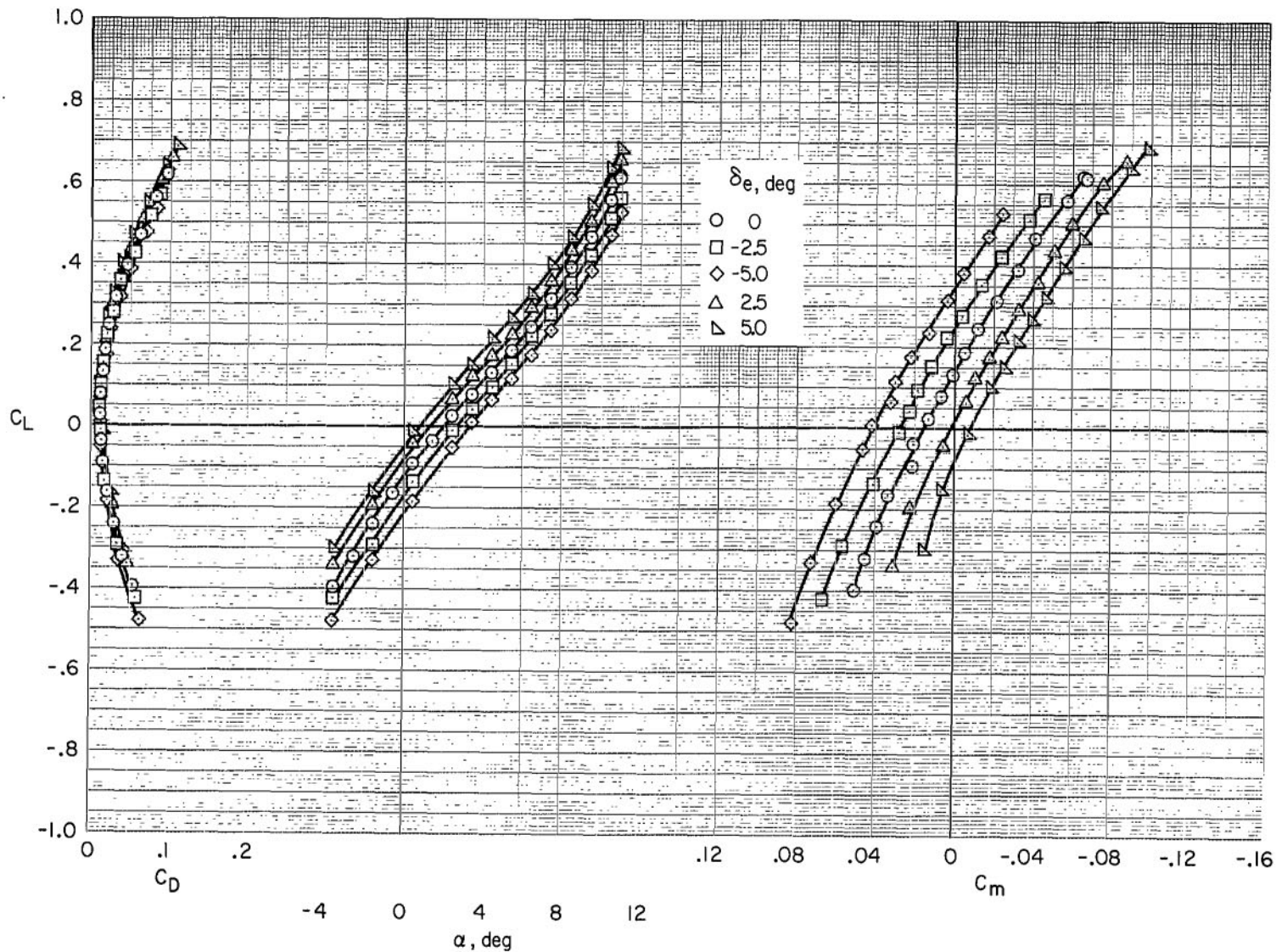
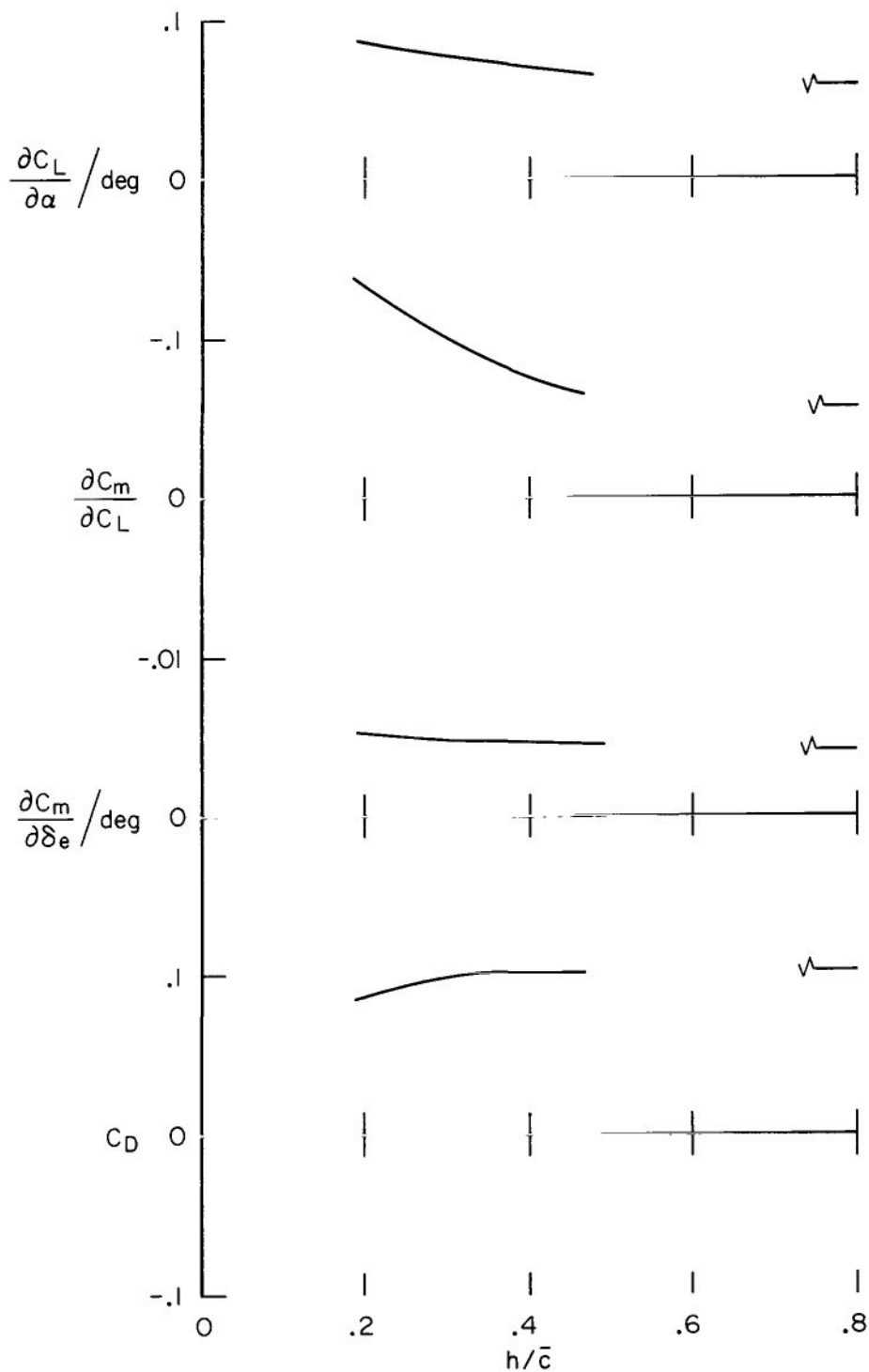
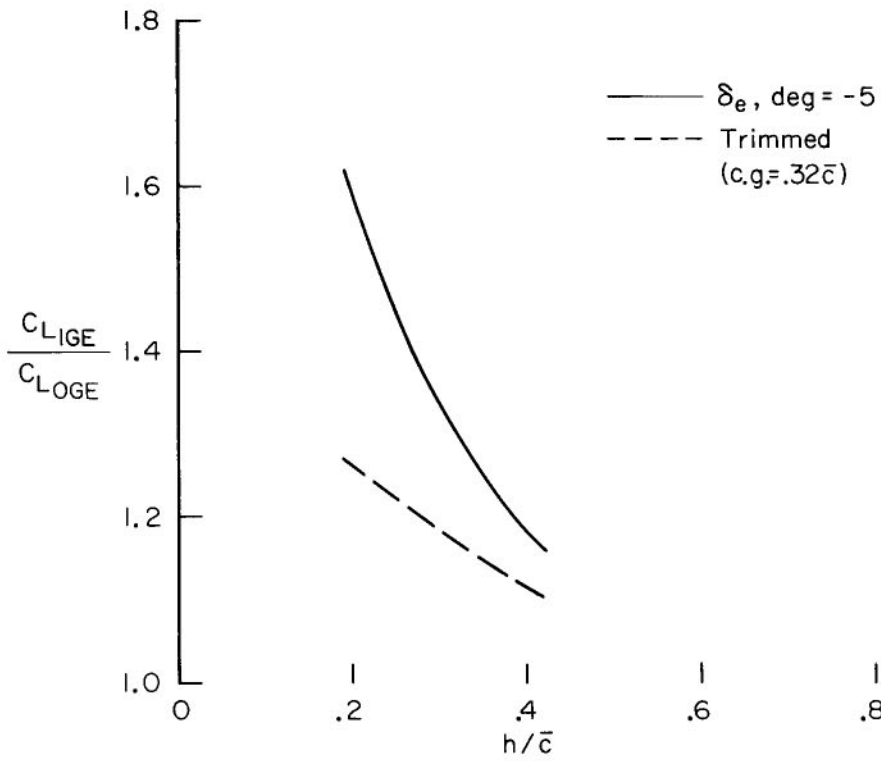


Figure 12.- The effect of elevon deflection on the characteristics of the model in the presence of the ground; $h/\bar{c} = 0.19$, $\delta_n = 30^\circ$, extended fuselage, nacelles removed.



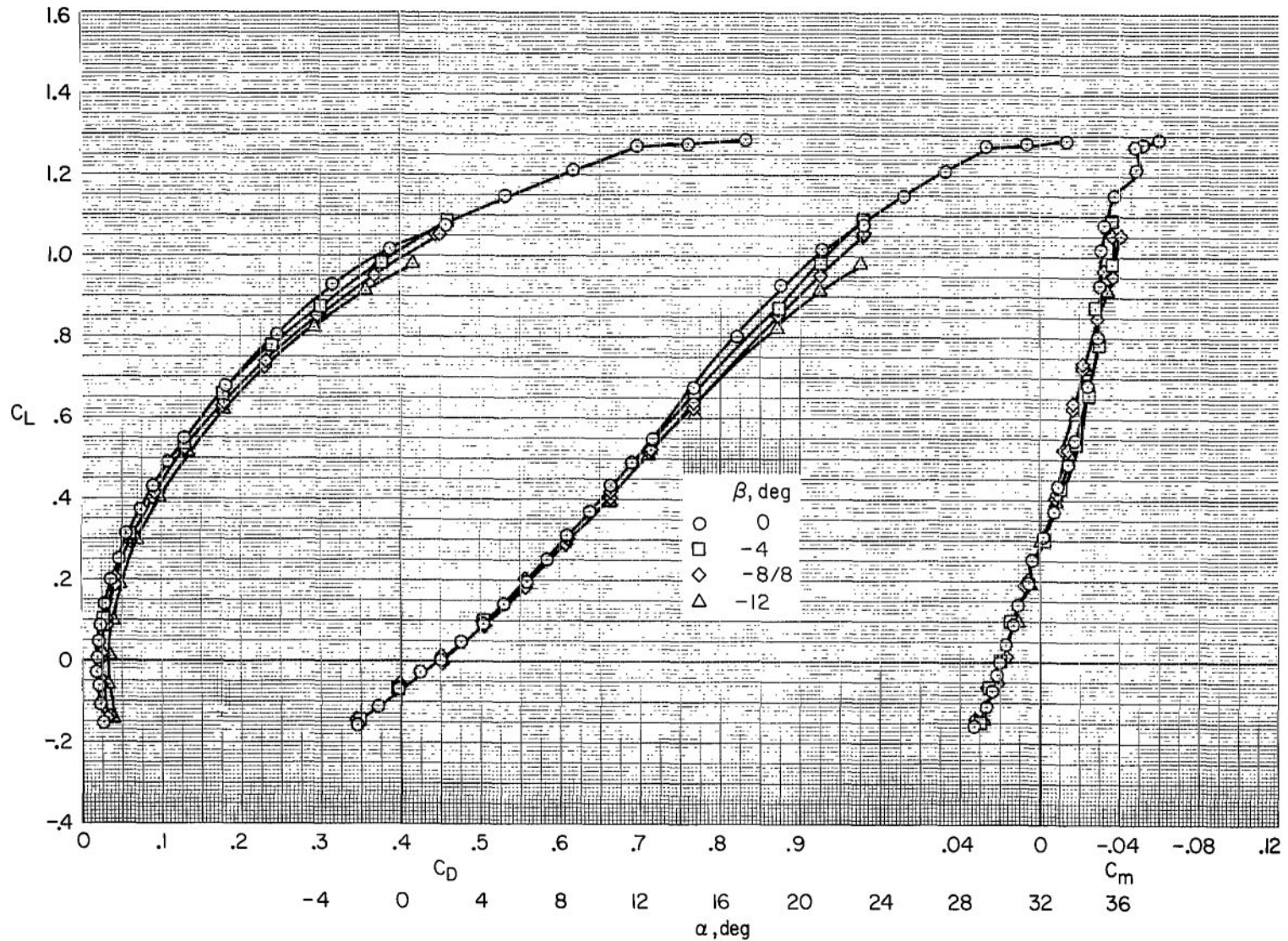
(a) $C_L = 0.5$, $\delta_e = -5^\circ$

Figure 13.- The effectiveness of variation of ground height on the characteristics of the model with the extended fuselage and the nacelles removed; $\delta_n = 0^\circ$.



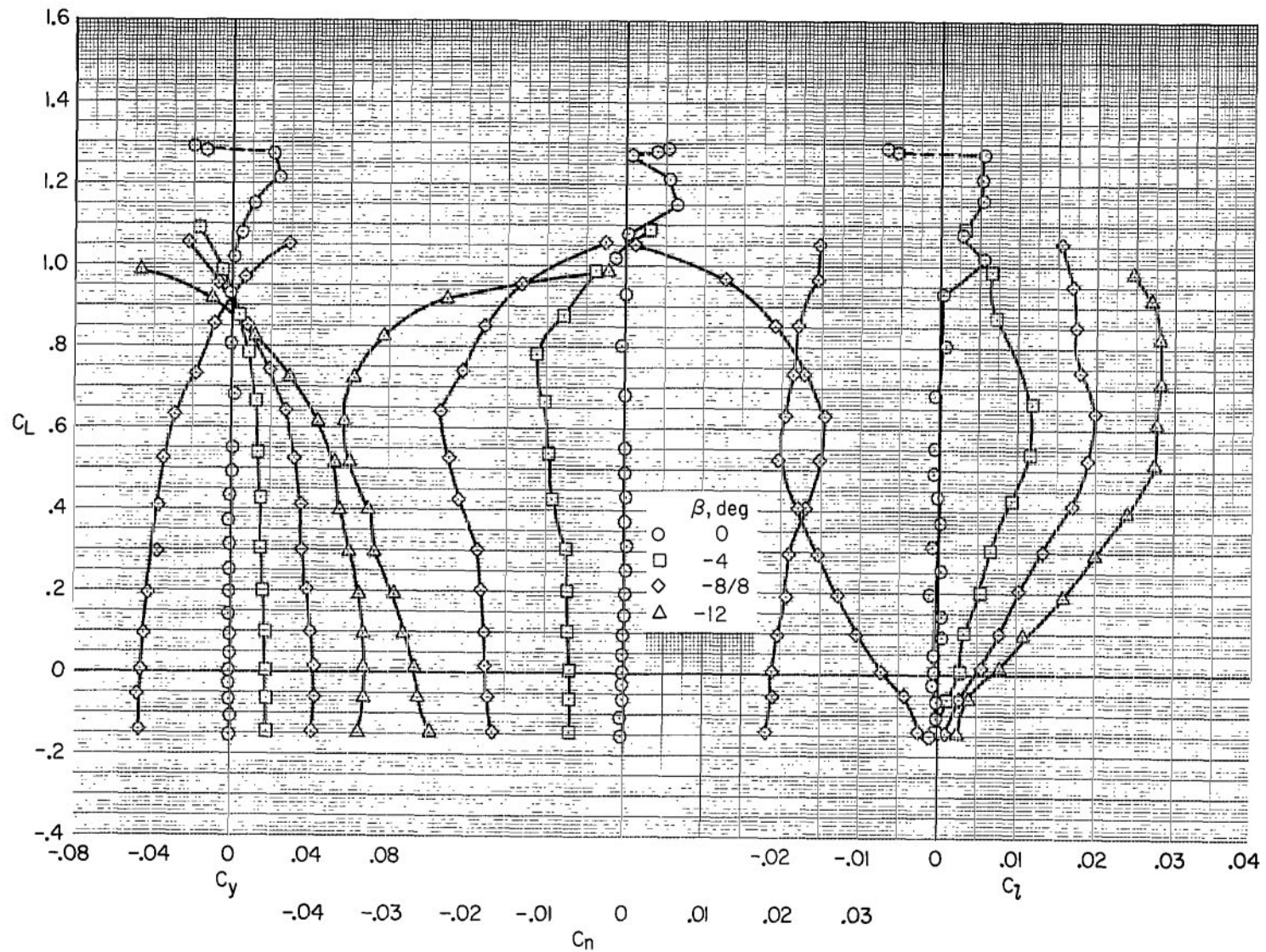
(b) $\alpha = 10^\circ$

Figure 13.- Concluded.



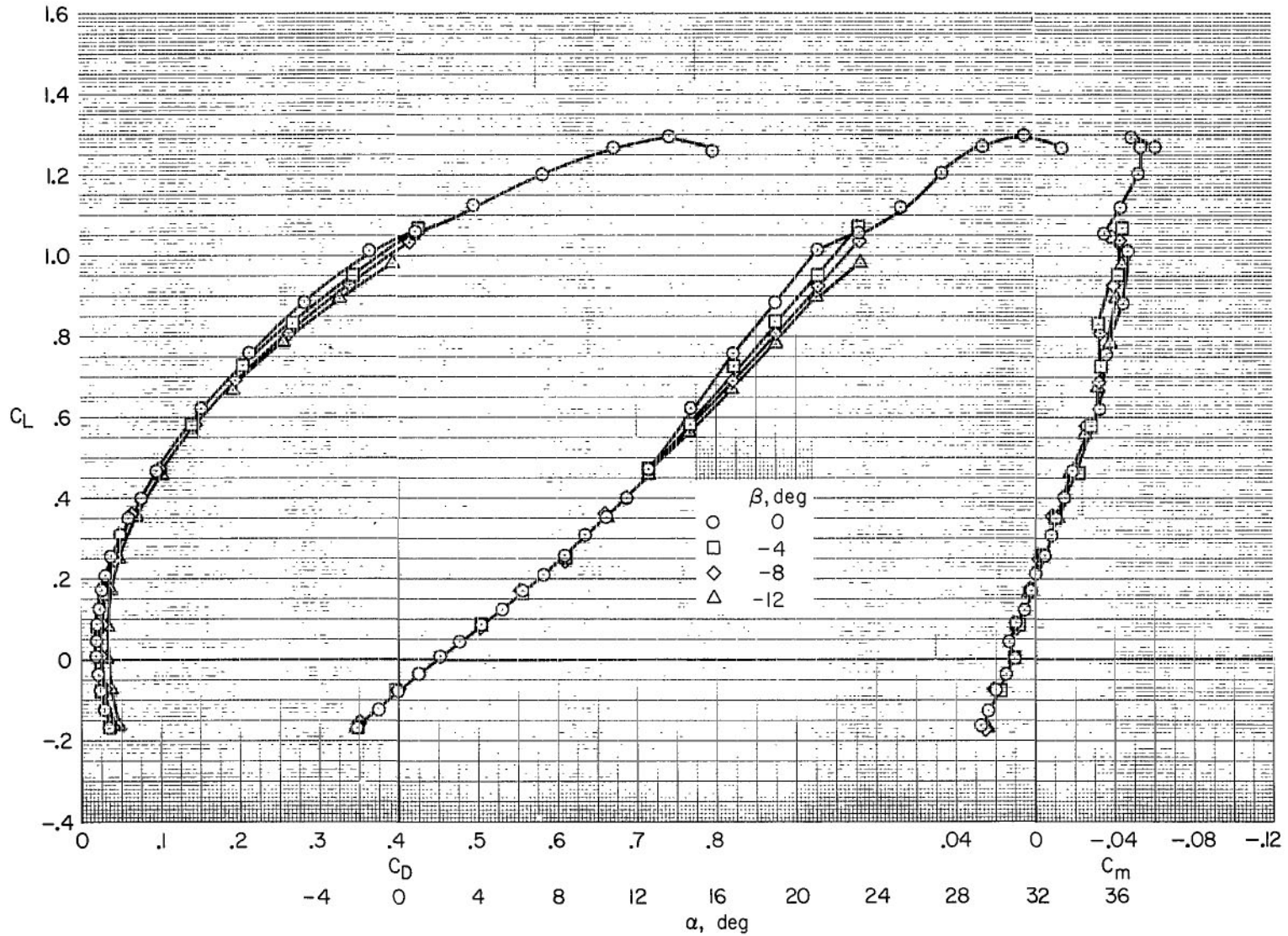
(a) $\delta_n = 0^\circ$, $\delta_e = 0^\circ$, C_L vs. C_D , α , C_m

Figure 14.- The effect of variations of sideslip on the characteristics of the model with the short fuselage; $h/\bar{c} = \infty$.



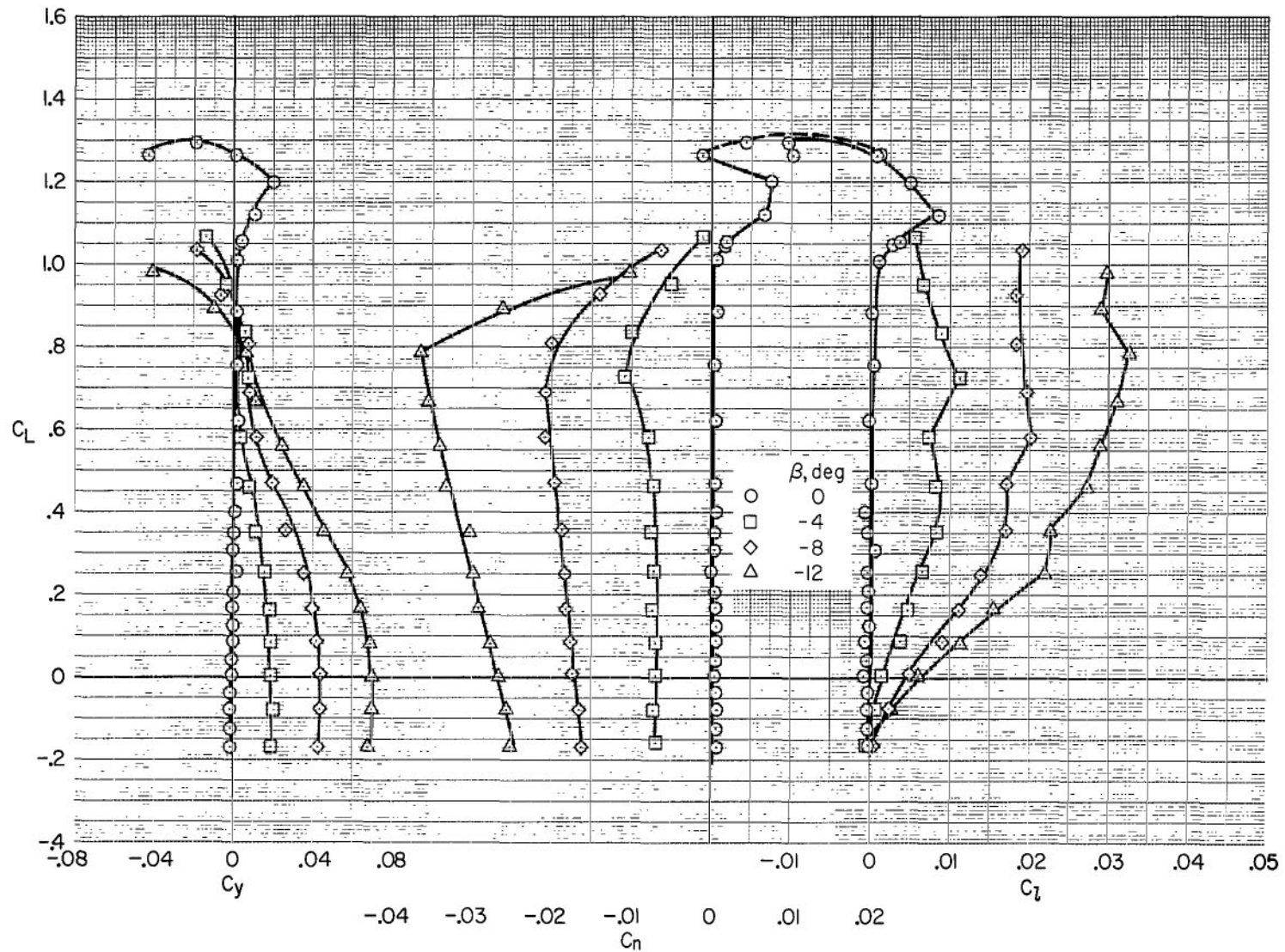
(b) $\delta_n = 0^\circ$, $\delta_e = 0^\circ$, C_L vs. C_y , C_n , C_z

Figure 14.- Continued.



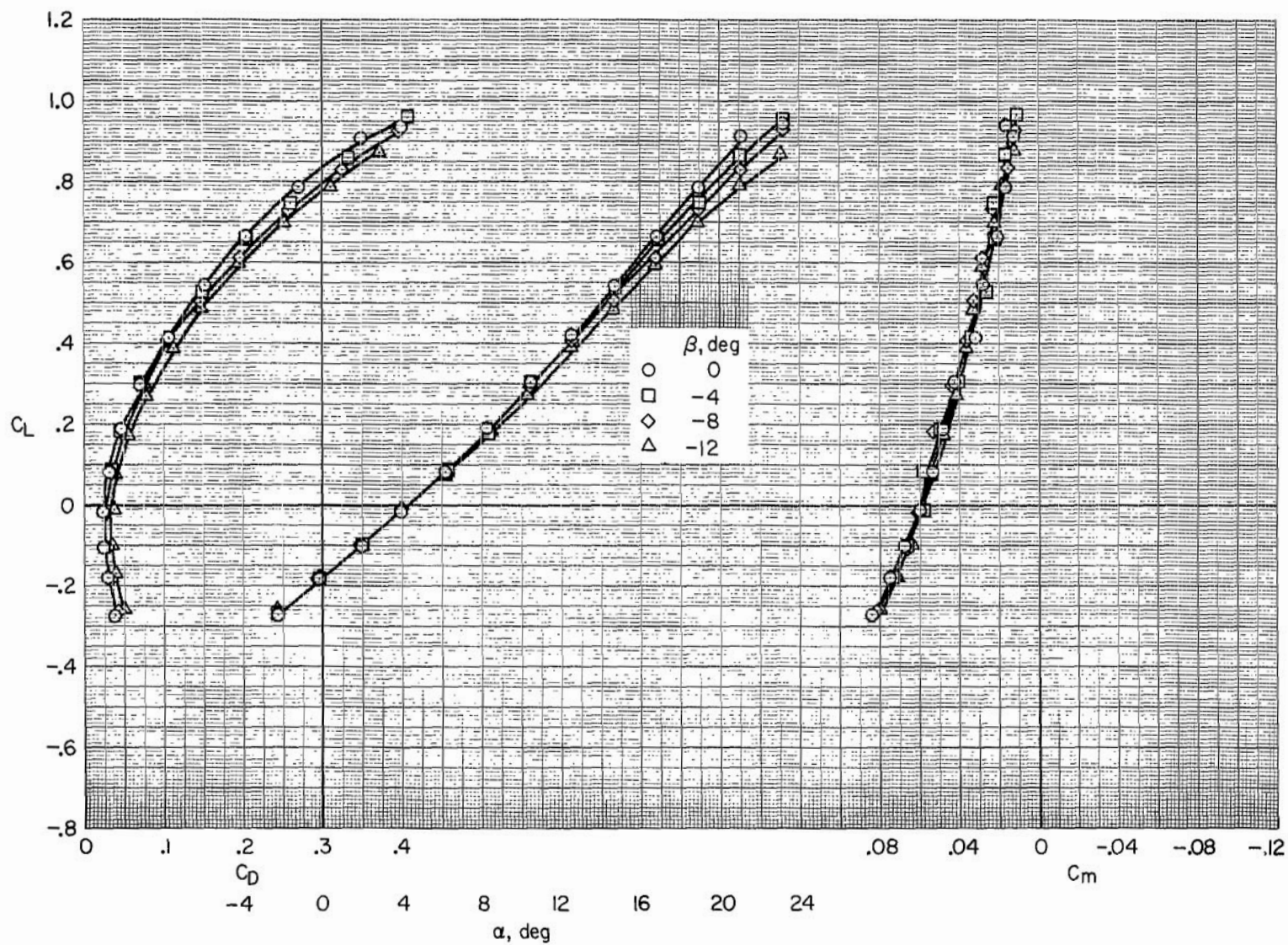
(c) $\delta_n = 30^\circ$, $\delta_e = 0^\circ$, C_L vs. C_D , α , C_m

Figure 14.- Continued.



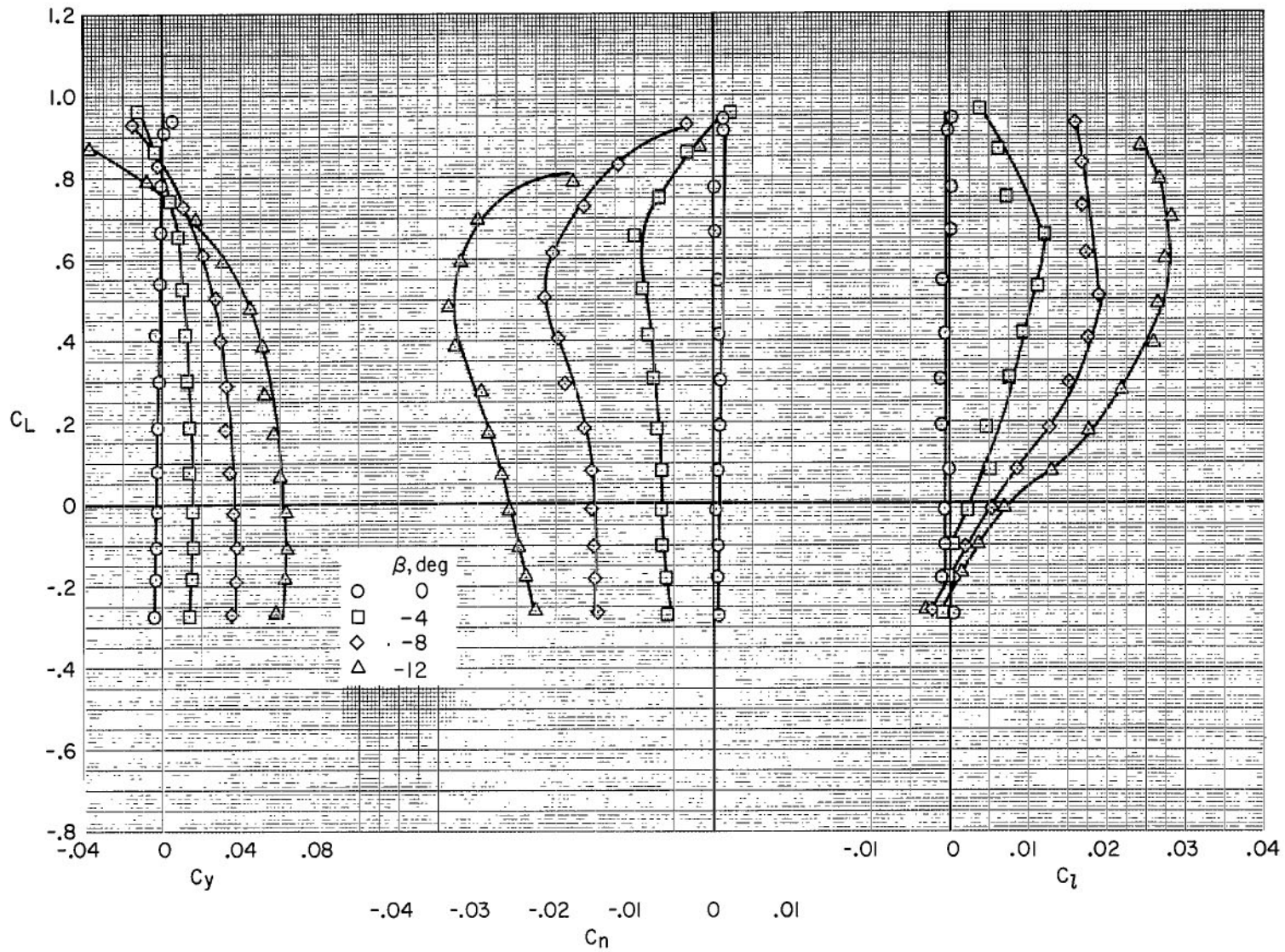
(d) $\delta_n = 30^\circ$, $\delta_e = 0^\circ$, C_L vs. C_y , C_n , C_l

Figure 14.- Continued.



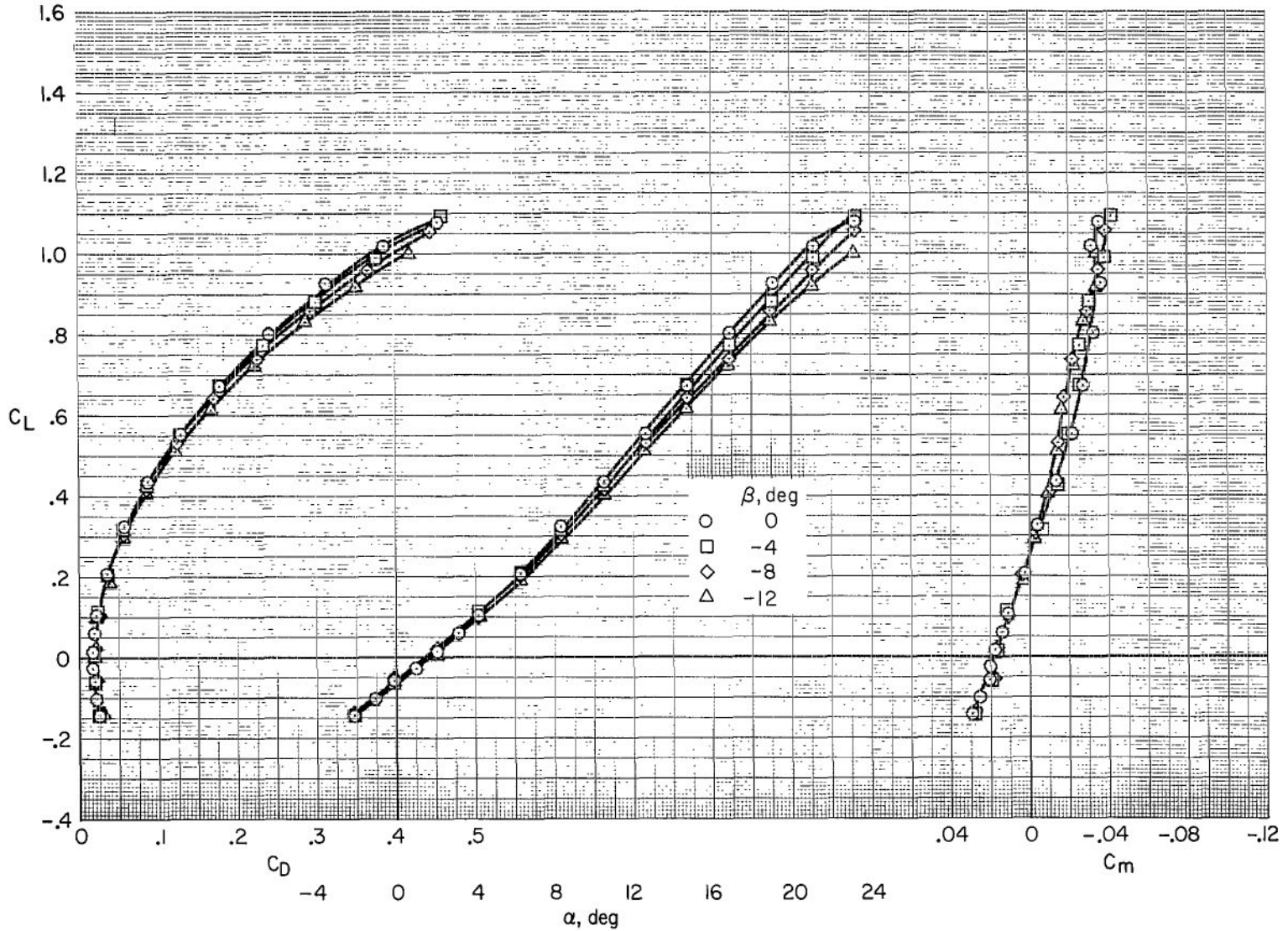
(e) $\delta_n = 0^\circ$, $\delta_e = -10^\circ$, C_L vs. C_D , α , C_m

Figure 14.- Continued.



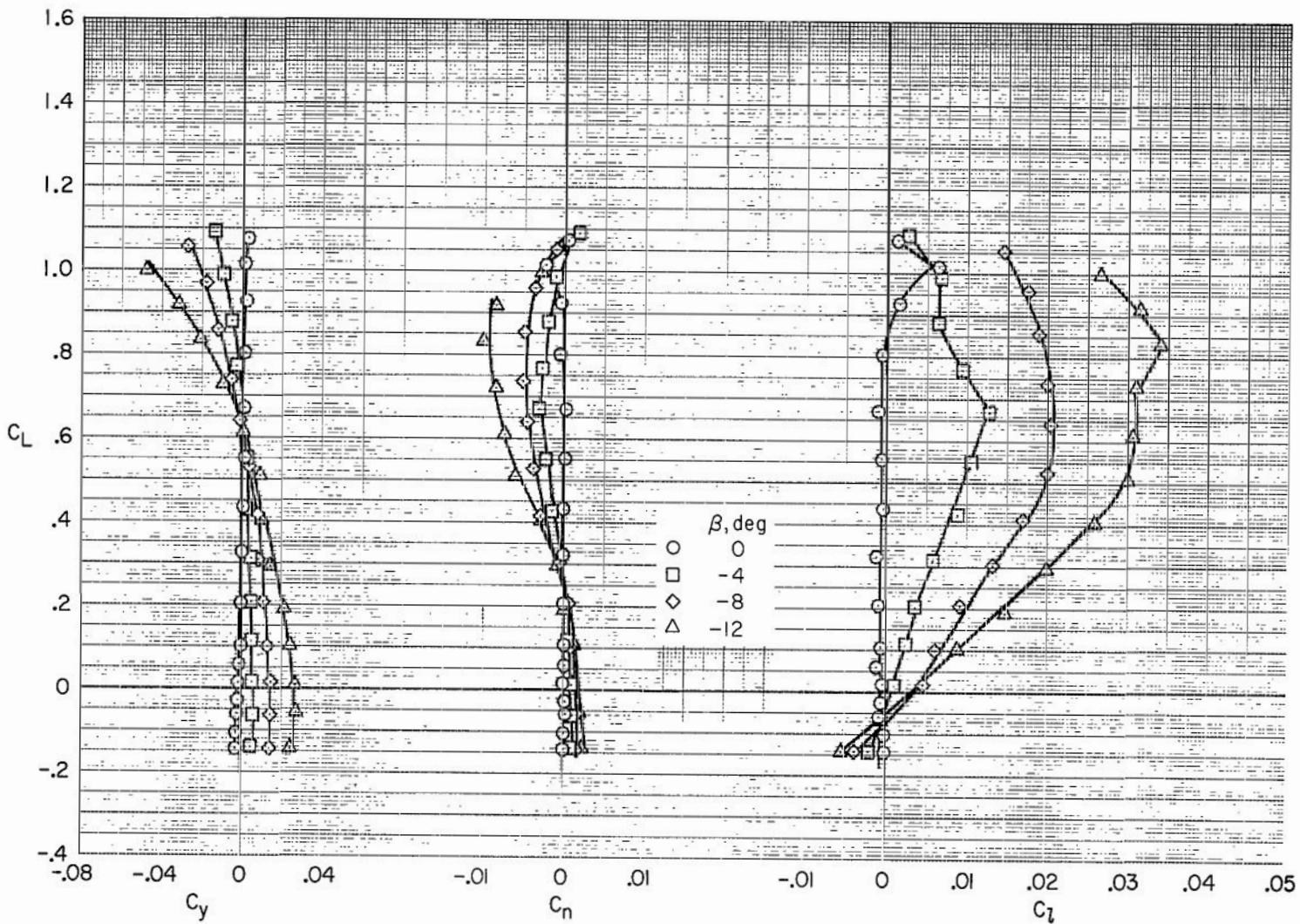
(f) $\delta_n = 0^\circ$, $\delta_e = -10^\circ$, C_L vs. C_y , C_n , C_l

Figure 14.- Concluded.



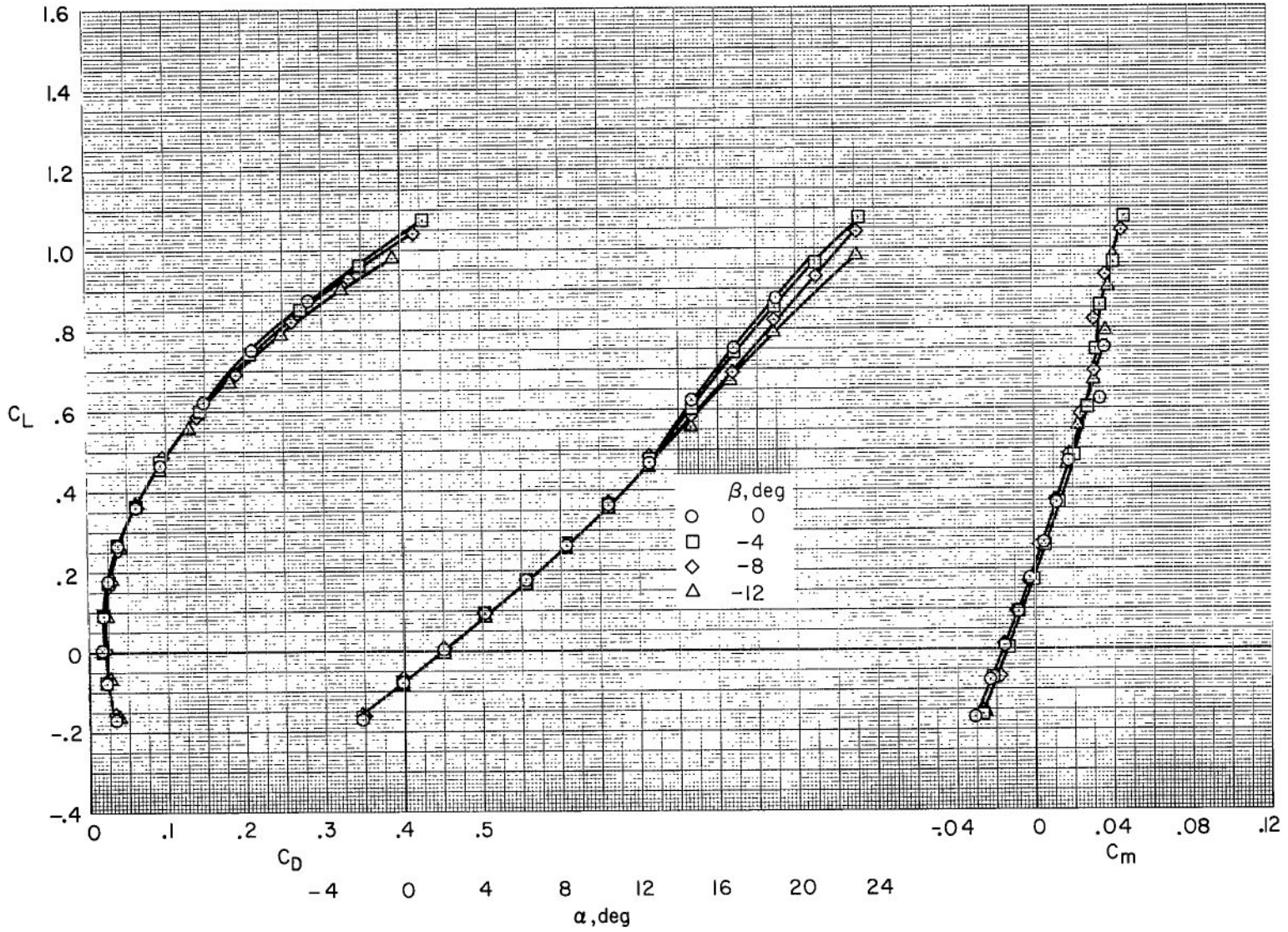
(a) $\delta_n = 0^\circ$, $\delta_e = 0^\circ$, C_L vs. C_D , α , C_m

Figure 15.- The effect of variations of sideslip on the characteristics of the model with the short fuselage and with the vertical tail removed; $h/\bar{c} = \infty$.



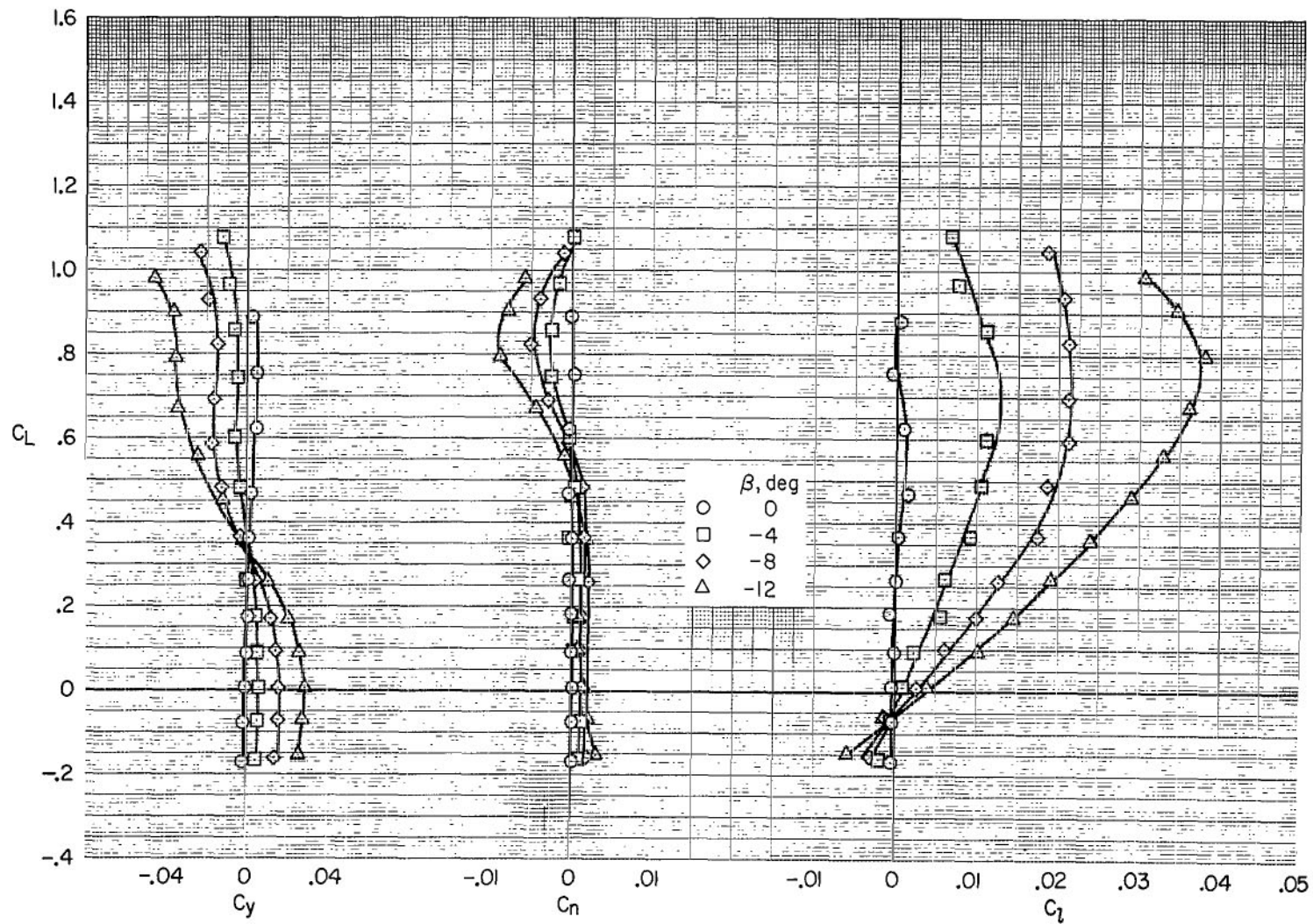
(b) $\delta_n = 0^\circ$, $\delta_e = 0^\circ$, C_L vs. C_y , C_n , C_l

Figure 15.- Continued.



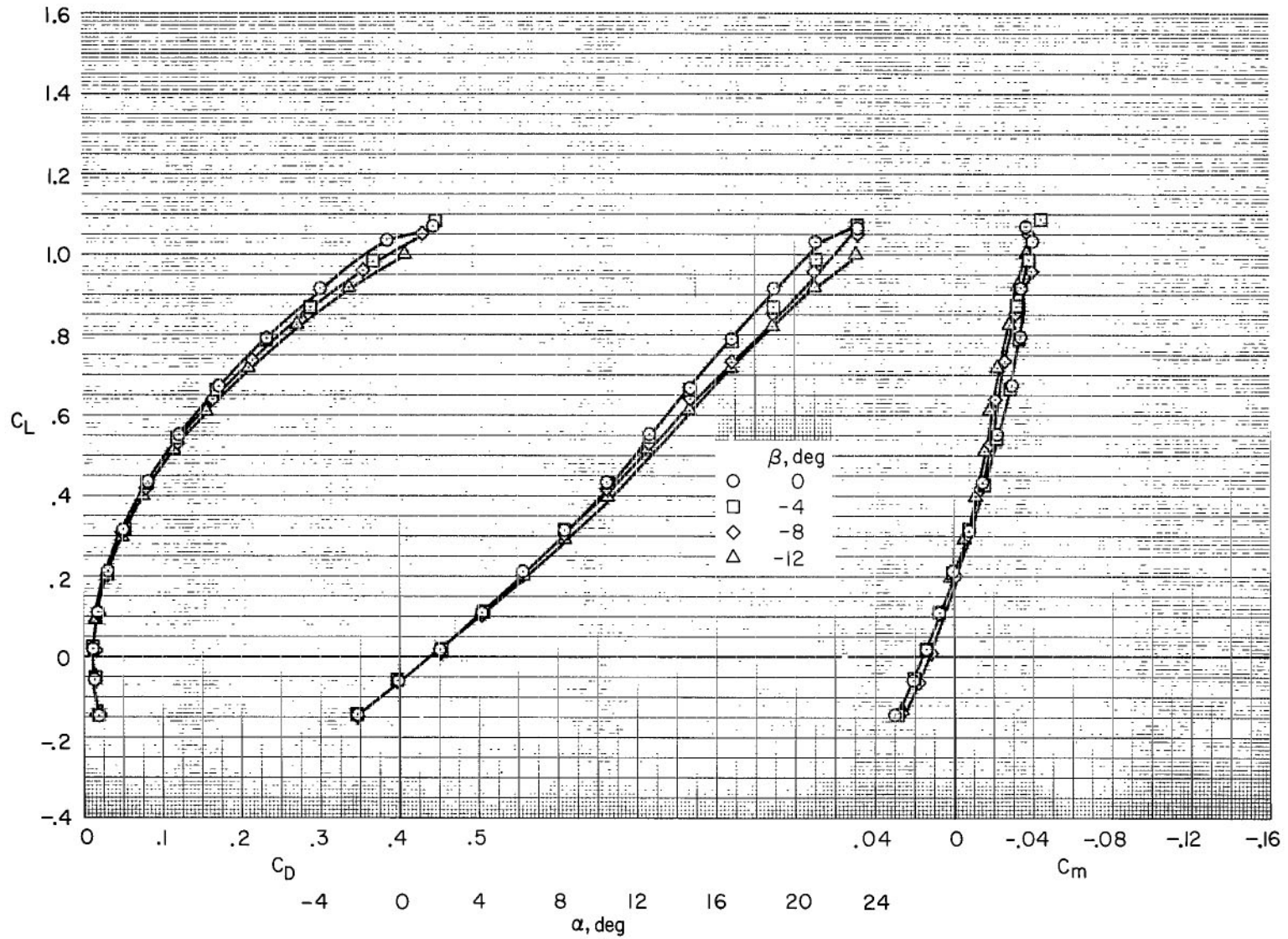
(c) $\delta_n = 30^\circ$, $\delta_e = 0^\circ$, C_L vs. C_D , α , C_m

Figure 15.- Continued.



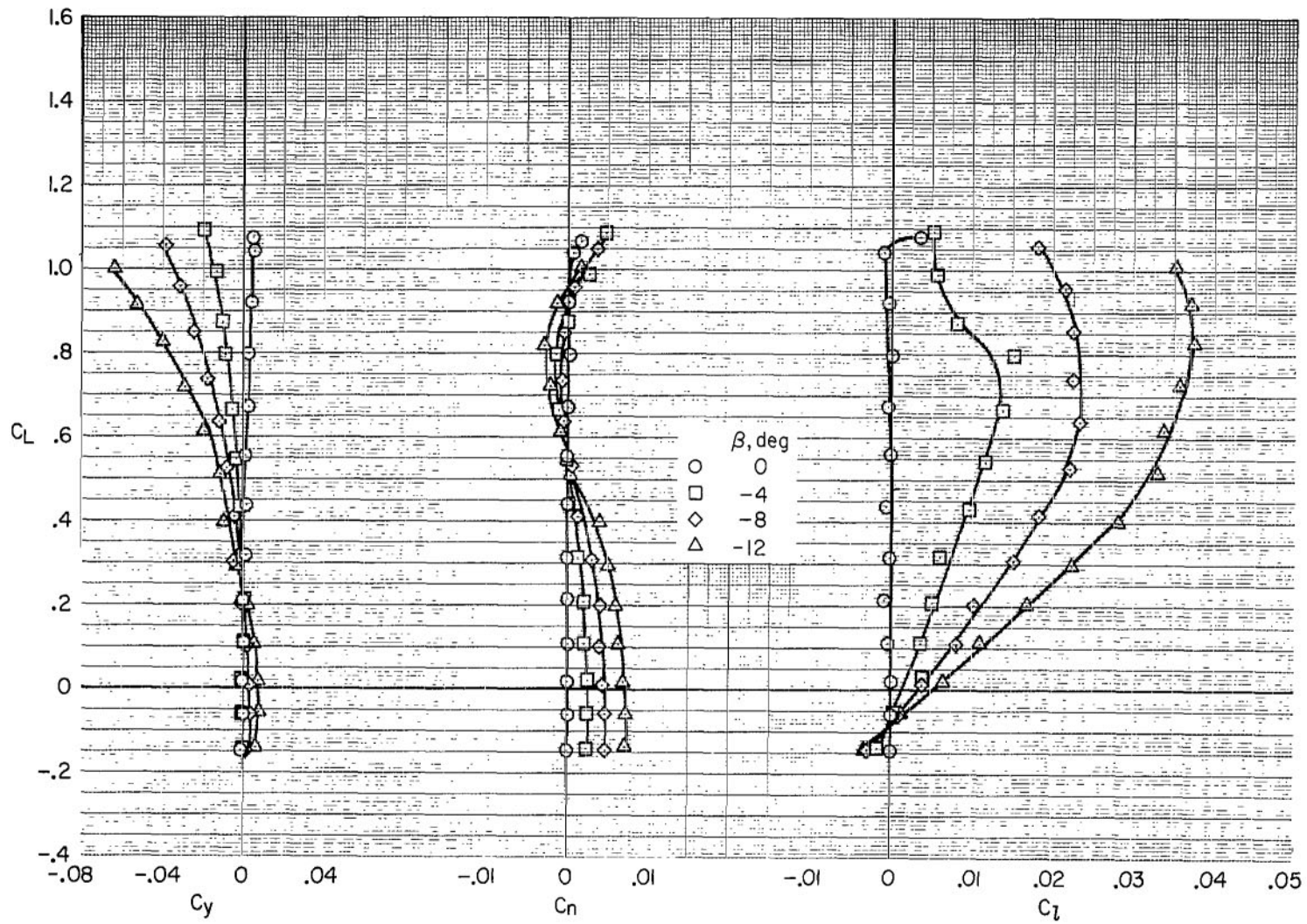
(d) $\delta_n = 30^\circ$, $\delta_e = 0^\circ$, C_L vs. C_y , C_n , C_l

Figure 15.- Concluded.



(a) C_L vs. C_D , α , C_m

Figure 16.- The effect of variations of sideslip on the characteristics of the model with the short fuselage and vertical tail and nacelles removed; $h/\bar{c} = \infty$, $\delta_n = 0^\circ$, $\delta_e = 0^\circ$.



(b) C_L vs. C_y, C_n, C_l

Figure 16.- Concluded.

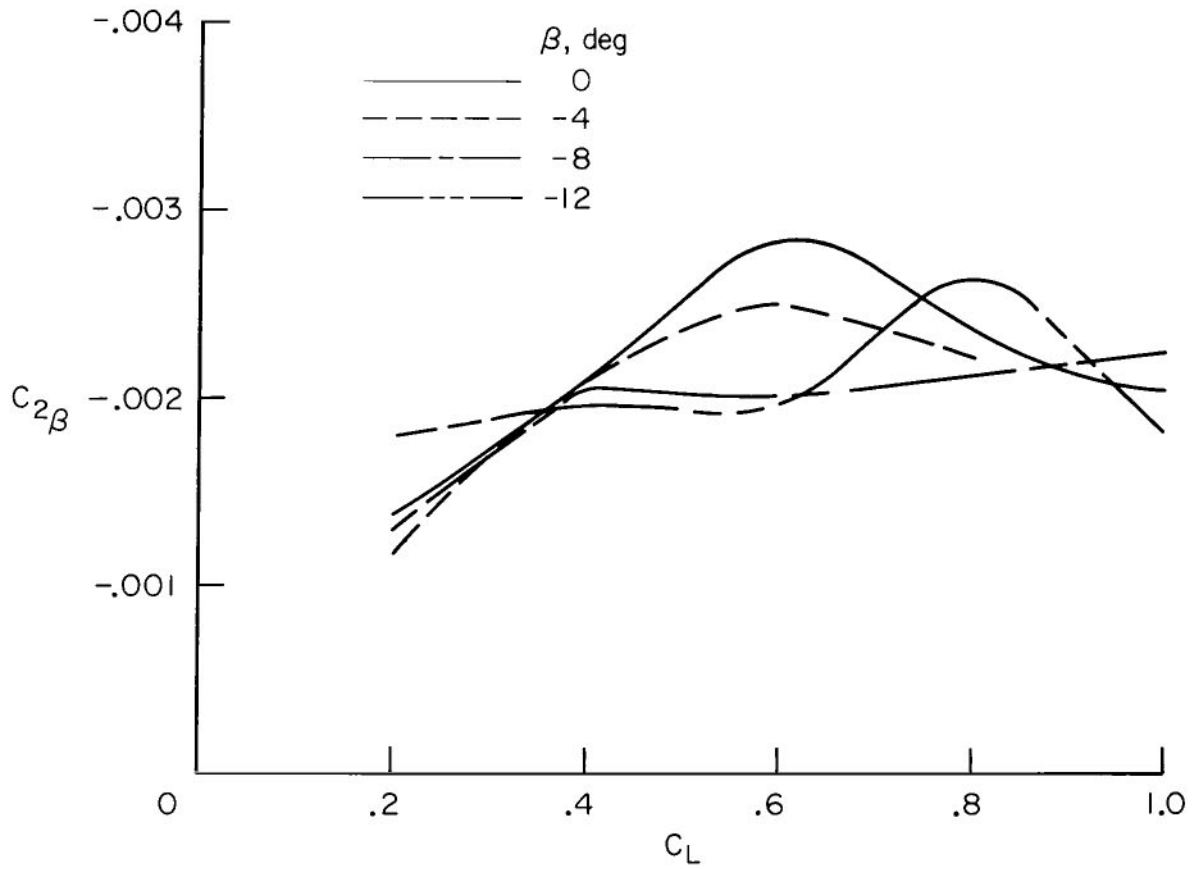
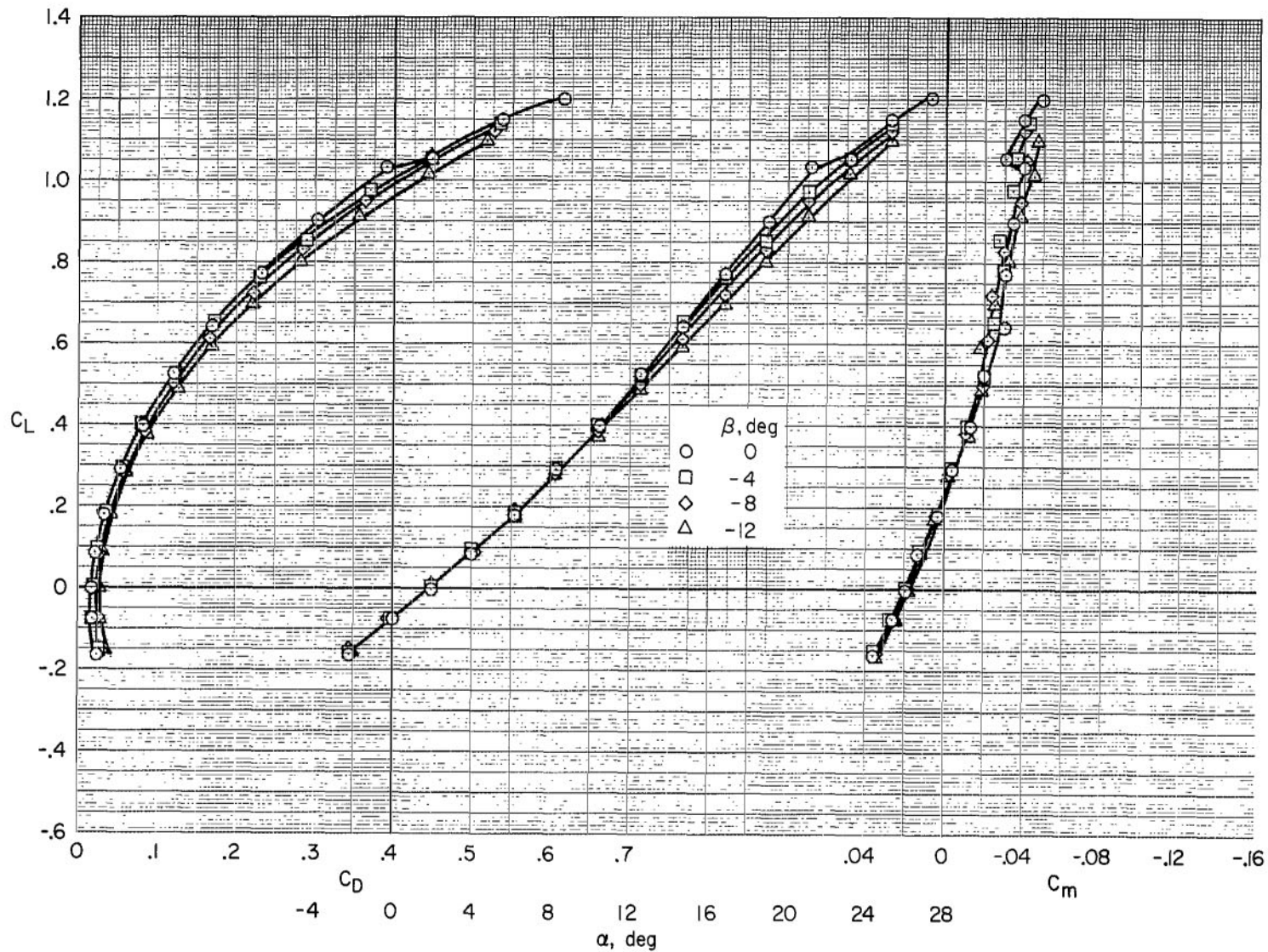


Figure 17.- The roll due to sideslip characteristics of the model with the short fuselage; $\delta_n = 0^\circ$, $\delta_e = 0^\circ$, $h/\bar{c} = \infty$, $\delta_a = 0^\circ$.



(a) C_L vs. C_D , α , C_m

Figure 18.- The effect of variations of sideslip on the characteristics of the model with the extended fuselage; $h/\bar{c} = \infty$, $\delta_n = 0^\circ$, $\delta_e = 0^\circ$.

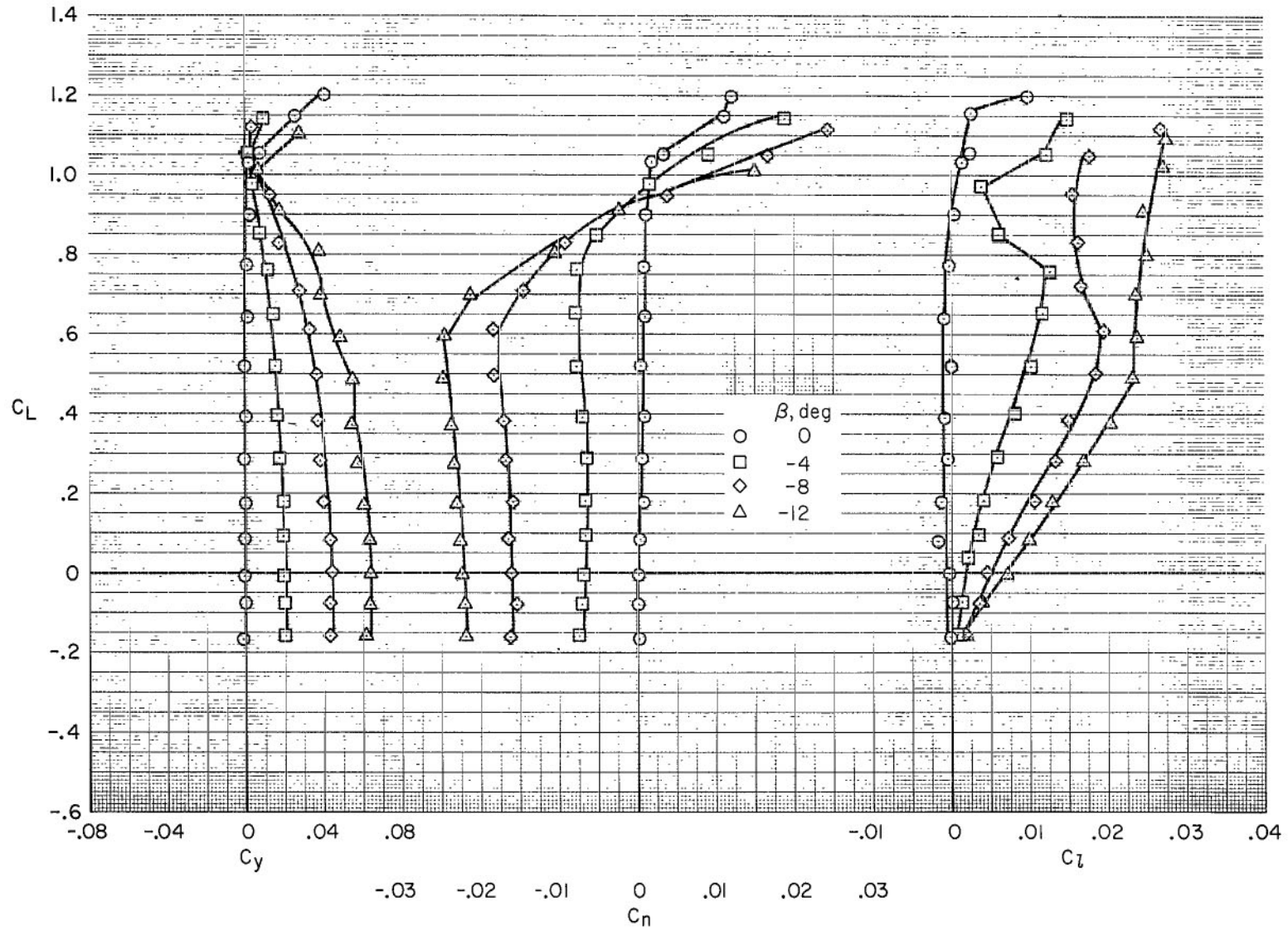
(b) C_L vs. C_y , C_n , C_l

Figure 18.- Concluded.

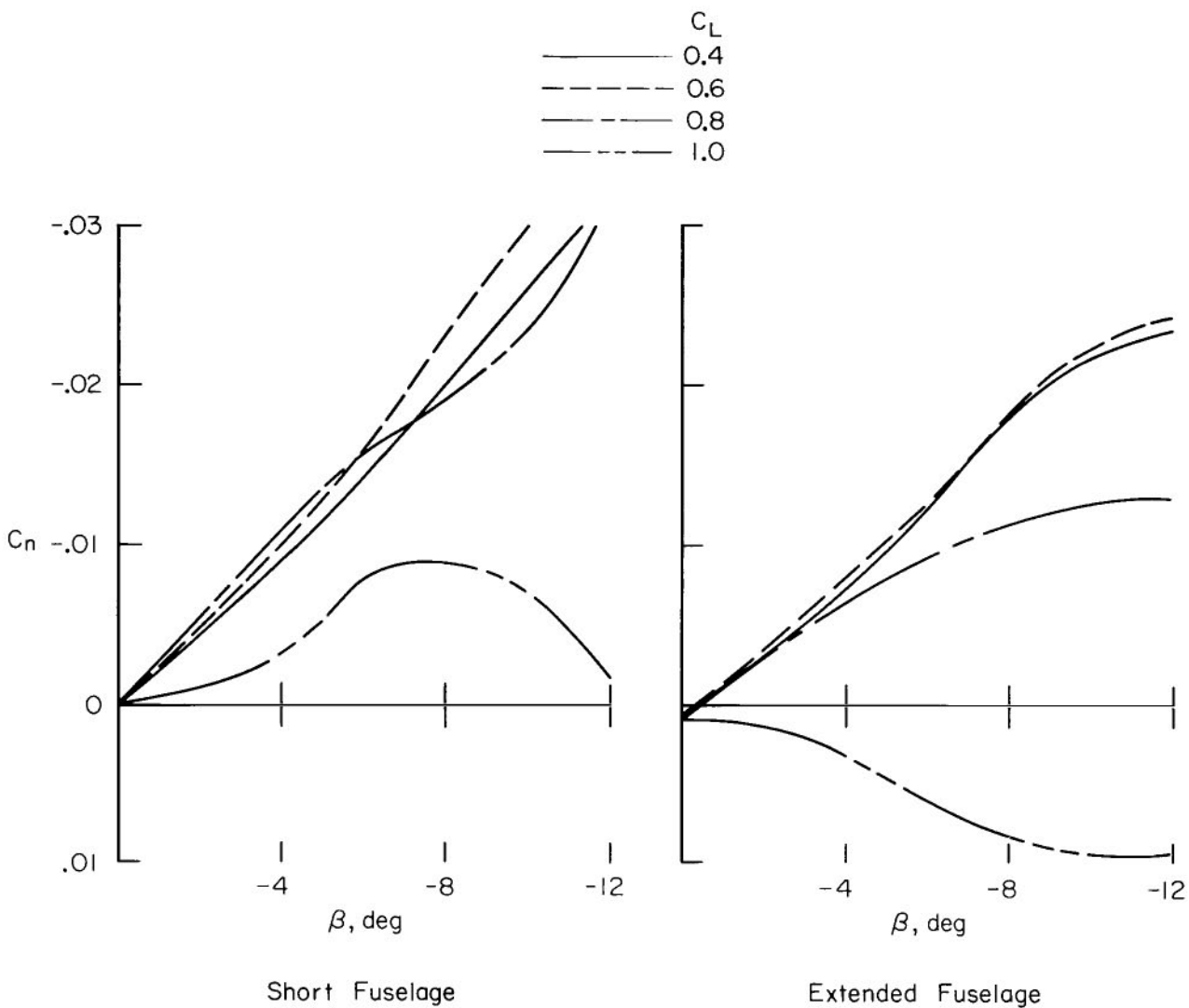
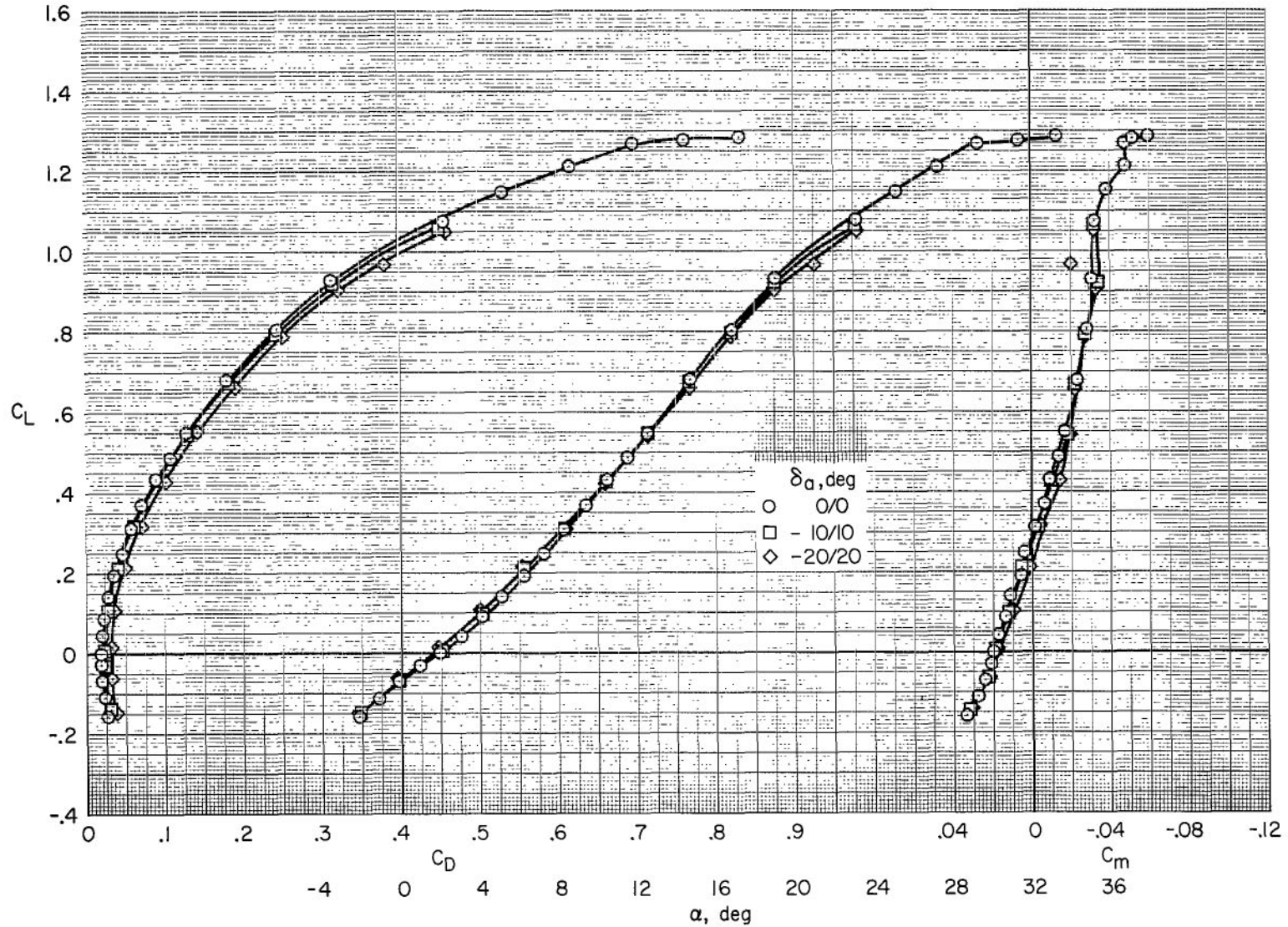
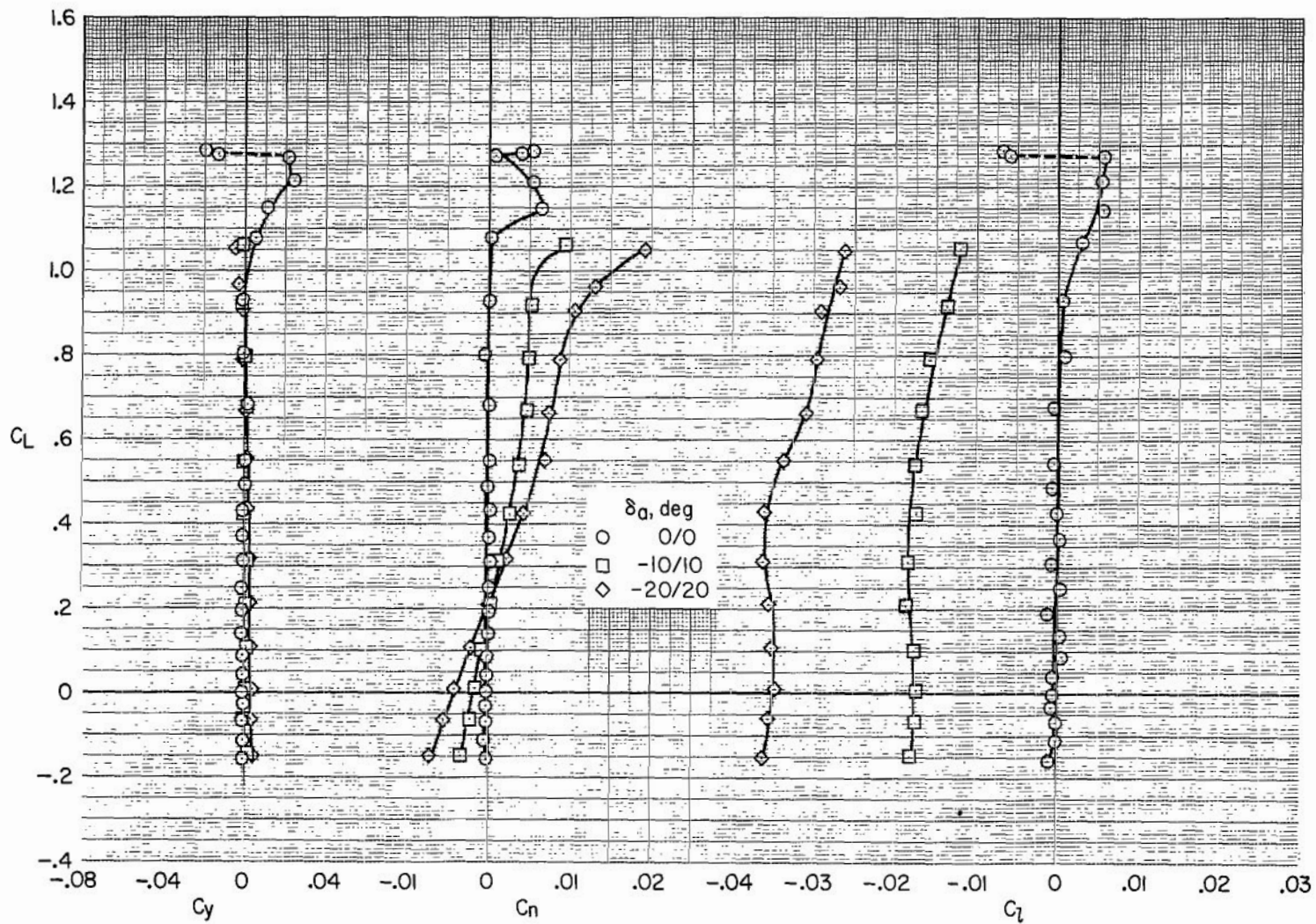


Figure 19.- The yawing moment due to sideslip characteristics of the model;
 $h/\bar{c} = \infty$, $\delta_n = 0^\circ$, $\delta_e = 0^\circ$, $\delta_r = 0^\circ$.



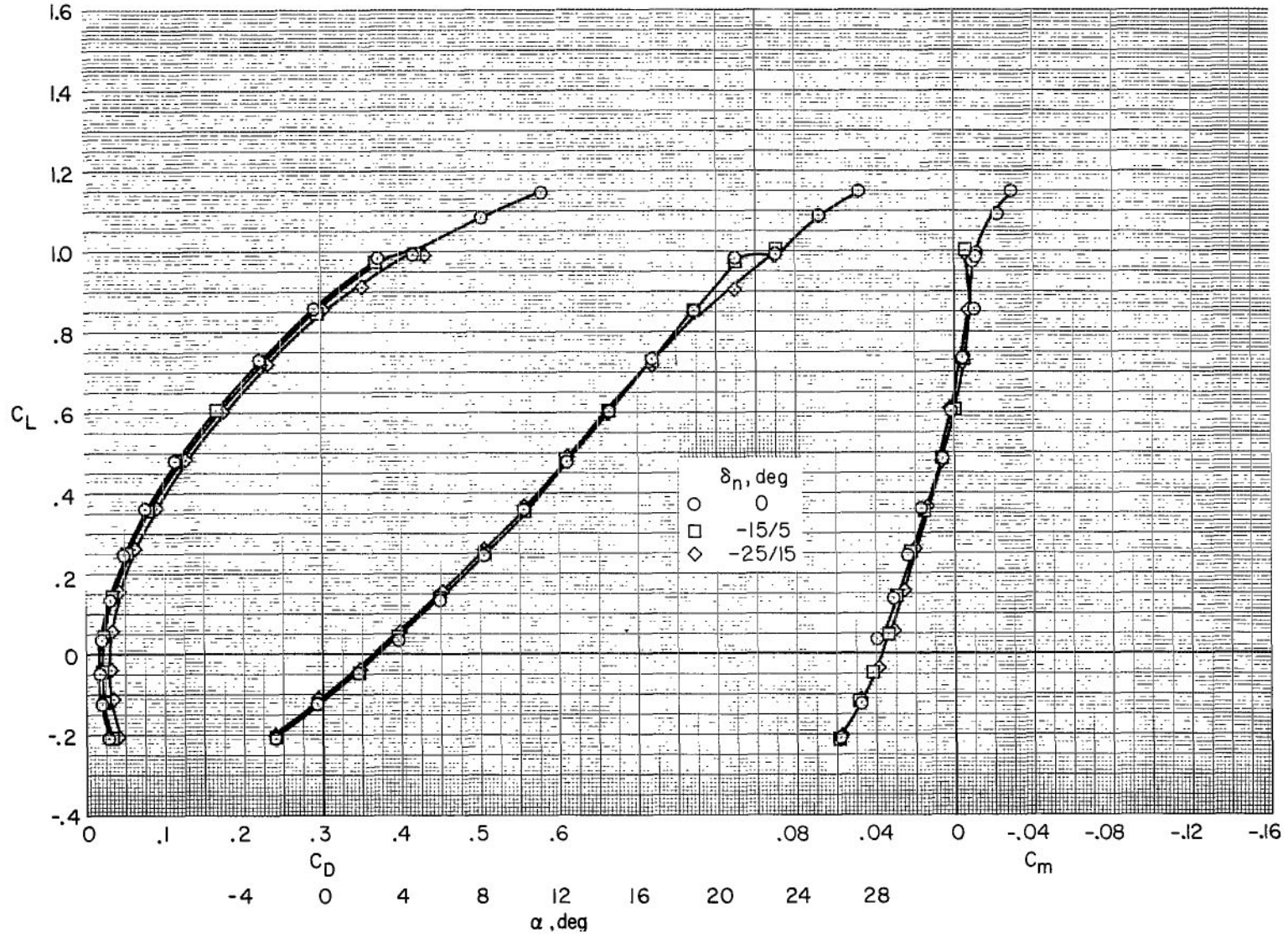
(a) $\delta_n = 0^\circ$, $\delta_e = 0^\circ$, C_L vs. C_D , α , C_m

Figure 20.- The effect of aileron deflection on the characteristics of the model with the short fuselage without sideslip; $h/\bar{c} = \infty$.



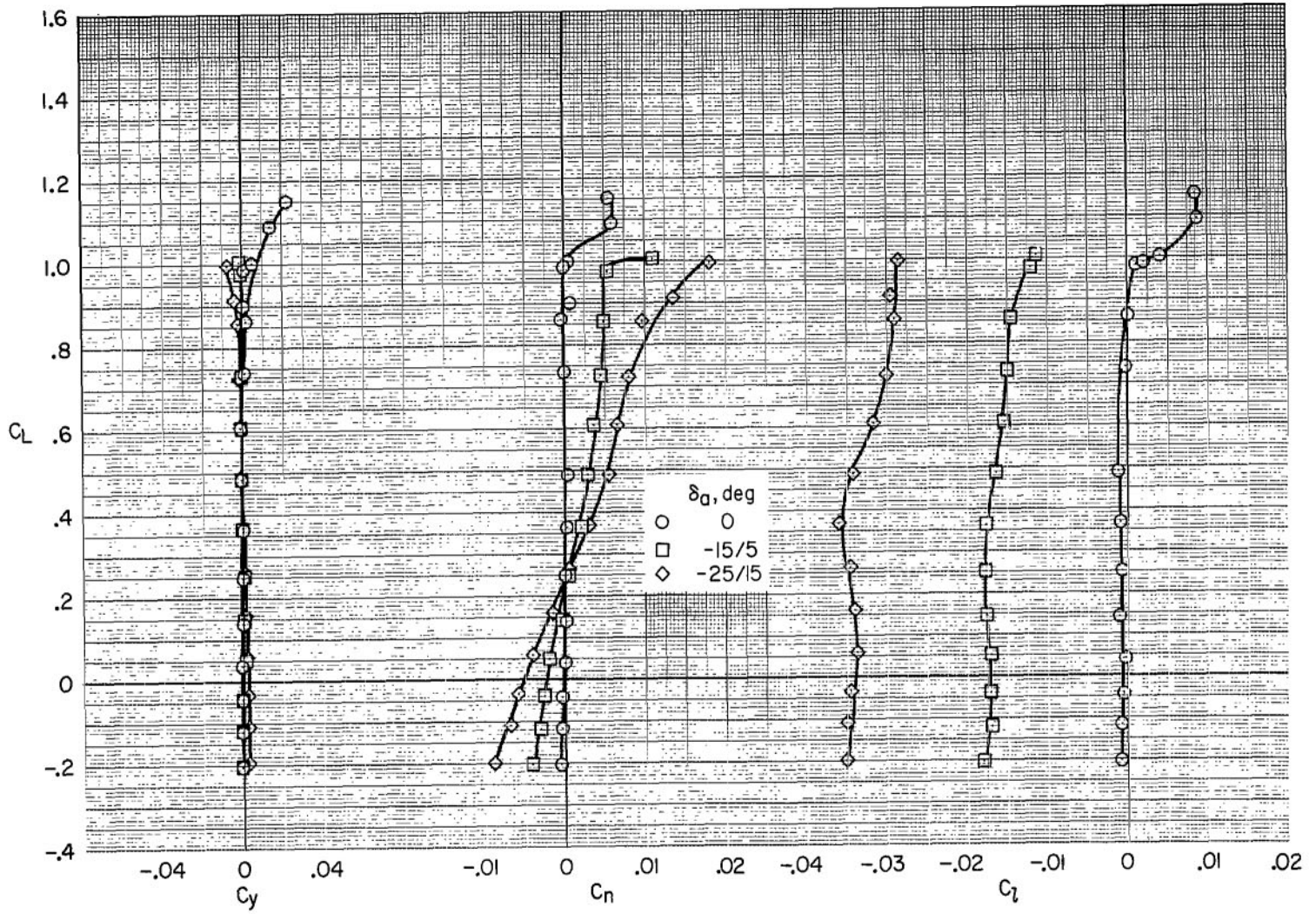
(b) $\delta_n = 0^\circ$, $\delta_e = 0^\circ$, C_L vs. C_Y , C_n , C_l

Figure 20.- Continued.



(c) $\delta_n = 0^\circ$, $\delta_e = -5^\circ$, C_L vs. C_D , α , C_m

Figure 20.- Continued.



(d) $\delta_n = 0^\circ$, $\delta_e = -5^\circ$, C_L vs. C_y , C_n , C_t

Figure 20.- Concluded.

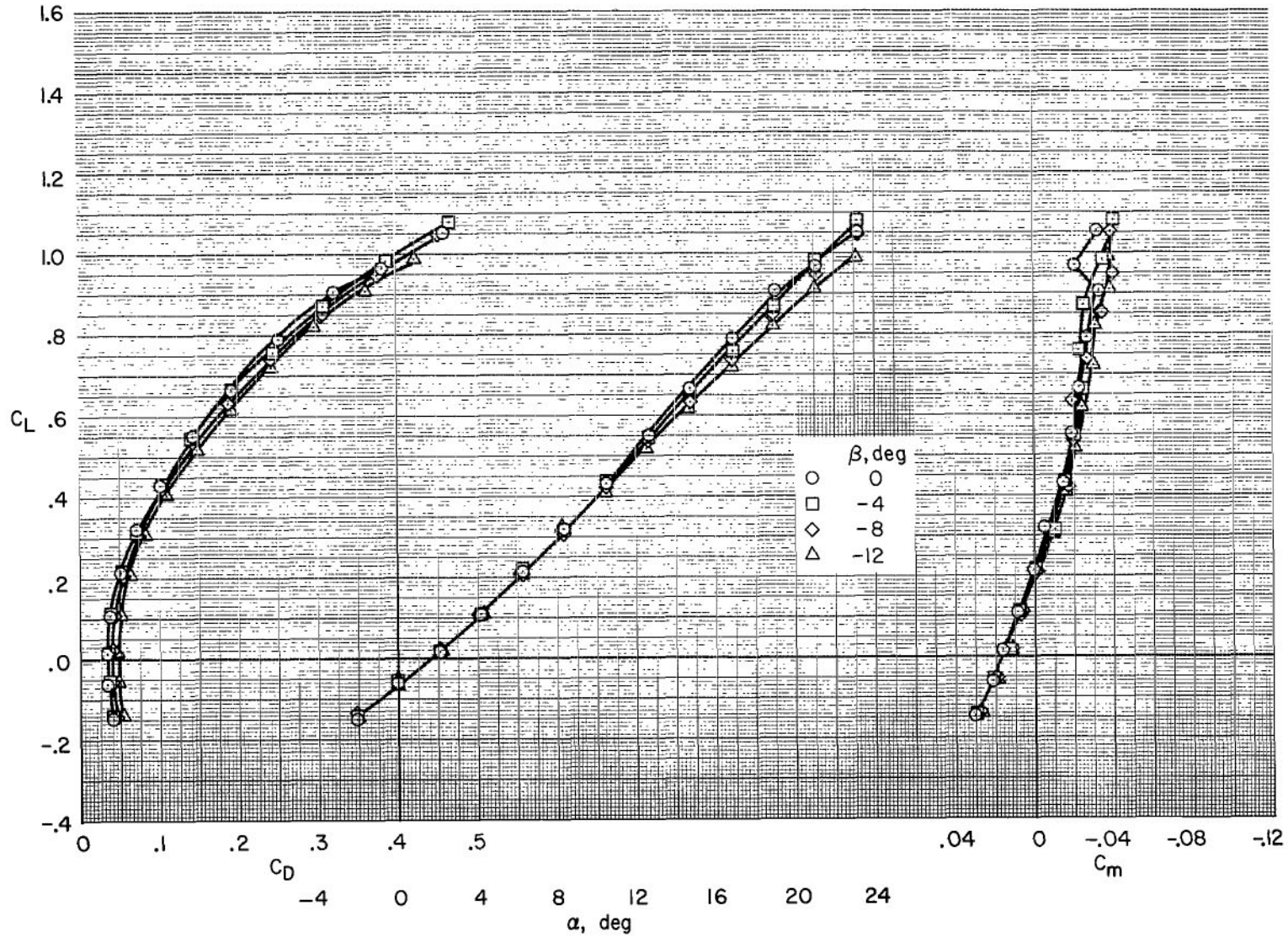
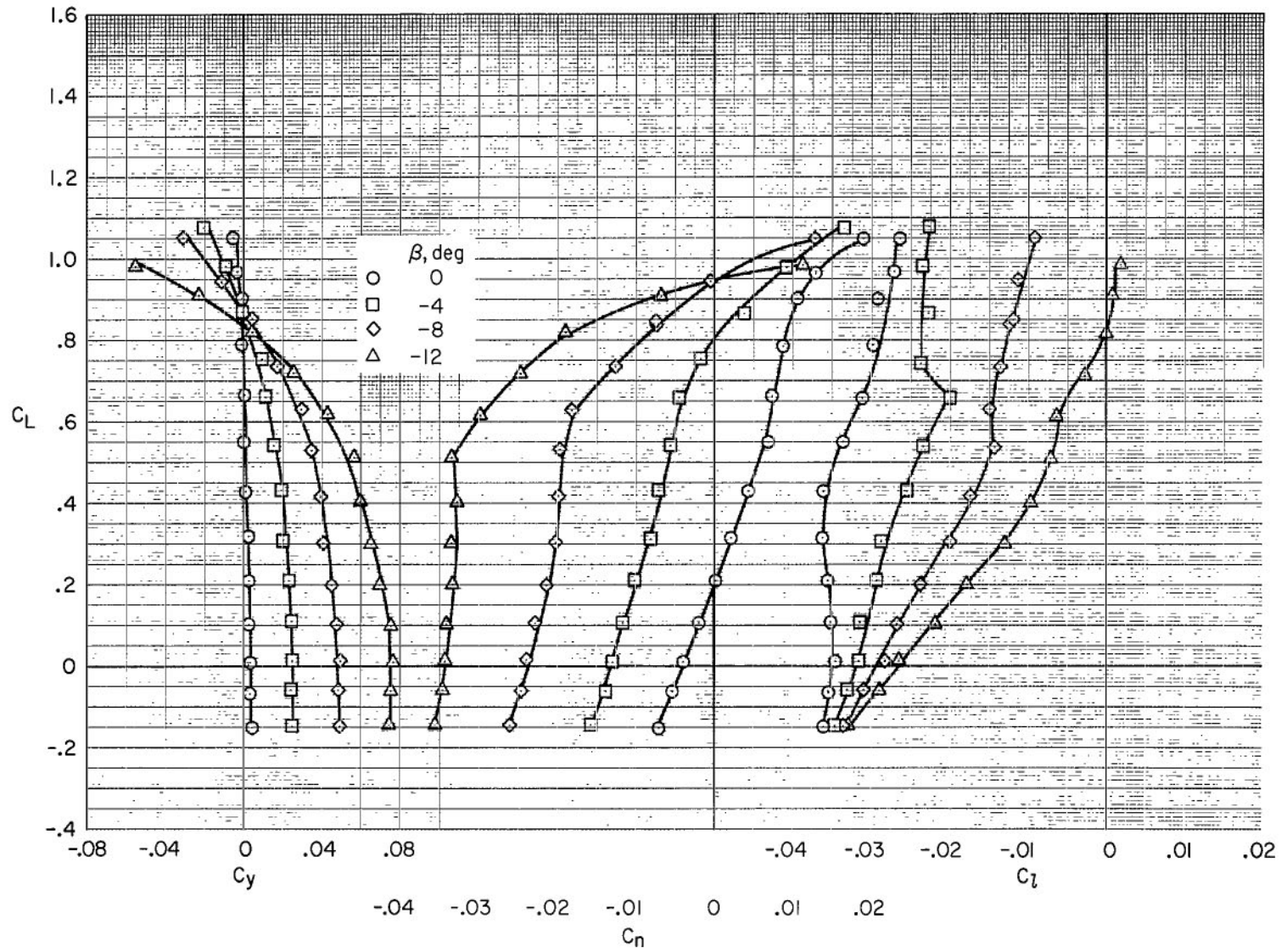
(a) C_L vs. C_D , α , C_m

Figure 21.- The effect of sideslip on the characteristics of the model with the short fuselage and with the ailerons deflected; $\delta_n = 0^\circ$, $\delta_e = 0^\circ$, $\delta_a = -20/20$, $h/\bar{c} = \infty$.



(b) C_L vs. C_y, C_n, C_l

Figure 21.- Concluded.

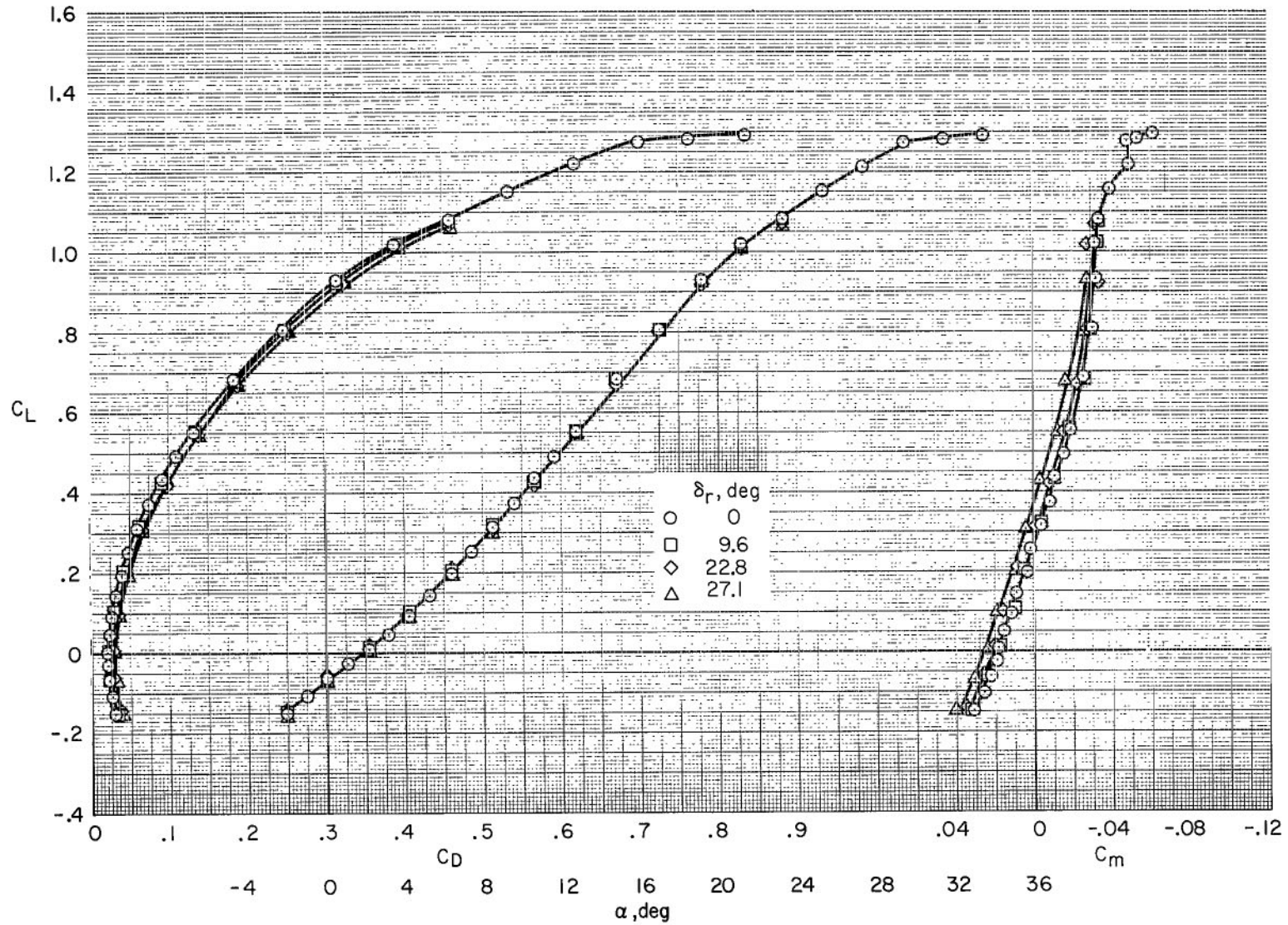
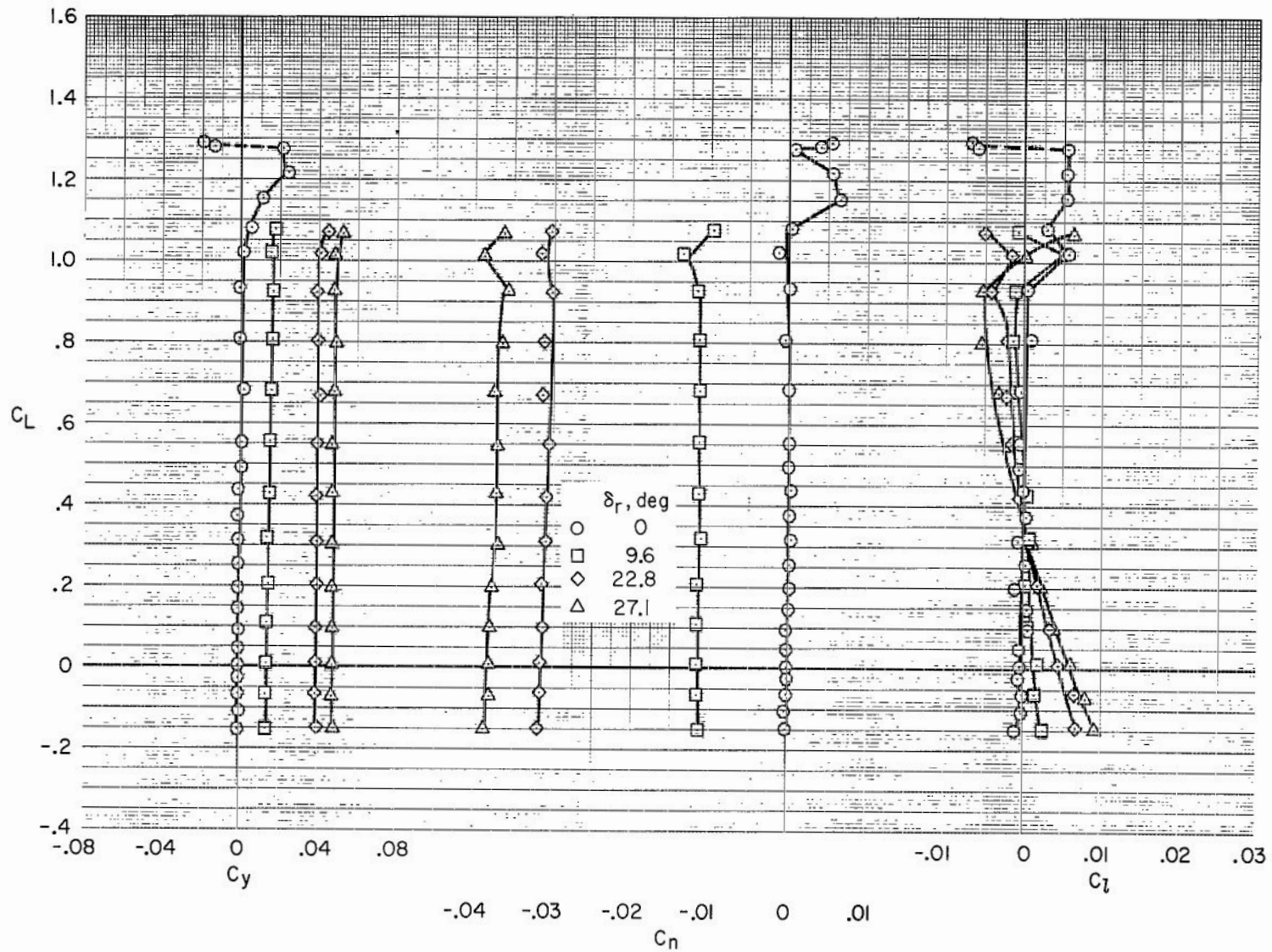
(a) C_L vs. C_D , α , C_m

Figure 22.- The effect of rudder deflection on the characteristics of the model with the short fuselage and without sideslip; $h/\bar{c} = \infty$, $\delta_n = 0^\circ$, $\delta_e = 0^\circ$.



(b) C_L vs. C_Y , C_n , C_l

Figure 22.- Concluded.

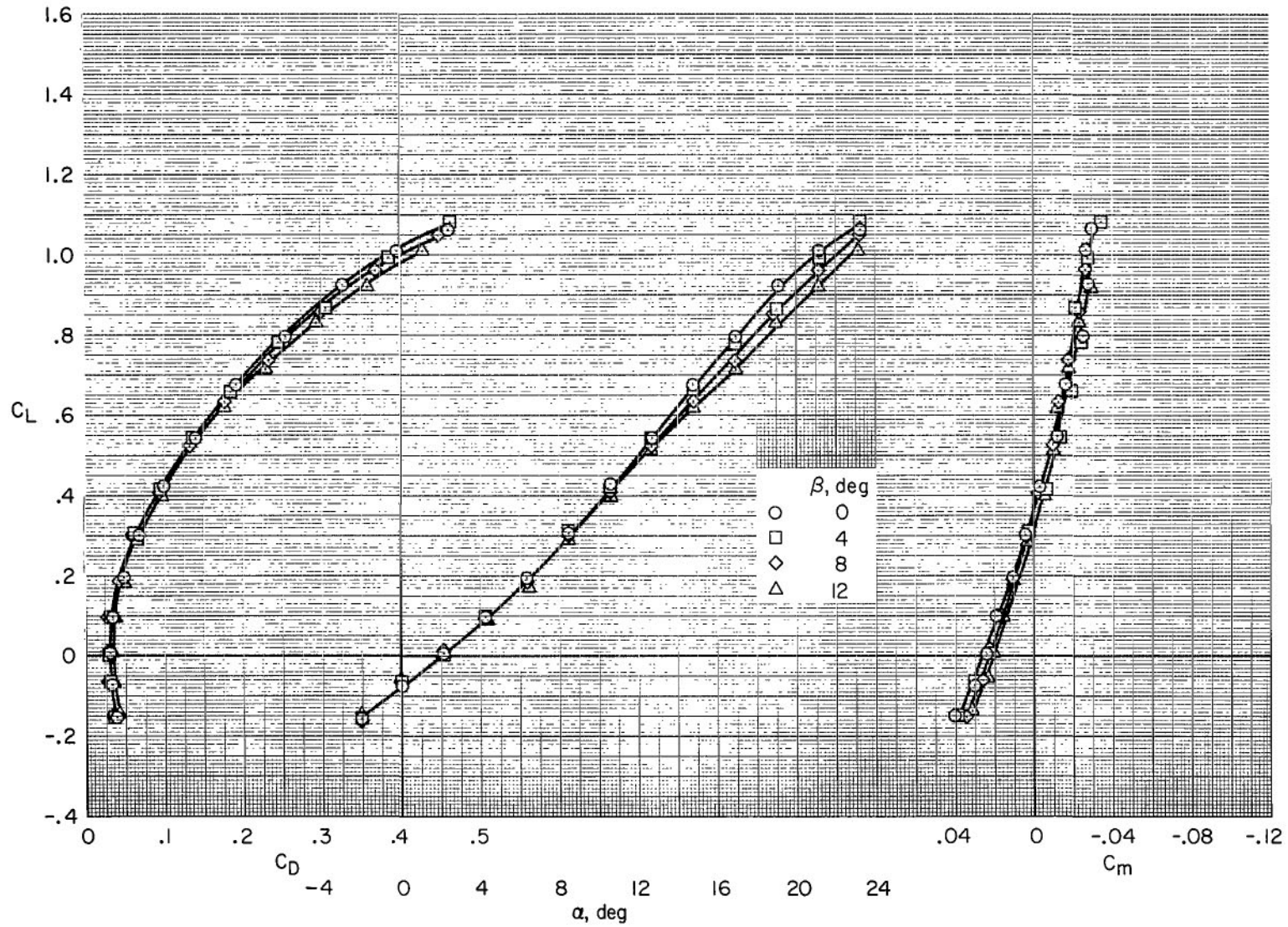
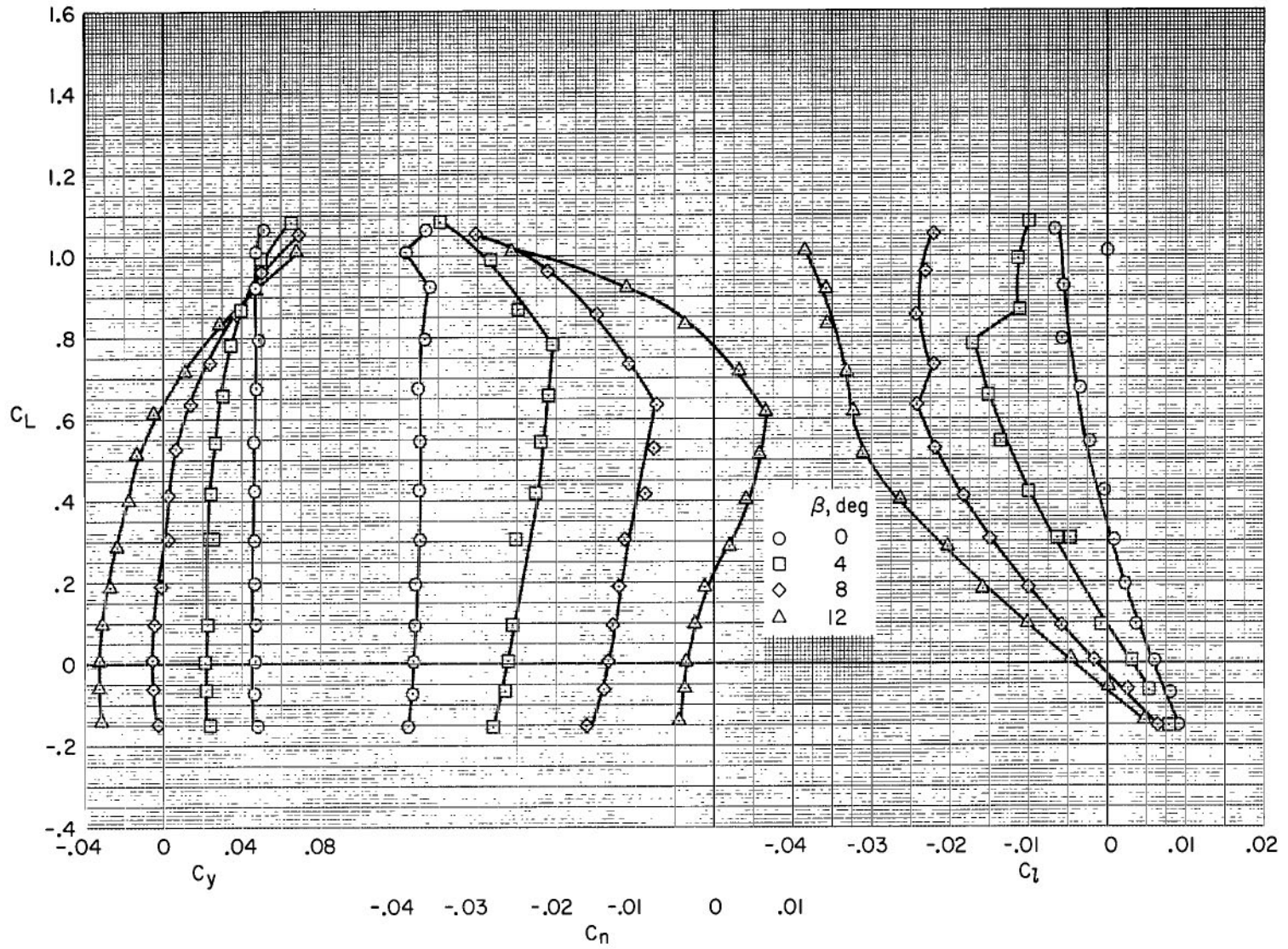
(a) C_L vs. C_D , α , C_m

Figure 23.- The effect of sideslip on the characteristics of the model with the short fuselage and with rudder deflected; $\delta_n = 0^\circ$, $\delta_e = 0^\circ$, $\delta_r = 27.1^\circ$, $h/\bar{c} = \infty$.



(b) C_L vs. C_Y , C_n , C_l

Figure 23.- Concluded.

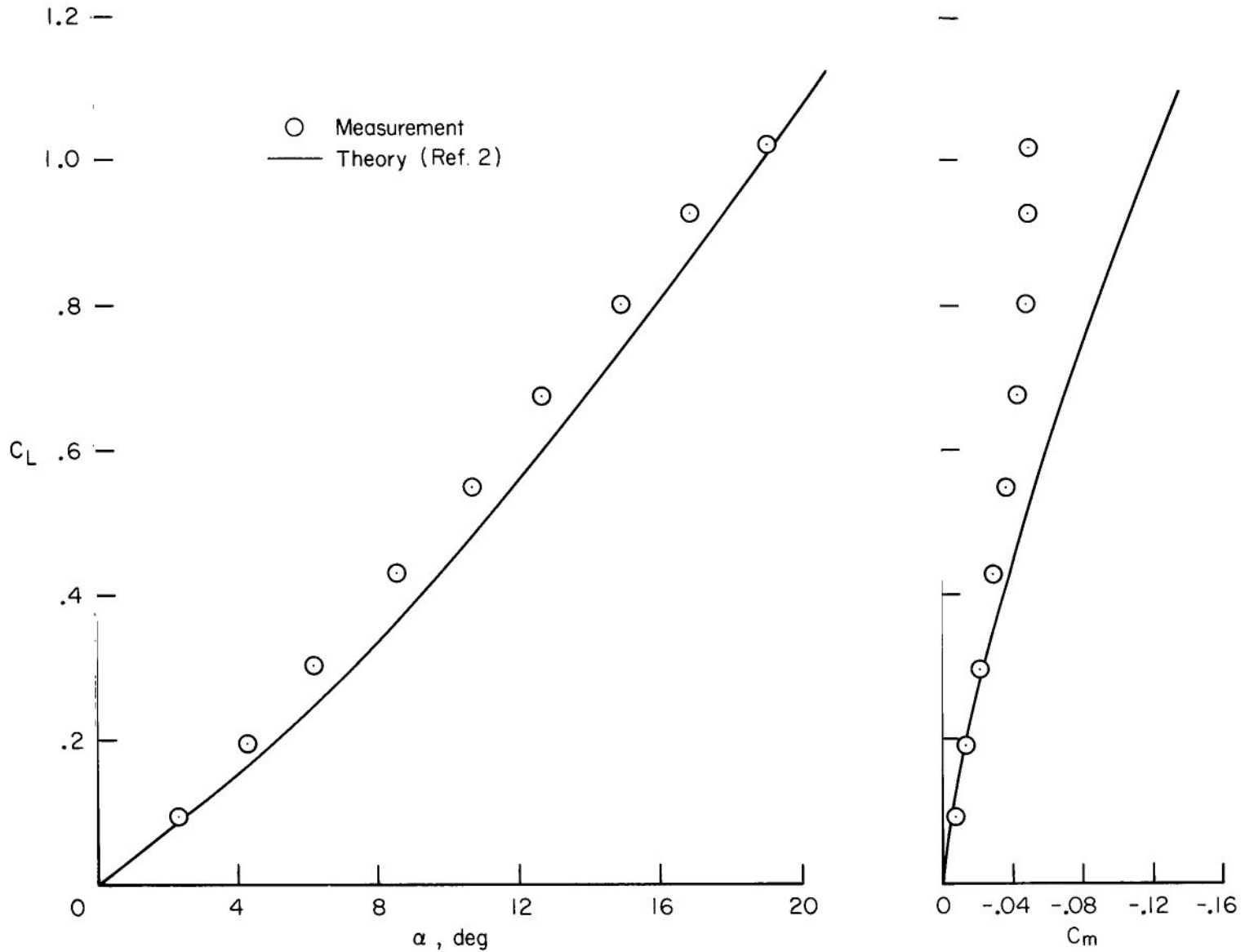


Figure 24.- Comparison of predicted lift and pitching moment for the configuration with the short fuselage with measurement; $\delta_e = 0^\circ$, $\delta_n = 0^\circ$, $h/\bar{c} = \infty$.

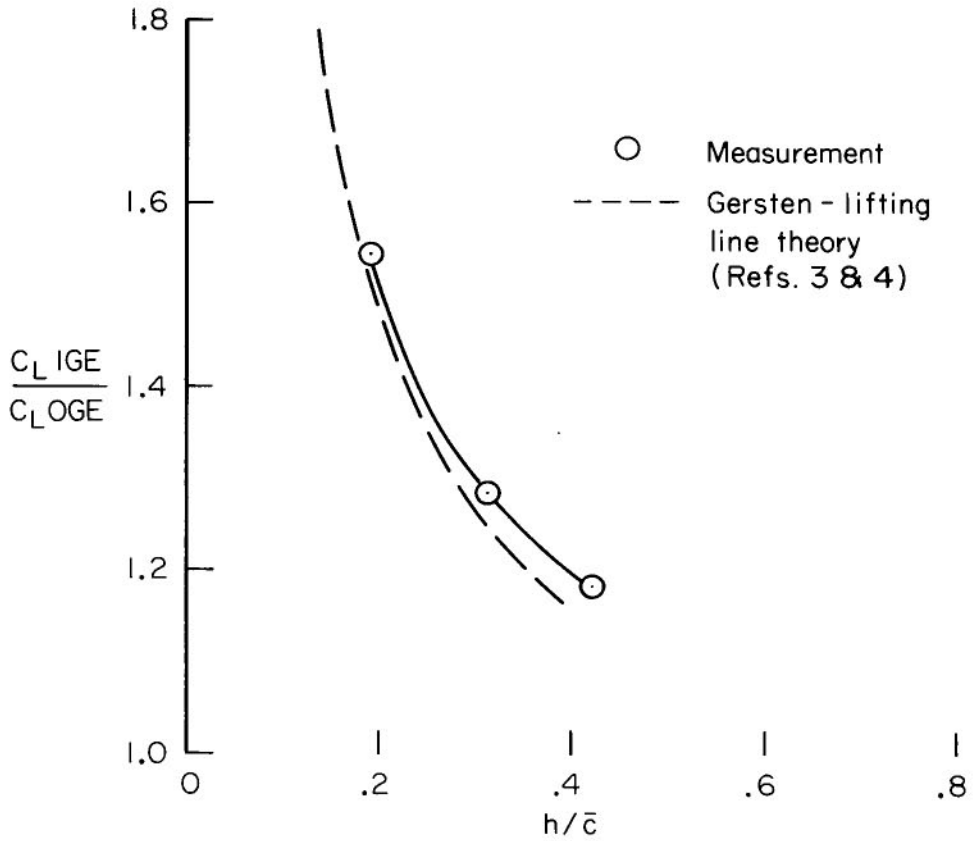
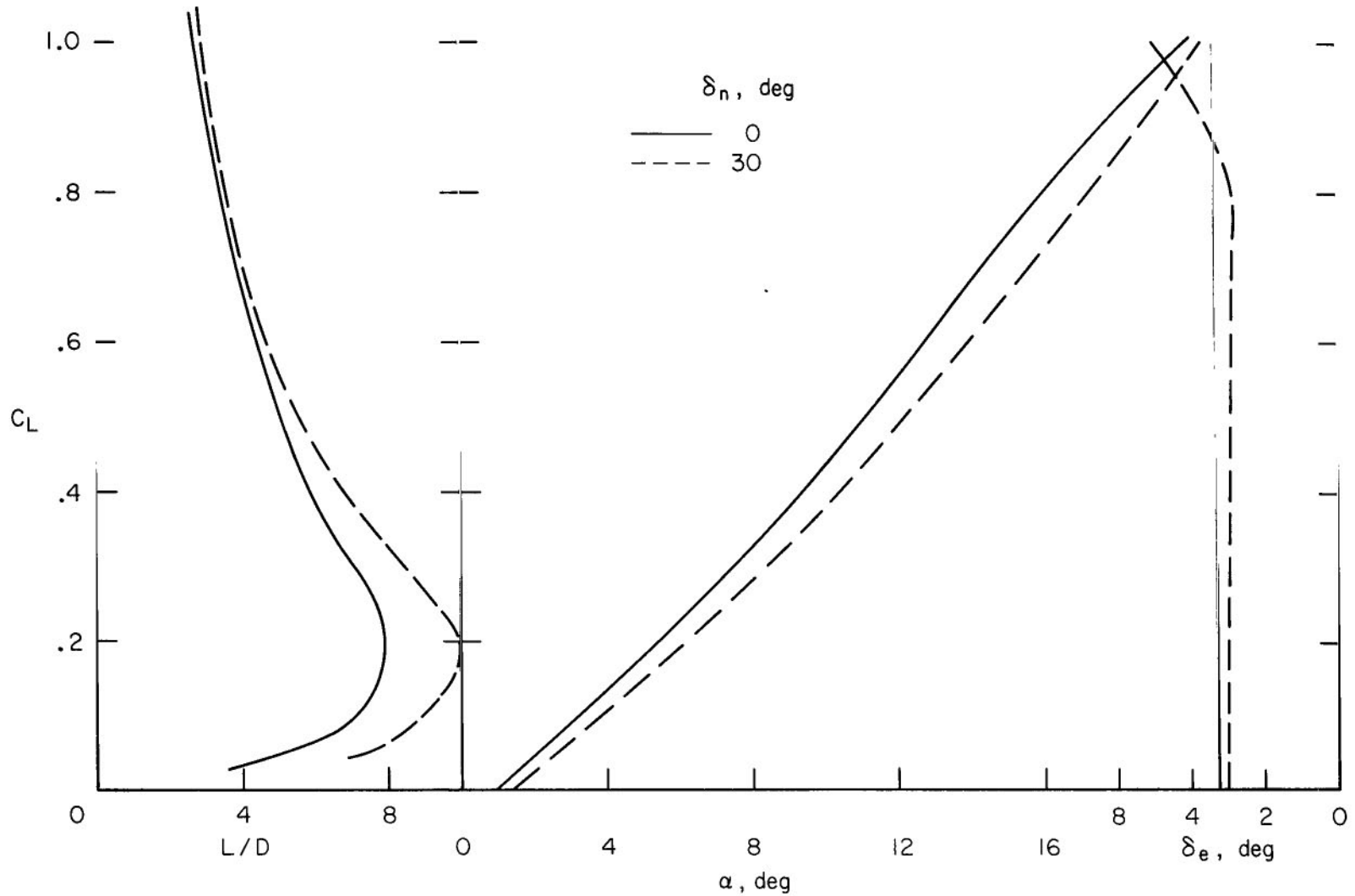
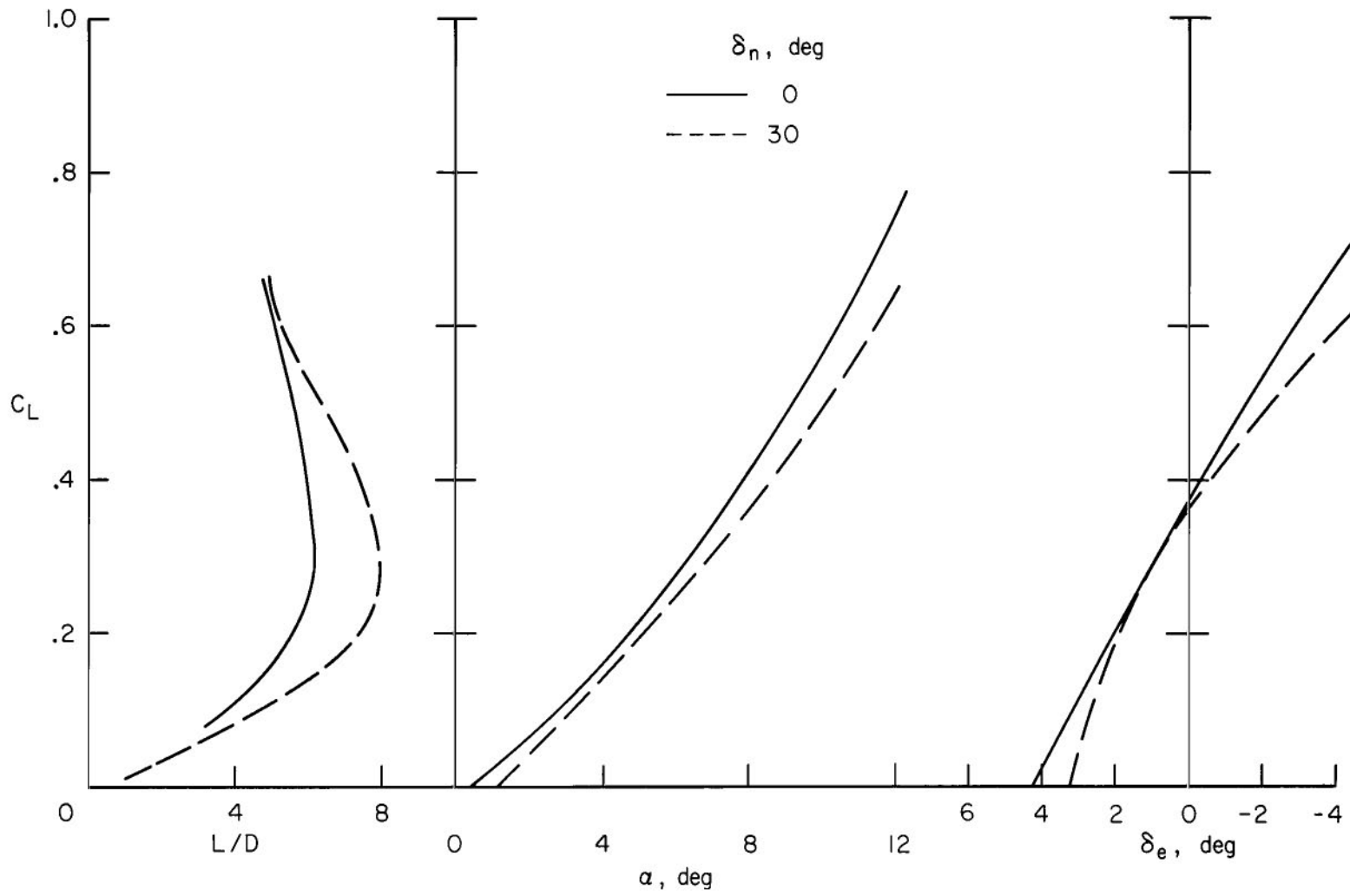


Figure 25.- Summary of measured ground effects with comparison with theory; $\alpha = 10^\circ$, $\delta_e = 0^\circ$, extended fuselage, nacelles removed.



(a) $h/\bar{c} = \infty$, $C_{D_{\min}} = 0.011$ (gear up), short fuselage, nacelles installed.

Figure 26.- The characteristics of the model trimmed about a static margin in ground effect of 8 percent of \bar{c} .



(b) $h/\bar{c} = 0.19$, $C_{D_{\min}} = 0.023$ (gear down), extended fuselage, nacelles removed.

Figure 26.- Concluded.

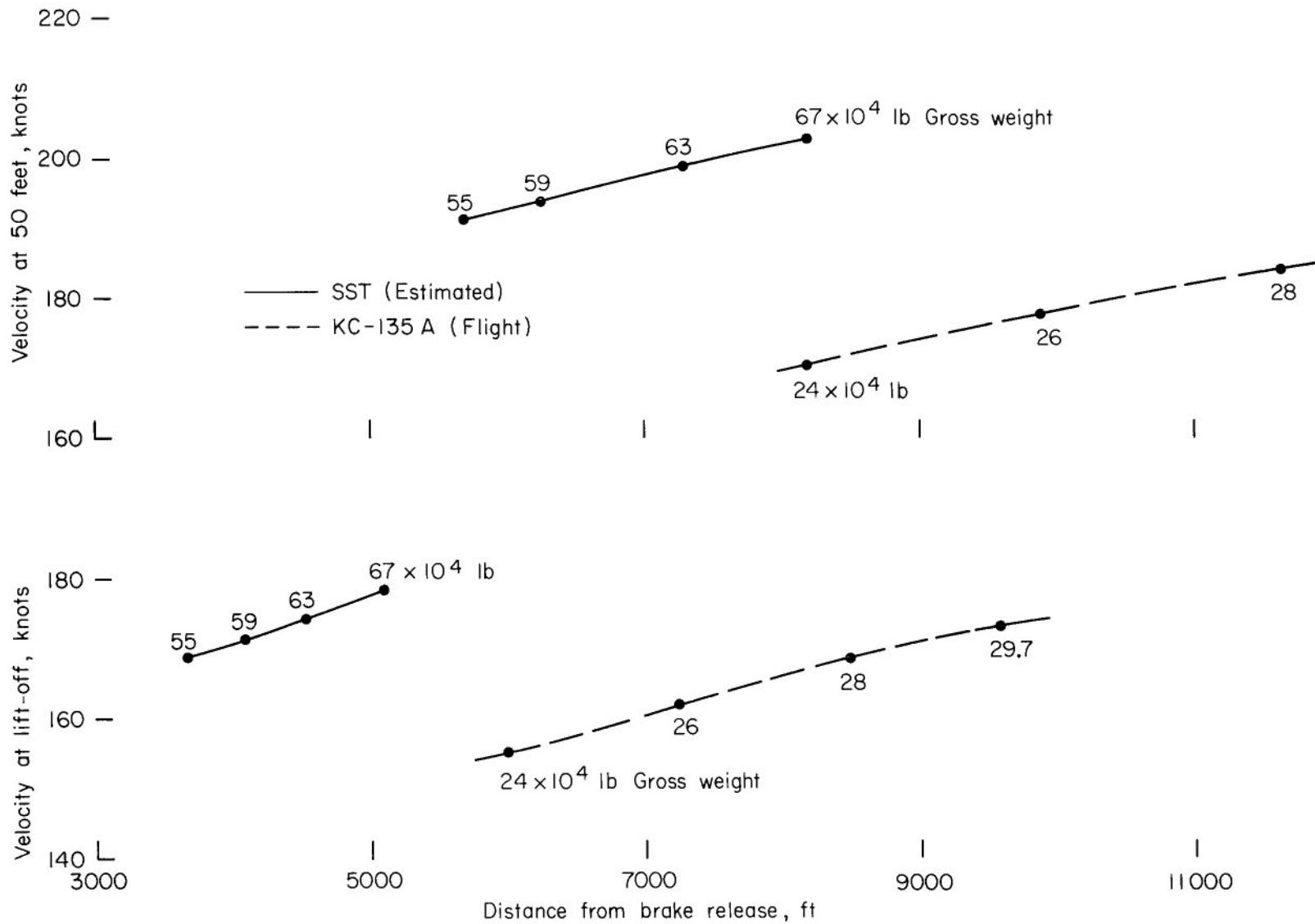


Figure 27.- Takeoff distances of SST and conventional subsonic jet. See table III for the parameters of the aircraft, standard day.

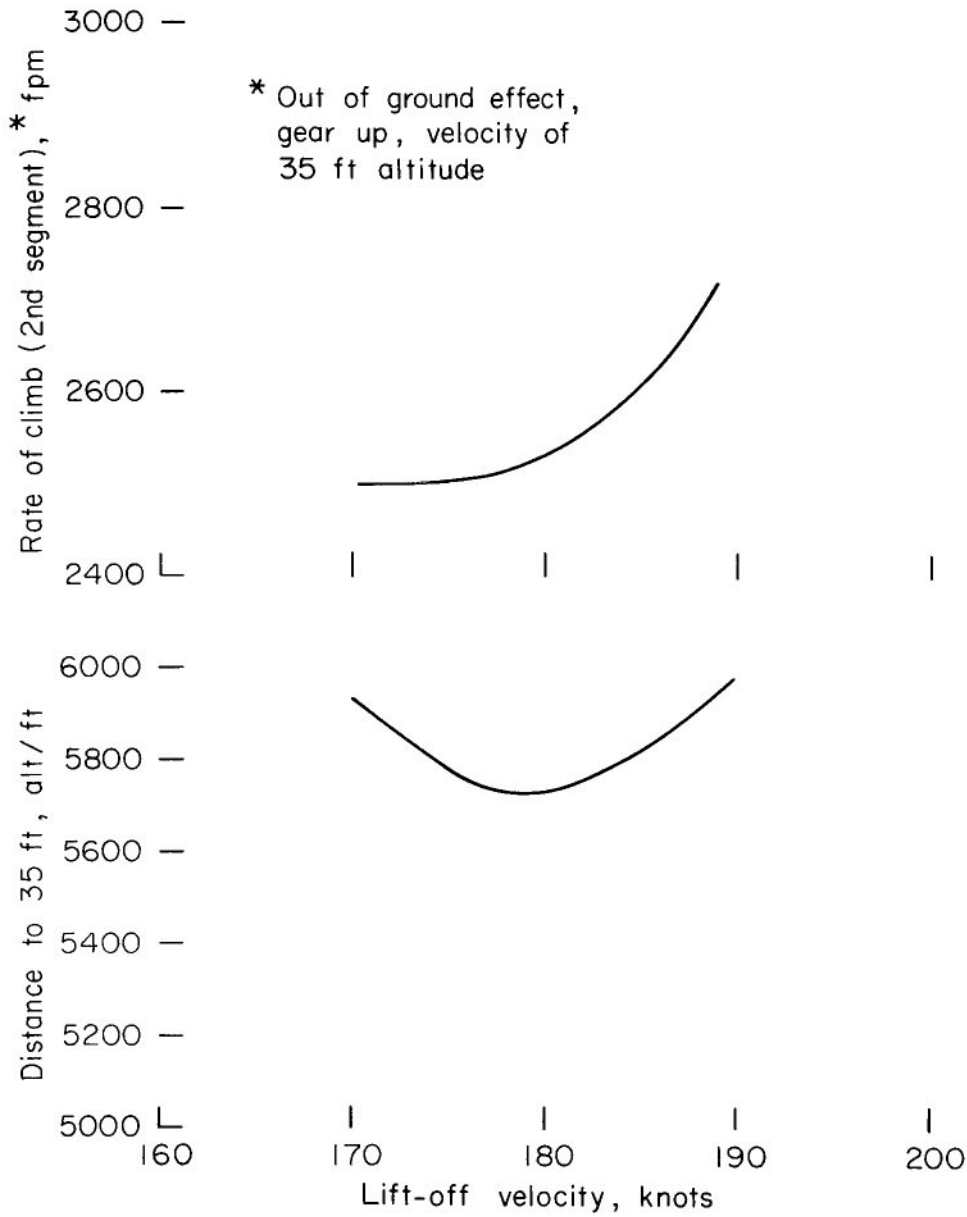


Figure 28.- The effect of lift-off speed on takeoff and climb performance, standard day.

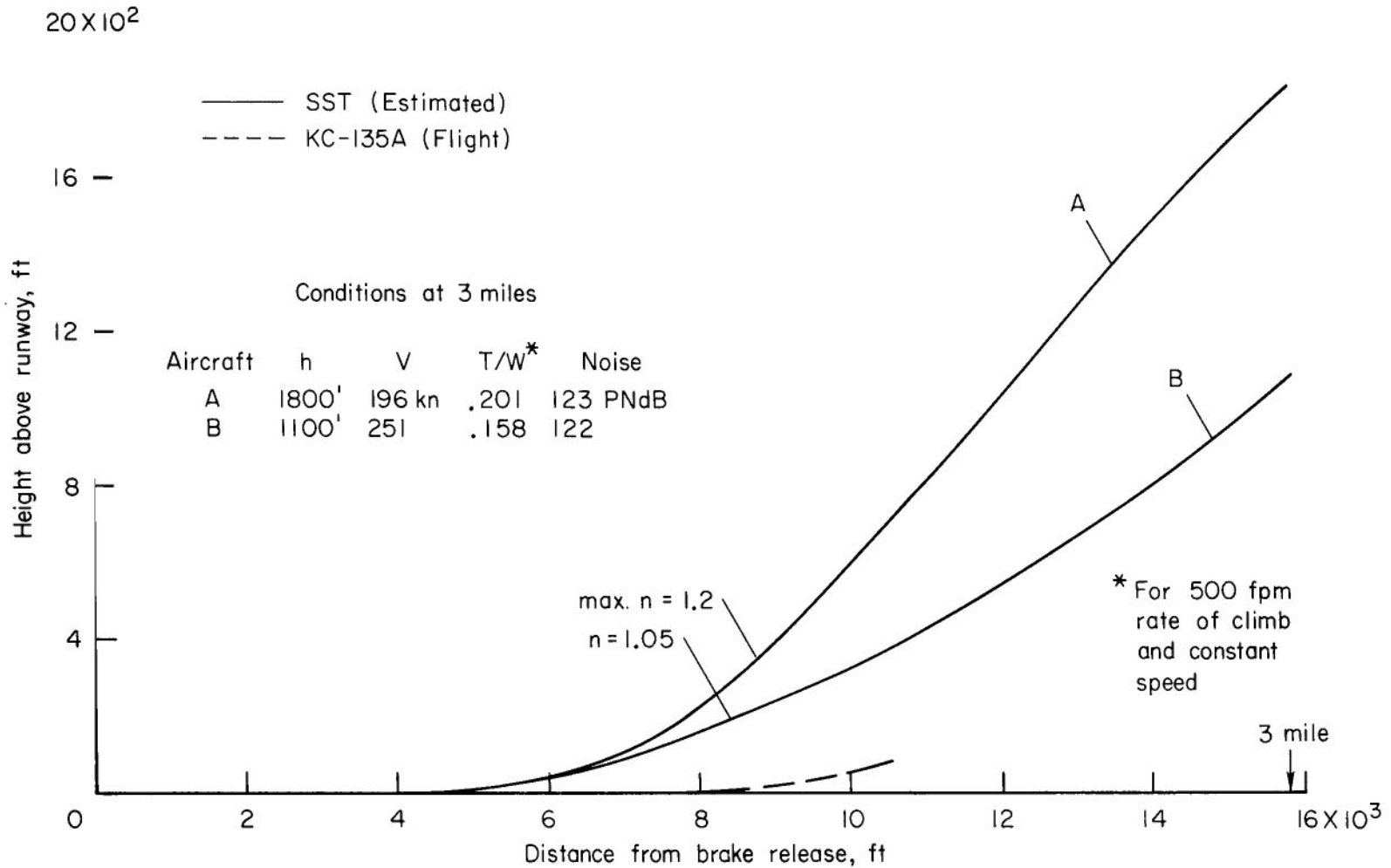


Figure 29.- Takeoff and climb profiles of an SST and a subsonic jet. See tables III and IV for the parameters of the aircraft.

FIRST CLASS MAIL

POSTMASTER: If Undeliverable (Section 152
Postal Manual) Do Not Return

"The aeronautical and space activities of the United States shall be conducted so as to contribute . . . to the expansion of human knowledge of phenomena in the atmosphere and space. The Administration shall provide for the widest practicable and appropriate dissemination of information concerning its activities and the results thereof."

— NATIONAL AERONAUTICS AND SPACE ACT OF 1958

NASA SCIENTIFIC AND TECHNICAL PUBLICATIONS

TECHNICAL REPORTS: Scientific and technical information considered important, complete, and a lasting contribution to existing knowledge.

TECHNICAL NOTES: Information less broad in scope but nevertheless of importance as a contribution to existing knowledge.

TECHNICAL MEMORANDUMS: Information receiving limited distribution because of preliminary data, security classification, or other reasons.

CONTRACTOR REPORTS: Scientific and technical information generated under a NASA contract or grant and considered an important contribution to existing knowledge.

TECHNICAL TRANSLATIONS: Information published in a foreign language considered to merit NASA distribution in English.

SPECIAL PUBLICATIONS: Information derived from or of value to NASA activities. Publications include conference proceedings, monographs, data compilations, handbooks, sourcebooks, and special bibliographies.

TECHNOLOGY UTILIZATION PUBLICATIONS: Information on technology used by NASA that may be of particular interest in commercial and other non-aerospace applications. Publications include Tech Briefs, Technology Utilization Reports and Notes, and Technology Surveys.

Details on the availability of these publications may be obtained from:

SCIENTIFIC AND TECHNICAL INFORMATION DIVISION
NATIONAL AERONAUTICS AND SPACE ADMINISTRATION
Washington, D.C. 20546